Applicability of analytical techniques to quantify trace metals in particulate matter for source apportionment in South Africa

E Van Loggenberg

orcid.org 0000-0003-3203-3029

Dissertation submitted in partial fulfilment of the requirements for the degree *Master of Science in Environmental Sciences with Atmospheric Chemistry* at the North-West University

Supervisor:	Prof PG van Zyl
Co-supervisor:	Prof JP Beukes

Graduation July 2020

23474920

“I will praise You on the mountain
And I will praise You when the mountain’s in my way
You're the summit where my feet are
So I will praise You in the valleys all the same
No less God within the shadows
No less faithful when the night leads me astray
You're the Heaven where my heart is
In the highlands and the heartache all the same”

~ Hillsong United

ABSTRACT

The impacts of atmospheric trace metal species in particulate matter (PM) on human health and the environment is well documented. Rapid advances in the development of analytical techniques used for characterisation and quantification of atmospheric trace metals have been made in recent years. Two analytical methods generally used for the analysis of trace metal species include wavelength-dispersive X-ray fluorescence (WD-XRF) and inductively coupled plasma mass spectrometer (ICP-MS) with each method associated with benefits and limitations. Limited research has been conducted to compare these techniques within the context of PM characterisation in the South African environment. Therefore, the aim of this study was to compare WD-XRF and ICP-MS for the analysis of trace metals in PM in order to assess the applicability of these techniques for source apportionment studies in South Africa.

Atmospheric PM samples were collected at two sites in South Africa. Size segregated ambient aerosol samples were collected at a regional background site, i.e. Welgegund, while indoor samples were collected in an informal settlement in Agincourt. Weekly ambient PM samples were collected on filters for two months with a Dekati three-stage cascade impactor, while 24-hour indoor samples were collected with a GX Cyclone comprising of a PM_4 inlet for four weeks. PM samples collected on filters were analysed with a WD-XRF spectrometer, after which aerosols were extracted with nitric acid digestion from these filters for analysis with an ICP-MS. In total, 31 trace metals were analysed by both analytical techniques. Only trace metal species that passed the assessment criteria were considered in the comparison of concentrations determined with WD-XRF and ICP-MS, which included 18 indoor trace metals (Na, Mg, Al, P, Ca, Ti, Cr, Mn, Fe, Co, Ni, Cu, Zn, Rb, Sr, Mo, Pd, Sb) and 16 ambient trace metals (Na, Mg, Al, P, K, Ca, Ti, Mn, Fe, Ni, Zn, As, Sr, Pd, Pt, Pb)

The trace metal concentrations determined with both analytical methods indicated higher trace metal concentrations in indoor samples compared to ambient samples, which was attributed to ambient aerosols being more dispersed compared to particulates associated with indoor emissions and different sources impacting the two sites. Furthermore, the highest trace metal concentrations were determined for Na, Mg, Al and Ca.

The percentages of samples for which concentrations of specific trace metals were above the limit of detection (LOD) of WD-XRF and ICP-MS differed for the two analytical techniques, while statistical correlations between trace metal concentrations determined with ICP-MS and WD-XRD also indicated very weak relationships between these species. In order to further assess these observed differences, concentrations determined for each trace metal species in each sample collected during the ambient and indoor campaigns with ICP-MS and WD-XRF

were directly compared. These direct comparisons of concentrations determined for specific trace metals in each sample did not reveal distinct trends in the concentrations determined for most species with these two analytical techniques. However, it did seem that higher concentrations of trace metal species associated with crustal sources were determined with WD-XRF, which was expected due to the nitric acid digestion underestimating silicate minerals in dust during ICP-MS analysis. Lower trace metal concentrations determined with ICP-MS was also attributed to interferences during the analysis of extracted samples. Lower trace metal concentrations determined with WD-XRF compared to ICP-MS was generally attributed to most trace metal species occurring in the fine size fraction. Comparison of the concentrations determined for each trace metal species with the two analytical methods did not reveal distinct confirmations with regard to the suitability of ICP-MS and WD-XRF for determination of concentrations of specific trace metals in South Africa. Therefore, future studies in order to improve the comparison of these two analytical methods for atmospheric trace metal analysis in South Africa are strongly recommended.

Keywords: ICP-MS; WD-XRF; Aerosols; Air quality; Indoor emissions; Welgegund

ACKNOWLEDGEMENTS

First and foremost, I would like to thank the Lord, Jesus Christ. Through whom anything and everything is possible. I would also like to sincerely thank the following people and institutions for their invaluable contributions and suggestions that made the completion of this dissertation possible:

- The North-West University (Potchefstroom Campus) for giving me the opportunity and financial support to enrol for my master's degree.
- Prof Stuart Piketh and Prof Roelof Burger, at the NWU climate research group, for the financial support throughout the completion of my degree
- My supervisor, Prof Pieter van Zyl, for his support, patience, knowledge and advice.
- My co-supervisor, Prof Paul Beukes, for his knowledgeable inputs, support and kind words throughout. As well as presenting this master's degree opportunity when I wasn't sure what to do next. For this, I am forever grateful.
- Dr Miroslav Josipovic, for his assistance and guidance during the sample collection of this study. As well as encouragement, kind words, and constant willingness to help throughout the completion of this dissertation.
- Mr. Joe Malahlela, Mr. Johan Hendriks and Brigitte Language, for their assistance in sample collection, sample weighing and sample analysis. Including their constant inclination to help in any way possible.
- My father, mother, sister and brother-in-law for their boundless love, support, encouragement and guidance in all I do. I love you the most.

TABLE OF CONTENTS

LIST OF FIGURES

LIST OF TABLES

LIST OF ABBREVIATIONS

AA	Atomic Absorption
AC	Alternating Current
ACRG	Atmospheric Chemistry Research Group
BIC	Bushveld Igneous Complex
CCN	Cloud Condensation Nuclei
cps	Counts Per Second
DC	Direct Current
ED-XRF	Energy-Dispersive X-Ray Fluorescence
GC	Gas Chromatography
IARC	International Agency for Research of Cancer
ICP-MS	Inductively Coupled Plasma Mass Spectrometry
ISFB	Indoor Solid Fuel Burning
LOD	Limit of Detection
MCE	Mixed Cellulose Ester
NSFB	Non-Solid Fuel Burning
OSFB	Outdoor Solid Fuel Burning
PGM	Platinum Group Metals
PM	Particulate Matter
ppb	Parts Per Billion
ppm	Parts Per Million
ppt	Parts Per Trillion
PSD	Particle Size Distribution
RSD	Relative Standard Deviation
SEM	Scanning Electron Microscopy
TSF	Tailing Storage Facility
TSP	Total Suspended Particles

WD-XRF	Wavelength-Dispersive X-Ray Fluorescence
WHO	World Health Organisation
XRF	X-Ray Fluorescence

CHAPTER 1: INTRODUCTION

In this chapter the relevance of the current study is considered, while the motivation for this study in view of background information relating to the measurement and analysis of atmospheric trace metal species is presented. The general aim and specific objectives for this study is also indicated.

1.1. Background & motivation

Atmospheric particulate matter (PM) is well-known for long- and short-term detrimental effects on both the environment (e.g. climate change, air quality, atmospheric visibility, acid deposition, eutrophication) and human health (e.g. cardiovascular disease, respiratory and allergic disease) (Bo *et al*., 2017; Liu *et al*., 2014; Nazir *et al*., 2011). Since the London smog of 1952 which attributed to approximately 4000 premature deaths, significant importance has been placed on an improved understanding of the chemical and physical properties of atmospheric PM. It is estimated that more than 1 500 scientific papers related to aerosols are currently published each year (Brunekreef & Holgate, 2002; Fuzzi *et al*., 2015; Harrison & Yin, 2000). Accordingly, critical focus has also been placed on the establishment of accurate and complete global emission inventories for atmospheric PM, which allows governments and federal agencies, such as the World Health Organisation (WHO) to accurately assess pollution and impacts associated with PM species. These emission inventories are crucial for the effective development of air quality standards and guidelines in order to improve air quality and protect the public against adverse health effects (Harrison & Yin, 2000; Niu *et al.*, 2009).

Atmospheric aerosols are emitted by numerous natural (e.g. wind-blown dust, volcanos, lightning induced savannah and grassland fires) and anthropogenic (e.g. industry, vehicles, man-made savannah and grassland fires) sources. Furthermore, secondary aerosols are formed due to oxidation of primary species e.g. oxidation of gaseous SO_2 to form SO_4^{2-}. PM have a diverse set of physical (e.g. particle size, particle shape) and chemical (e.g. composition) properties. The influence of these species on human health and the environment are determined by their physical and chemical properties (Prospero *et al.*, 1983; Pöschl, 2005; Fuzzi, 2015). Smaller particulates, for instance, with an aerodynamic diameter <1 µm can penetrate into the lower respiratory tract. In addition, a complete understanding of the chemical composition of PM is crucial in assessing the impacts of these species. It is therefore crucial to assess the precision, accuracy and sensitivity of analytical techniques utilised to quantify the composition of PM (Niu *et al.*, 2009).

Rapid advances in the development of analytical techniques used for the measurement of PM have been observed throughout the years (Brown & Milton, 2005). Multiple analytical

techniques are commercially available at present, which include advanced *real-time* measurement techniques. It is important to acknowledge that none of techniques are without limitations (Feldmann *et al*., 2009). Furthermore, there is no agreed upon method that is considered the most reliable. This is mainly attributable to the fact that an instruments' response is determined by PM shape, size, concentration, etc. Whilst laboratory-generated PM standards comprised of a known size, shape, and concentration are used to calibrate instruments. Countless uncertainties remain when analysing ambient- and/or indoor PM as their size, shape, and concentration may differ significantly from particle-to-particle (Fuzzi *et al.*, 2015; Kgabi, 2010; McMurry, 2000; Okuda *et al.*, 2013). According to the majority of literature, the particle size fraction and the chemical composition of the particulate matter act as the greatest obstacles for most analytical techniques. Therefore, one should consider measurement techniques of these species that are most reliable for the specific species of interest in a study.

X-ray fluorescence (XRF) and the inductively coupled plasma mass spectrometer (ICP-MS) are two of the most popular analytical techniques generally used to quantify trace metal species in PM, even though they are fundamentally different and indicate biases towards different particulates (size and composition). The wavelength-dispersive XRF (WD-XRF) spectrometer is a diverse non-destructive analytical technique used to obtain both quantitative and qualitative multi-elemental information of inorganic- or organic substances. In brief, a WD-XRF spectrometer can be explained as a system in which a sample is irradiated with X-rays. In turn, the secondary X-rays (or X-ray fluorescence) is measured with a wavelength dispersive detection system. That is, secondary X-rays are identified by means of a diffraction crystal which separate the X-rays based on their wavelength. The WD-XRF spectrometer is traditionally applied for the quantification of the most abundant elements, which are generally associated with the coarse fraction PM (PM_{10}). Whereas, an ICP-MS is a destructive analytical technique used for the quantitative and qualitative chemical analysis of a substance. An ICP-MS system ionises a liquid sample into a fine mist by means of an inductively coupled plasma. The ionised aerosol comprises the various isotopes of the different elements in a sample. These ions are quantified by means of a mass-spectrometer, according to the mass-to-charge ratio of each ion. The ICP-MS systems are capable of accurately determining elemental concentrations as low as parts per billion (ppb). It is known that XRF has lower detection limits for crustal elements, e.g. Si, S, P, Cl and Fe typically associated with the coarse fraction. However, the XRF might underestimate elements typically found in finer size fractions, which is generally associated with combustion processes, secondary chemical reactions and condensation. Therefore, the ICP-MS seems to be more suitable to determine trace metals in

finer PM fractions due to lower detection limits related to this analytical method. However, ICP-MS could underestimate elements associated with the coarse PM fraction. Another disadvantage of the ICP-MS, is that samples must first undergo acid digestion before ICP-MS analyses can be completed, which in turn, increases the risk of sample contamination and loss of particulate matter (Herner *et al*., 2006; Niu *et al.*, 2009; Salcedo *et al*., 2014). Furthermore, most commercial ICP-MS systems do not readily analyse silicon (Si), consequently underestimating elements generally comprised of a siliceous matrix such as Al, Fe, Ca, Na, K and Mg. This is unless the siliceous matrices are decomposed with appropriate, but rather dangerous acid digestion methods, and the system consists of expensive corrosive-resistant materials.

Even though WD-XRF and ICP-MS are the most commonly applied analytical techniques used for the quantification of atmospheric PM, limited research has been conducted on the comparison between these techniques. Especially within the context of PM characterisation in the South African environment. South Africa is considered the largest industrialised economy in Africa, with vast deposits of several mineral resources (including gold; platinum; iron and chromium) dispersed over the entire country. Thus, South Africa consists of substantial mining and metallurgical activities and therefore, a substantial amount of anthropogenic pollution sources comprised of PM-bound trace metals (Swartz, 2016; van Zyl *et al*., 2014). In this study, PM will be collected on filter media at two sites in South Africa exposed to both primary and secondary source PM. Additional filters that have already been collected for a previous study will also be analysed. The filters will be subjected to WD-XRF and ICP-MS analyses to determine the trace metal composition. The obtained data will be used to compare and assess the suitability of the different methods for different applications.

1.2. Aims & Objectives

The primary aim of this study was to compare two analytical methods, i.e. WD-XRF and ICP-MS typically used to quantify trace metals in PM sampled on filters in order to assess the applicability of these techniques for source apportionment studies in South Africa. It is aimed to assess the strengths and limitations associated with each of these two analytical methods. The general aim of this study was achieved through the following specific objectives:

- Quantify trace metal composition of PM samples collected on filters by means of non-destructive WD-XRF analysis,
- Quantify trace metal composition of the same samples with a destructive acid digestion technique for ICP-MS analysis, and
- Compare results obtained from the different methods so as to identify possible biases of techniques with regard to composition and source apportionment of PM.

CHAPTER 2: LITERATURE REVIEW

Chapter 2 will provide a brief but relevant description about the most important aspects of particulate matter, such as: particle size, source and emission, as well as the significance of particulate matter in air pollution, climate change and human health. Furthermore, a critical literature review will be given on analytical techniques used to quantify atmospheric particulate matter. ICP-MS and WD-XRF, utilised in this study, will be discussed comprehensively by examining the basic components of each technique individually, as well as the basic principles of functionality. External factors, such as filter media and sample preparation, that may adversely affect the accuracy and effectiveness of the techniques are also discussed.

2.1. Introduction to atmospheric particulate matter

Atmospheric particulate matter (PM) or aerosols can broadly be defined as a liquid and/or solid suspended in a gas (atmosphere). PM can be non-volatile species such as crustal material (oxides), trace metals, salt, soot and pollen or formed from semi-volatile compounds. However, it is important to note that the relationship between non-volatile and semi-volatile species are interchangeably linked to one another. PM are classified on the premise of their source, i.e. natural PM and/or anthropogenic PM, which is typically reflected by the PM composition and particle size. Furthermore, PM can either be emitted directly into the atmosphere (primary PM) or formed by means of gas-to-particle transformation (secondary PM) as indicated by Figure 2.1 (Kgabi, 2010; McMurry, 2000; Prospero *et al*., 1983; Venter, 2015).

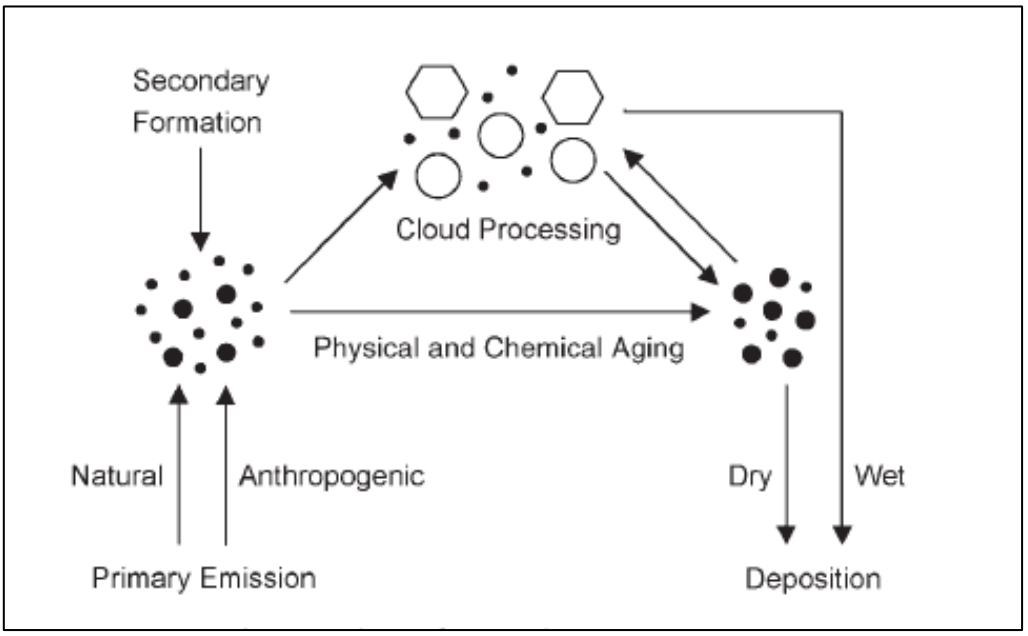

Figure 2.1: Cycle of particulate matter in the atmosphere (Pöschl, 2005)

The two principal mechanisms responsible for removal of PM include wet deposition and/or dry deposition as indicated by Figure 2.1 (Booyens, 2018; Brimblecombe, 1996; Pöschl, 2005, Swartz, 2016). According to Prospero (as stated by Booyens, 2018) wet deposition removes 80 – 90% of PM from the atmosphere. Wet deposition removes PM by means of rainout: integration of PM within cloud as cloud condensation nuclei (CCN) or washout: in which PM is removed from the atmosphere by precipitation or any other hydrometeor below cloud-base (Pöschl, 2005; Prospero, 1983; Swartz, 2016). Dry deposition is the removal of PM without precipitation. Sedimentation of particles is attributable to gravitational settlement, convection, diffusion, and adhesion to Earth's surface (Booyens, 2018; Kgabi, 2006; Pöschl, 2005; Prospero, 1983).

The Earth's atmosphere is a highly complex system within which numerous reactions occur continuously, which allows atmospheric aging of PM. PM undergoes physical and chemical transformations, which result in a change of the chemical composition, particle size and structure that may differ significantly from the originally emitted particle (Pöschl, 2005; Prospero *et al.*, 1983). It is these variances associated with PM that give rise to the uncertainties when measuring ambient PM. It is also these particular properties that play a vital role when investigating the effects of PM on the environment and human health.

2.2. Particle size, particle emission & particle size

PM sizes range over more than four magnitudes and are classified in relation to the aerodynamic diameter of particles. Size fractions include: the ultrafine fraction, $PM_{0.1}$ (particles ≤ 0.1µm) and PM_1 (particles ≤ 1 µm); fine fraction, $PM_{2.5}$ (particles ≤ 2.5 µm); and the coarse fraction, PM_{10} (particles ≤ 10µm) (Booyens *et al.*, 2015; Graney *et al.*, 2003; Pöschl, 2005; McMurry, 2000). Coarse PM are generally associated with natural primary particles. These particles are mainly composed of pollen, sea salt, soot or formed by means of mechanical abrasion of earth surface (erosion, farming, volcanic eruptions, wind-blown dust/soil). fine fraction primary particles are mainly emitted by means of anthropogenic activities, such as incomplete fossil fuel combustion or high temperature processes (Brimblecombe, 1996; Butterfield & Quincey, 2007; Fuzzi *et al.,* 2015; Pope & Dockery, 2006; Prospero *et al.*, 1983). Ultra-fine and fine fraction PM are largely formed by means of transformation, nucleation condensation and coagulation (secondary PM) (Prospero *et al.*, 1983). Furthermore, according to Kulmala *et al.* (as stated by Venter, 2015) secondary PM may from as result of homogeneous or heterogeneous condensation. Homogeneous condensation occurs when new particles are formed due to nucleation of gases. Whereas heterogeneous condensation occurs when gases condensate and/or coagulate on pre-existing particles. As previously mentioned, this study mainly focused on PM-bound trace metals, which can be emitted by

both natural and anthropogenic sources. Table 2.1 and Table 2.2 provide a list of major natural and anthropogenic sources of ambient trace metals PM respectively. As well as the elemental markers (trace metals) generally associated with corresponding sources.

Table 2.1: Sources of ambient natural trace metals in the atmosphere and the corresponding elemental markers

Source	PM-Bound Trace Metals
Vegetation	According to Jacobson (as stated by Venter, 2015), vegetation is comprised of low concentrations metals. These trace metals include antimony (Sb), arsenic (As), cadmium (Cd), chromium (Cr), cobalt (Co), copper (Cu), lead (Pb), manganese (Mn), nickel (Ni), titanium (Ti), and zinc (Zn). These elements are emitted into the atmosphere as volatile metals when vegetation burns (veld-fires) or decay. Emitted metals then condense onto existing particle such as soot or ash.
Dust	Approximately 45% of PM is comprised of dust. Crustal material is characterised by a diverse composition, generally reflecting the sum of metal oxides most abundant in soil/geology, such as aluminium (Al), calcium (Ca), iron (Fe) and silicon (Si). Concentrations of elements present in crustal material as PM depends on the climate and local geology (Davidson *et al*., 2005; Marconi *et al*., 2014; Harrison& Yin *et al.*, 2000; van Zyl *et al.*, 2014). Dust is responsible for roughly 50% of Cr, Mn, vanadium (V) in PM, and 20% of Cu, molybdenum (Mo), Pb, Sb, Zn in PM (Allen *et al.*, 2001; Venter, 2015).
Volcanism	Roughly 20% of Sb, As, Cd, Cr, Cu, Pb, mercury (Hg), and Ni are due to the sporadic eruptions of volcanoes (Allen *et al.*, 2001; Venter, 2015).
Ocean Spray	10% of total PM-bound trace metals are formed by wind (spray), waves and bursting of bubbles at the ocean surface (Venter, 2015).

Table 2.2: Sources of ambient anthropogenic trace metals in the atmosphere and the corresponding elemental markers

Sources	PM-Bound Trace Metals
Oil Power Plant	Fe, Ni, V, Zn (Deguillaume *et al.*, 2005; Venter, 2015).
Coal Power Plant	Al, Sb, As, Cd, Cr, Co, Cu, Fe, Pb, Mn, Hg, Ni, V, Zn (Venter, 2015).
Smelting Industries	Cd, Cr, Fe, Mn, Ni, Si, V, Zn (Venter, 2015).
Steel Mills	Cr, Cu, Fe, Pb, Mn, Ni, Zn (Venter, 2015).

Table 2.2 (continued): Sources of ambient anthropogenic trace metals in the atmosphere and the corresponding elemental markers

Sources	PM-Bound Trace Metals
Vehicle Emissions	Cd, Cu, Fe, Pb, Ni, palladium (Pd), platinum (Pt), rhodium (Rh), Zn (Kulshrestha *et al*., 2014; Onbowale & Owoade, 2015; Venter, 2015).
Waste Incineration	Sb, As, Cd, Co, Cu, Fe, Pb, Mn, Hg, Ni, tin (Sn), Zn (Venter, 2015).

Indoor PM sources can differ from those mentioned in Table 2.1 and Table 2.2, which can included particles from skin, hair, clothing fibre, combustion of solid fuel used for cooking and heating, cigarette smoke, and building materials of the building itself (Khoder, M.I., 2009; Kulshrestha *et al*., 2014). However, it is important to acknowledge that due to air exchange between outdoor- and indoor environments, the trace metals mentioned above in Table 2.1 and Table 2.2. cannot completely be omitted from an indoor environment. Studies such as Kulshrestha *et al*. (2014) have even stated that the greatest source of urban indoor trace metals are derived from outdoor anthropogenic sources, such as vehicular emissions and tyre abrasion. Table 2.3. provides a list of indoor PM-bound metal sources. As well as the elemental markers (trace metals) generally associated with the specified source.

Table 2.3: Sources pf indoor trace metals in the atmosphere and the corresponding elemental markers

Source	PM-Bound Trace Metal
Outdoor PM	Primarily dust that infiltrated from the outdoor environment. Can either be due to natural dust (refer to Table 2.1. *Dust* and *Vegetation*) or particles from anthropogenic activities such as metallurgical processes or vehicle emissions/tyre abrasion (refer to Table 2.2.) in the nearby proximity of building (Khoder *et al*., 2009; Kulshrestha *et al*., 2014).
Combustion of Solid Fuel (Wood)	Ca, Cu, K, Mn, P, Zn (Onbowale & Owoade, 2015)
Combustion of Solid Fuel (Coal)	As, Cd, Cr, Cu, Ni, Pb, Zn (Kulshrestha *et al*., 2014; Liu *et al*., 2017)
Combustion of Solid Fuel (Animal Manure)	As, Cd, Cr, Cu, Fe, Mn, Ni, Pb (Irshad *et al*., 2013; Mudway *et al*., 2005)
Combustion of Solid Fuel (Crop Waste)	Cu, K, Ni, Pb, Zn (Onbowale & Owoade, 2015; Venter, 2017)
Cigarette Smoke	Cd, Cr, Ni, Zn (Khoder *et al*., 2009; Kulshrestha *et al*., 2014)

2.3. Particulate matter & impacts

Air pollution is considered a major environmental risk factor world-wide. However, air pollution is a natural occurring phenomenon that has existed long before mankind. PM were emitted by volcanic eruption, wind-blown dust, lightning, sea spray and natural fires. Nonetheless, anthropogenic activities since the industrial revolution and mechanisation of processes has (have) significantly increased PM emissions (Bo *et* al., 2017; Monks *et al.*, 2009; Venter, 2015). According to the National Environmental Management: Air Quality Act (No. 39 of 2004) of South Africa, air pollution can broadly be defined as any change in the geochemical composition of the air caused by smoke, soot, dust, gas and/or fumes, odorous substances, and solid particulate matter of any kind. Air quality monitoring in developing countries such as South Africa is not strongly enforced and/or monitored by the law. Resources are rather invested in the economic growth of the country. South Africa, however, is considered the most industrialised country in Africa – consisting of numerous mineral deposits throughout the country and consequently a significant amount of mining-, metallurgical- and smelting activities. Emission of metals (including heavy metals) generally associated with these activities can result in significant problems for the surrounding environment (Swartz, 2016; Vanhoof *et al.*, 2003; van Zyl *et al*., 2014). In addition, a large percentage of South Africans reside in low-income settlements. It is well-known that these residents are most severely affected by indoor PM. This is mainly attributable to the fact that the residents of low-income settlements generally use solid fuel, such as wood, coal, animal dung, and crop waste as their primary energy source for cooking and space heating in poorly ventilated dwellings (Language *et al*., 2016; Smith, 2002). Emission of both indoor- and ambient PM have a significant influence on both the environment (climate change) and human health, which will be discussed in the subsequent sections.

2.3.1. Climate change

The effect of PM on the global climate is complicated. Many uncertainties remain as result of spatial and temporal unpredictability of PM concentration. Uncertainties associated with the reactivity of condensed phases (Davidson *et al.*, 2006; Deguillaume *et al.*, 2005; Sundström *et al.*, 2015). Primarily, atmospheric PM influence the Earth's climate by altering the solar radiative budget, by means of direct- or indirect radiative forcing (Deguillaume *et al.*, 2005; Venter *et al*., 2015). Scattering and absorption of solar radiation is known as direct radiative forcing. Furthermore, scattering and/or reflection of solar radiation cause a decrease of Earth's temperature (negative forcing). Whereas absorption of radiation causes an increase of Earth's temperature (positive forcing). Indirect radiative forcing results when PM act as CCN. Indirect radiative forcing of PM may govern certain optical properties of the atmosphere as well as

cloud lifetime (Monks *et al.*, 2009; Pacyna & Pacyna, 2001; Venter, 2015). For example, an increase in CCN result in bigger brighter clouds due to an increase of small cloud droplets. Consequently, short wavelength radiation is reflected to the atmosphere resulting in a decrease of Earth's temperature (Davidson *et al.*, 2005; Deguillaume *et al.*, 2005).

2.3.2. Human health

During the 1970s and 1980s, a significant increase in cardiopulmonary disease and mortality was observed in the USA and UK. This was mainly attributed to the high concentration PM in the air (air pollution). Several studies have since also concluded that an indescribable link between human health and PM (especially PM-bound trace metals) exist (Chow, 1995; Harrison & Yin, 2000; Pope & Dockery, 2006). The influence of PM on human health mainly depend on particle size, shape and particle composition. Furthermore, particle properties such as physicochemical properties, toxicity, residence time in atmosphere, concentration, and solubility also play a vital role (Chow, 1995; Davidson *et al.*, 2005; Harrison & Yin, 2000; Vousta & Samara, 2002). It is important to note that both natural and anthropogenic sources are responsible for PM that may affect air quality and human health. However, Vousta & Samara (2002) refers to numerous studies that have found anthropogenic PM exist primarily as water-soluble forms – making elements more readily bioavailable. Furthermore, according to the Medical Research Council (Burden of Disease Research Unit), indoor PM more adversely affect human health than ambient PM. This does not come as a surprise, as people spend 87% of their day indoors and only 6% outside. Additionally, the Medical Research Council (Burden of Disease Research Unit) ranked ambient air pollution as the ninth and indoor air pollution as the third leading risks associated with the global burden of disease (Language *et al*., 2016; Onabowale & Owoade, 2015).

Coarse particles ($PM_{2.5-10}$) are inhaled into the upper respiratory tract. Which may lead to allergic reaction and/or sinus ailments. Ultra-fine and fine particles ($PM_{2.5}$) are considered to have a greater effect on human health than coarse particles. This notion is based on the potential of fine particles to penetrate deeper and settle into the respiratory system and/or alveolar regions, due to its small size (Harrison & Yin, 2000; Pope & Docker, 2006; Vousta & Samara, 2002; Watson *et al.*, 2010; Woo *et al.*, 2001) In fact, Harrison & Yin (2000) states that the harmfulness of particles increase with decreasing size – consequently ultra-fine particles are deemed most harmful. Ultra-fine and/or fine particles are generally associated with severe cardiovascular and pulmonary damage. Or in severe cases, death. Furthermore, particles are also able to penetrate through cell membranes – affecting important organs such as the brain (Watson *et al.*, 2010).

PM-bound trace metals, especially transition metals such as Cr, Cu, Mn, Ni, Zn are known to have a significant influence on human health and are commonly associated with increased toxicity (Harrison & Yin, 2000; Liu *et al*., 2017; Rasmussen, 2007). Although trace metals consist of numerous elements that are each distinguished by their own set of characteristics, these metals are commonly characterised as redox-active in biological systems. Consequently, trace metals in PM, e.g. Fe or Cu, induce or catalyse chemical change resulting in free radical such as the hydroxyl radical. These radicals are known to cause inflammation of human tissue (Harrison & Yin, 2000). According, to the International Agency for Research on Cancer (IARC, 2012) as stated by Okuda *et al.* (2013) several metals/metal-compounds such as As, Be, Cd, Cr^{6+}, and Ni are considered carcinogenic to humans.

2.4. Measurement of atmospheric particulate matter

In 1885 the first attempt to measure the mass of PM in the atmosphere was made by drawing air through a filter paper. Prior to 1885, the degree of pollution was primarily only noticed by its effect on human health (irritation of nose and/or throat) or its influence on the surrounding environment (degradation of visibility). However, great advances have been made in the development of analytical techniques used for the quantification of PM (Chow *et al.,* 1995). Today, multiple techniques (both online and off-line) are available for the multi-elemental quantification of low concentration atmospheric PM samples (Alfarra, 2004; Booyens, 2018; Feldmann *et al*., 2009; McMurry, 2000). It is important however, to acknowledge that none of these instruments are without limitations.

2.4.1. Online analytical techniques

Online techniques continuously measure the real-time PM concentration in the atmosphere. Allowing for time- and environmental (temperature and humidity) relevant data capturing. Online techniques also minimise potential of artefact contamination and sample loss (volatilisation) which are generally associated with off-line analytical techniques. It is without surprise that several sources have deemed online techniques the greatest advancement made in the development of analytical techniques in the past 20 years. However, these instruments are generally expensive and require trained personnel for operation and maintenance procedures (Alfarra, 2004; Booyens, 2018; McMurry 2000).

2.4.2. Offline analytical techniques

Sample collection for off-line technique is conducted independently from analysis. That is, samples are generally collected on some type of substrate (filter, foil or film) by instruments such as an impactor, sampling pump and denuder. Subsequently, samples are packaged, stored and transported to the laboratory that houses the preferred off-line technique. Sample collection and handling are perhaps the greatest disadvantage associated with off-line

techniques, as it significantly increases the potential of contamination (Alfarra, 2004; Booyens, 2018; McMurry, 2000). Several off-line analytical techniques are commercially available, such as atomic absorption (AA), scanning electron microscopy (SEM), gas chromatography (GC), X-ray fluorescence (XRF) and inductively coupled plasma mass spectroscopy (ICP-MS). Off-line techniques are more readily used as they are less expensive and more feasible than online methods (Alfarra, 2004; Booyens, 2018). In the subsequent sections the basic principles of the two most commonly used techniques, i.e. inductively coupled plasma mass spectrometer (ICP-MS) and the wavelength-dispersive X-ray fluorescence (WD-XRF) are discussed, while the systematic biases, such as contamination and/or loss of target element, for each technique are also presented.

PM is commonly collected from the atmosphere by filtration, as it is easy and cost efficient. A variety of filter types are commercially available (Raynor *et* al., 2011). For atmospheric sample collection, filters such as cellulose fibre, quartz/glass fibre, membrane, and/or mixed fibre are used. However, there is no agreed upon filter that is considered the most appropriate for sample collection. Several studies have stated that the suitability of filters depends on the type of sample under consideration and the analytical technique it will subsequently be subjected to. Ideally the collection of PM should be conducted on multiple substrates to ensure accurate chemical characterisation of the sample. A few physical and chemical properties of filters have been identified that should be considered before selecting a type of filter material (Chow, 1995; Raynor *et al*., 2011). These properties include (Chow, 1995; Raynor *et al*., 2011; US-EPA, 1999)

(1) The mechanical and temperature stability of filter material. Filters that are divided should uphold its structural integrity as brittle filters will increase the potential of a negative bias in the gravimetric mass obtained.
(2) Chemical stability of filter material. In other words, the filter should not readily react with the sample particles collect on it, or react with gasses that are not of importance for a study.
(3) Low blank concentrations. When selecting a filter material, it is important to take into consideration its blank concentration. A high blank concentration will increase biases in the results obtained, compromising the data study.
(4) Sampling efficiency. 99% or more of the atmospheric PM drawn though the filter material should be collected on them regardless of the PM size and/or shape.
(5) Cost and obtainability. Filter material should be readily obtainable and at a reasonable price whilst still taking the sampling efficiency in to consideration.

For this study, mixed cellulose-ester membrane (MCE) filters were utilised for sample collection. As the name indicates, the filters are composed of mixed cellulose esters including cellulose nitrate and cellulose acetate. MCE-filters are characterised by a few advantages such as, easily dissolved (acid digestion) at a low temperature (70°C) for ICP-MS analysis, low blank weight, and obtainable at a relative low cost. However, MCE-filters also have multiple disadvantages including poor sampling efficiency due to high flow rate, high sensitivity to moisture, poor mechanical stability and are often considered fragile/brittle. Another significant disadvantage is MCE-filters not only collect PM on the surface but also allow PM to penetrate the filter. Primarily penetration of fine and/or ultra-fine PM occurs (Chow, 1995; US-EPA, 1999).

2.5. Inductively coupled plasma mass spectrometry

The (ICP-MS) system was developed in the early 1980's. ICP-MS is one of the most popular analytical techniques available today. It's massive popularity amongst scientists are mainly attributable to its rapid quantitative and/or qualitative multi-elemental analysis capability. Not to mention that currently ICP-MS systems have the lowest limit of detection (LOD) available for routine analytical chemistry with LODs of parts per billion (ppb) and parts per trillion (ppt) for the majority elements on the periodic table (see Figure 2.2) (Brown & Milton, 2005; Holler *et al*., 2007; Kgabi, 2006; Lachas *et al*., 1998; Thomas, 2004).

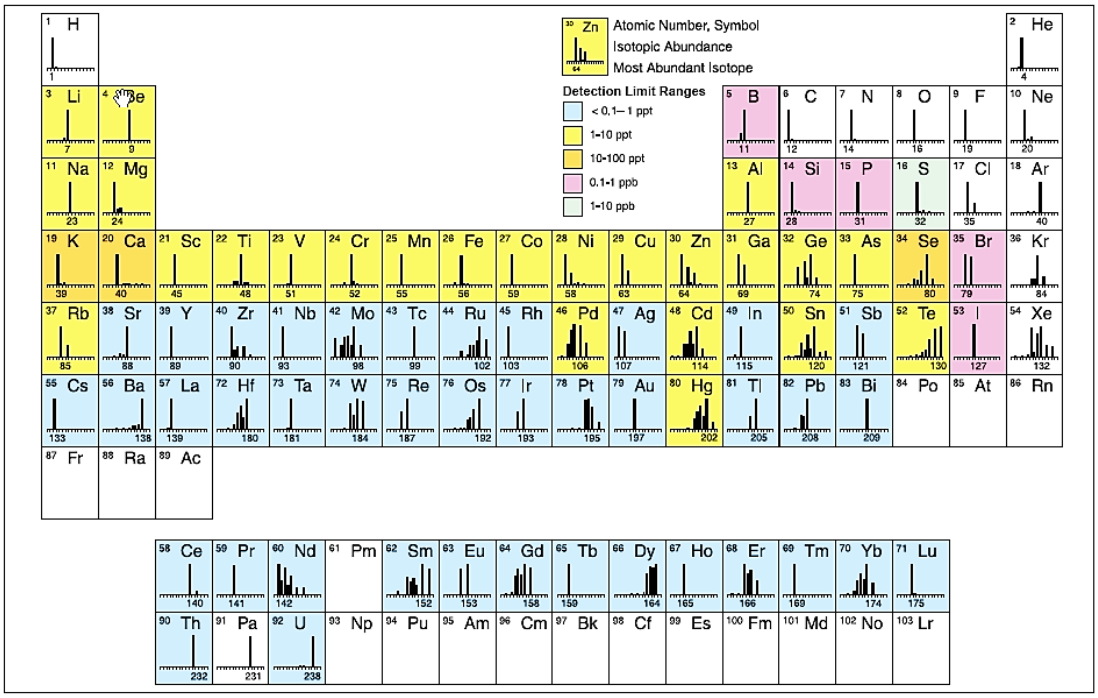

Figure 2.2: Limit of detection (LOD) capability for ICP-MS (Bazilio & Weinrich, 2012)

Figure 2.3 indicates the basic component within an ICP-MS system. Although all ICP-MS systems comprise of similar principle components, it is important to note that not all ICP-MS

systems are created equally. Meaning, different varieties of these components are commercially available (Thomas, 2004). In brief, the sample enters the system and is converted into a fine aerosol spray by means of pressurised Argon gas. In turn, the mass spectrometer separates ions according to a mass-to-charge ratio (m/z). ICP-MS systems are rather complex and consists of several different components (Thomas, 2004).

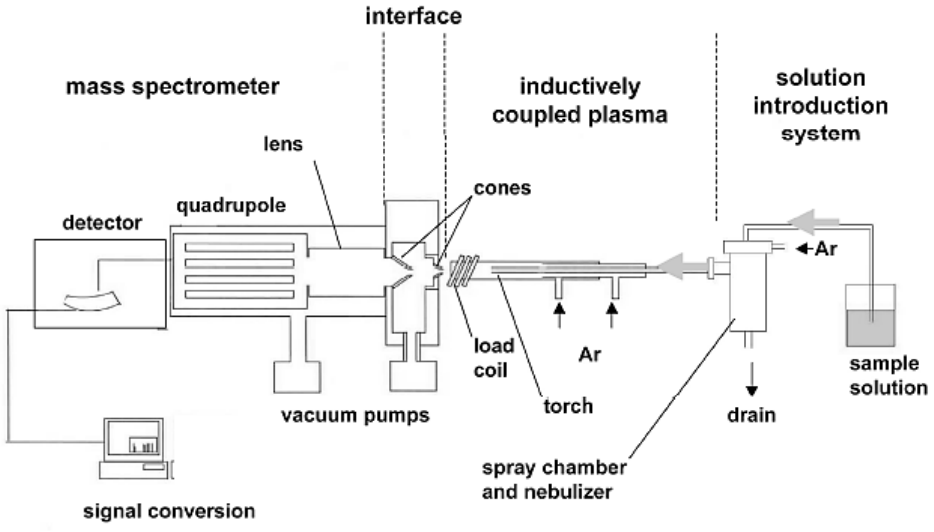

Figure 2.3: Schematic diagram illustrating the basic components of an ICP-MS system (Gilstrap, 2009)

In section 2.5.1. a comprehensive description will be given of the function of each component. As well as specific reference to components within the Agilent 7500ce ICP-MS system used for this study.

2.5.1. A comprehensive ICP-MS review

2.5.1.1. Sample introduction

The sample introduction component of an ICP-MS system is considered one of its greatest disadvantages. In fact, several studies refer to it as the *"Achilles heel"* of ICP-MS. Not only is approximately just 1-2% of the sample able to enter the system, but also ICP-MS systems were developed to primarily perform analysis on liquid samples. Consequently, samples other than liquids must be subjected to pre-analysis preparation, such as acid digestion as in this case study. This frequently leads to contamination and biases in resulting data. Fortunately, newer ICP-MS systems have been developed that allow for introduction of solid and/or slurry samples (Holler *et al.*, 2007; Thomas, 2004). The sample introduction system is comprised of two main components, i.e. the nebuliser and the spray chamber (Holler *et al.*, 2007; Kgabi, 2006; Thomas, 2004).

The nebuliser:

The liquid sample is generally introduced by means of a peristaltic pump(s). The Agilent 7500ce system consists of a ~~n of~~ 3-channel and 10 roller-pump, allowing constant computer-controlled pump/flow of sample regardless of difference in viscosity between samples. The pneumatic nebuliser is considered the most popular for ICP-MS. Several different pneumatic nebulisers are commercially available, including concentric-, micro concentric-, microflow-, and crossflow nebulisers (Bazilio & Weinrich, 2012; Kgabi, 2006; Thomas, 2004). The Agilent 7500ce system contains a concentric nebuliser – more specifically a MicroMist glass concentric nebuliser. The MicroMist glass concentric nebuliser introduces the sample into the? back of the? nebuliser. The sample flows through the inner capillary of the nebuliser. Argon gas enters the outer tubing of the nebuliser at 90° angle. Diameter of outer tubing decrease towards the end of the nebuliser, causing Argon gas to accelerate as it exits the nebuliser. Consequently, high-speed Argon gas disintegrates the liquid sample – resulting in formation of a fine aerosol (as indicated by Figure 2.4) (Thomas, 2004).

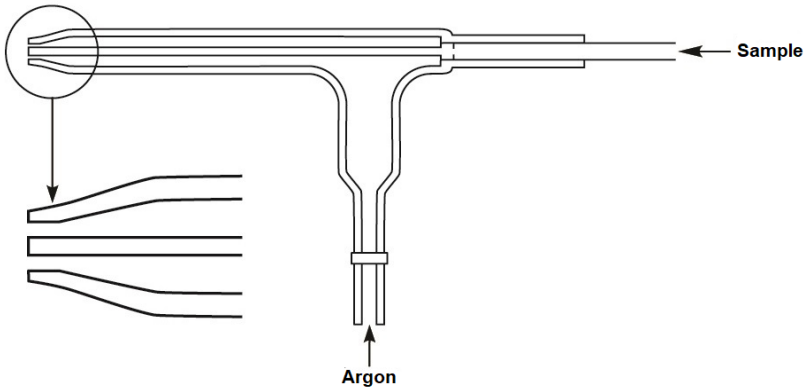

Figure 2.4: Schematic illustration of a concentric nebuliser (Thomas, 2004).

Popularity of the concentric nebuliser can be ascribed to its numerous advantages such as excellent sensitivity and stability, especially for “clean” samples. However, MicroMist glass concentric nebulisers frequently experience blockages due to its small orifices upon introduction of heavy matrix samples (Thomas, 2004).

The spray chamber:

The Agilent 7500ce ICP-MS systems contains a Quartz-Scott double pass spray chamber. As previously mentioned, the spray chamber is responsible for the removal of particles larger than 10µm from the created aerosol. The Quartz-Scott double pass spray chamber design achieves particle separation by guiding the aerosol into a central tube. The larger particles settle in the spray chamber due to gravity and are evacuated from the system by means of a drain tube.

Smaller particles present in aerosol are kept in suspension and are prevented from exiting the system by maintaining a positive pressure within the drain tube. Forcing the smaller particles between the outer wall of the spray chamber and central tube. Consequently, only the small particles are exposed to the plasma torch via a sample injector (Kgabi, 2006; Thomas, 2004).

2.5.1.2. Ion formation

The plasma torch:

The plasma in an ICP-MS system is one of the most vital components. The plasma is responsible for the formation of positively charged ions, which in turn is subjected to the mass spectrometer for detection and measurement of analytical concentration (Thomas, 2004). The formation of plasma in the ICP system is due to the interaction between a powerful magnetic field (formed by radio frequency passing through a copper coil) and Argon gas (flowing through a concentrical quartz tube, known as a torch). As a result, argon gas is ionised – forming a high temperature plasma when high voltage spark is applied (Bazilio & Weinrich, 2012; Thomas, 2004).

Ionisation of the sample:

Aerosol containing the fine particles derived from the spray chamber is accelerated through the sample injector into the base of the plasma (Thomas, 2004). It is important to note that the plasma is characterised by multiple heating zones as indicated by Figure 2.5.

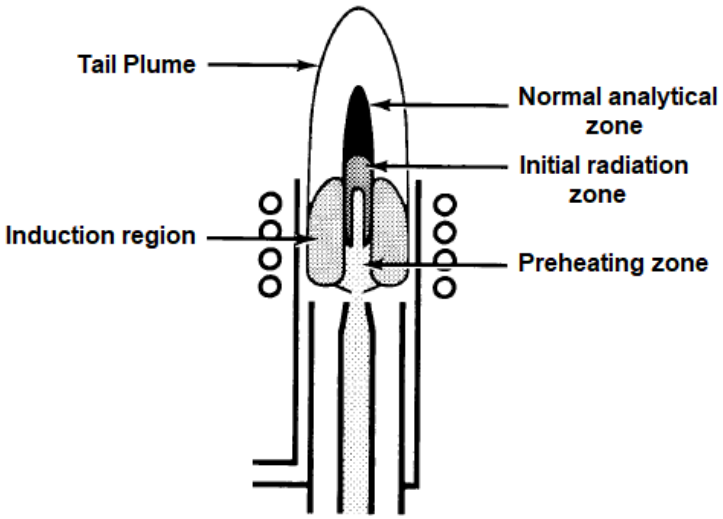

Figure 2.5: Heating zones of plasma (Boss & Fredeen, 2004)

Liquid sample (aerosol) is introduced to high temperature plasma. The sample proceeds through the different heating zones of the plasma and undergoes several phase conversions. Figure 2.6 illustrates the mechanisms of sample conversion during ionisation of sample (Boss & Fredeen, 2004; Thomas, 2004).

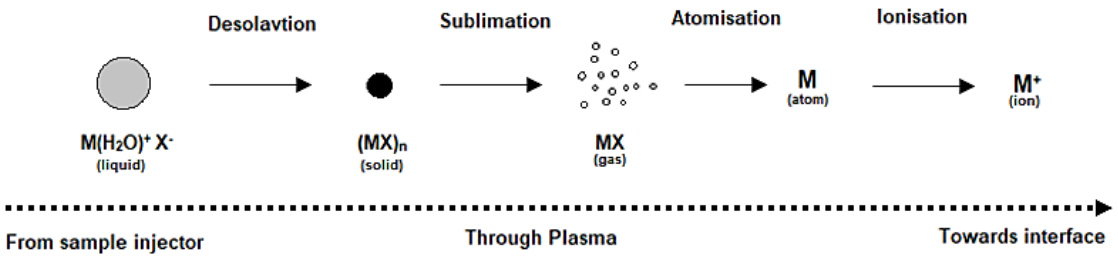

Figure 2.6: Conversion process of sample when introduced to plasma (ICP) source

Firstly, water molecules are removed from liquid sample (desolvation) – resulting in a small solid particle. Next, the solid particle is converted into a gas (sublimation) and then into ground state atoms of sample (atomisation). Finally, at the analytical zone (6 000 – 7000 K) sample is composed of its ground state atoms and protons (ionisation) – indicating the elemental composition of the sample (Bazilio & Weinrich, 2012; Boss & Fredeen, 2004; Thomas, 2004).

2.5.1.3. The interface region

The interface region can be described as the point where the protons emitted by ICP-torch enter the mass spectrometry region of an ICP-MS system. The interface region consists of two main components, i.e. the sampler cone and skimmer cone, which are kept at 1-2 Torr by a mechanical pump. The cones are generally made from nickel (as is for the Agilent 7500ce system) but may be constructed from more corrosive resistant materials such as platinum and/or sapphire (Bazilio & Weinrich, 2012; Thomas, 2004).

The primary function of the interface region is to direct the protons emitted from the plasma torch (760 Torr) towards the sampler cone subsequently the skimmer cone and finally into the heart of the ICP-MS system – the mass spectrometer (10^{-6} Torr) whilst maintaining the electrical integrity of protons. This proceeding may seem fairly simple, however, according to Thomas (2004) the interface region posed as the greatest obstacle during the development of the ICP-MS system due to the unkept electrical integrity of protons. This was mainly attributable to the unwanted secondary electrical discharge (pinch effect) between the plasma and sampler cone. Consequently, an increase in doubly charged interfering species were observed, giving rise to spectral interferences. As well as significant changes in the kinetic energy of the protons directed towards the mass spectrometer. Making the optimisation of ion optics difficult. Fortunately, today there are several different resolutions available to eliminate the pinch effect, e.g. grounding of the induction coil to prevent potential voltage difference (Bazilio & Weinrich, 2012; Thomas, 2004).

2.5.1.4. Ion optics

The ion optics component is situated between the skimmer cone (interface region) and mass spectrometer. Ion optics consist of one or multiple electrostatically controlled metallic cones at a pressure of approximate 10^{-3} Torr (Thomas, 2004). The primary task of the ion optic component is the removal of protons from the plasma and subsequently, to direct the retrieved protons into the mass spectrometer. Secondly, the ion optic component is responsible for preventing unwanted species (solid particles, neutrons, and photons) from entering the mass spectrometer. These species promote signal instability and an increase of background noise, which have an adverse effect on the efficiency and performance of ICP-MS system (Thomas, 2004). A proprietary off-axis Omega lens is utilised in the Agilent 7500ce system to prevent solid particles, neutrons, and photons from interacting with the mass spectrometer.

2.5.1.5. The mass spectrometer

The heart of the ICP-MS system – the mass spectrometer. The mass spectrometer is responsible for the separation of ions according to their mass-to-charge (m/z) ratio. Multiple mass spectrometers are commercially available, including the quadrupole-, the time-of-flight- and the double-focussing mass spectrometer (Holler *et al.*, 2007; Thomas, 2004).

Quadrupole Mass Analyser:

The most common mass separation devices used in ICP-MS systems, as well as in the Agilent 7500ce system, is the quadrupole mass analyser. Popularity of the quadrupole mass analyser can be ascribed to it being more compact, rugged, and cheaper than the other mass analysers available (Bazilio & Weinrich, 2012; Thomas, 2004). The quadrupole mass analyser consists of four cylindrical or hyperbolic rods of same length and diameter that act as electrodes (see Figure 2.7).

Opposite rods are connected electrically. A direct current field (DC) and a time-dependent alternating current field (AC) is applied to a pair of rods. By governing the AC/DC ratio on each pair determines the mass-to-charge (m/z) ratio of ions allowed to accelerate through the rods. Ions of different m/z ration are removed from quadrupole (Bazilio & Weinrich, 2012; Holler *et al.*, 2007; Thomas, 2004). Subsequently, ions of the selected m/z ratio emerging from quadrupole are converted into electrical pulse by the detector – delivering the mass spectrum. The process is repeated as the ac and dc voltages on rods are increased whilst upholding a constant ac/dc ratio – determining the next m/z ratio of ions to be analysed (Holler *et al.*, 2007; Thomas, 2004).

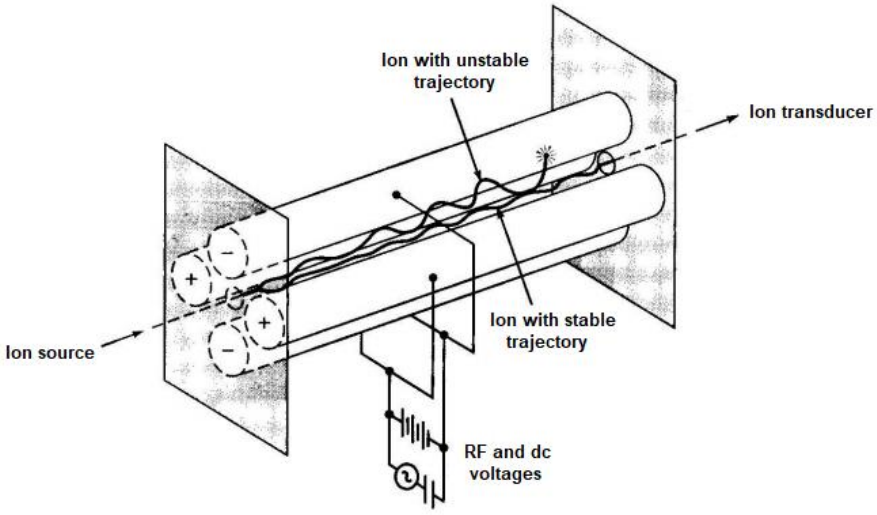

Figure 2.7: Schematic illustration of a quadrupole mass analyser (Holler et al., 2007)

2.5.1.6. The detector: dual-mode discrete dynode electron multiplier

The detector of the mass spectrometer is responsible for the conversion of the ions emitted by the quadrupole mass analyser into an electrical pulse. In turn, the electrical pulse represents the number of analyte ions present in the sample, which is used for the quantitation of elemental concentration by comparing the electric signal with calibration standards. It is also important to note that the detector greatly influences the low detection limits which? ICP-MS systems are well-known for (Thomas, 2004). The Agilent 7500ce system consists of a simultaneous dual-mode discrete dynode detector. Detectors are generally off-axis to decrease potential background noise and/or interferences due to unwanted species emitted from ions. As an ion emerges from quadrupole it is directed towards a set of dynodes. The ion then strikes the first dynode, electrons are released. The resulting electrons are then attracted and accelerated to the next dynode with electrons being released upon each strike. This process is repeated at each dynode resulting in multiplication of electrons. Finally, a stream of electrons is captured by multiplier collector or an anode (Thomas, 2004). With the ICP-MS system used in this study comprising of a dual-mode detector, the linear dynamic range increases from five to nine orders. Basically, the dual-mode detector allows for two scans (both high- and low concentrations) within one scanning process Not only does the dual-mode detector decrease sampling time, but also allows for maximum data collection on a single transient signal.

2.5.2. Acid digestion

As previously mentioned, although ICP-MS systems have recently been developed to allow for the introduction of solid and/or slurry samples, the majority of ICP-MS systems (like the one used for this study) still require the introduction of liquid samples. Therefore, solid samples (e.g. rocks) or samples comprising of solid particles are subjected to a decomposition procedure prior to the analysis. Ensuring the complete conversion of a solid sample to a liquid in which the analyte is dispersed evenly. Multiple methods are available for the decomposition of solid samples (ISO DINEN, 1972; Matusiewicz, 2016; Salcedo *et al*., 2014). Table 2.4 presents a summary of all the decomposition methods applied in this case study, as well as the different circumstances under which it can be conducted.

Table 2.4: Different digestion techniques available for the decomposition of samples.

Wet Chemical Decomposition (Acid Digestion)		
Digestion Technique	**Reagents**	**Application**
	Open Systems	
Conventional Heating	HNO_3, HCl, HF, H_2SO_4, $HClO_4$, H_2O_2	Inorganic/Organic
Microwave Heating	HNO_3, HCl, HF, H_2SO_4, $HClO_4$, H_2O_2	Inorganic/Organic
Ultraviolet Digestion	H_2o_2, $K_2S_2O_8$, HNO_3, O_3	Water/Slurries
Ultrasound Assisted Acid Digestion	H_2o_2, HNO_3	Inorganic

Acid digestion is not only one of the most popular methods used in current research but also one of the oldest methods. Acid digestion utilises mineral acids, such as hydrochloric- (HCl), nitric- (HNO_3), hydrofluoric- (HF), or sulphuric (H_2SO_4) acid for the complete dissolution of sample and matrix. Ideally, a mixture of an oxidising acid (HNO_3, hot conc. $HClO_4$, or hot conc. H_2SO_4) and a non-oxidising acid (HCl, HF, H_3PO_4, diluted $HClO_4$, or diluted H_2SO_4) is used (Bettilinelli *et* al., 1989; ISO DINEN, 1972; Matusiewicz, 2016; Swami *et al*., 2001). Furthermore, the digestion of samples are encouraged by subjecting the samples to a source of energy, such as heat or an increase of pressure by conducting the decomposition procedure in a closed vessel (Bettilinelli *et* al., 1989; ISO DINEN, 1972; Matusiewicz, 2016). For this case study, acid digestion in an open system (atmospheric pressure), with conventional heating was(were) applied for sample treatment.

Acid digestion in an open system is characterised by numerous advantages. It is inexpensive, allows for digestion of both organic- and inorganic sample matter as well as being a feasible and safe technique that does not require a specialised laboratory technician. However, it is also engrossed by well-known disadvantages – making this the most important and difficult

step to ensure accurate ICP-MS analysis due to the multiple errors it can produce. Two of the greatest disadvantages of an open acid digestion system is its potential ~~for~~ incomplete decomposition of the sample matter and the significant potential of contamination. Contamination potential can be decreased by adding a reflux condenser, as was done in this case study (ISO DINEN, 1972; Karanasiou *et* al., 2004; Matusiewicz, 2016; Swami *et al*., 2001).

Acid digestion of samples for ICP-MS analysis is probably the most important step for an accurate and reliable analysis. Several studies have indicated the importance of pH in relation to the solubility of inorganic samples. For instance, the solubility of trace metals such as Cd, Cu, Mn, Zn, and Fe increase with a decrease in pH. In neutral pH conditions, trace metals act stable and do not readily dissolve. As the pH increases, certain trace metals may once also indicate an increase, allowing for decomposition methods such as alkaline fusion. In addition, it was found that trace metals speciated in carbonate-, metal oxide-, silicate- and organic fractions are poorly soluble. Whereas absorbed trace metals and/or salts are more readily dissolved. Therefore, it is of great importance when choosing the reagents to conduct acid digestion. Table 2.5 indicates properties of the acids applied in this case study. These properties are important to consider as they determine the degree with which the dissolution of certain samples is successful (Deguillaume *et al.*, 2005; ISO DINEN, 1972).

Table 2.5: Properties of acids used for acid digestion

Nitric Acid (HNO_3)
Oxidising agent: $(CH_2)_n + 2HNO_3 \rightarrow CO_2 + 2NO + 2H_2O$
Boiling point: 122°C (HNO_3 65%)
Vapour pressure: ~25 bar at 225 °C
Doesn't form soluble nitrates with: Au, Pt, Al, B, Cr, Ti, Zr
Hydrochloric Acid (HCl)
Non-oxidising Acid
Boiling point: 84°C (HCl32%)
Vapour pressure of ~25 bar at 205°C
Forms insoluble chlorides with: Ag, Hg, Ti
Forms insoluble oxides with: Al, Be, Cr, Sb, Sn, Si, Ti, Zr

2.5.3. ICP-MS interferences

ICP-MS interferences are well-known and even characteristic to certain “problem elements”. Unfortunately, these interferences are brought forth by the very advantages (high sensitivity and rapid multi-elemental analysis) that makes the ICP-MS such a popular analytical technique. Luckily, recent development and optimisation of software as well as instrumental components minimise the negative effects of interferences (Evans & Giglio, 1993; Thomas, 2004).

ICP-MS interferences are categorised into two main groups, i.e. spectral- and matrix interferences (Evans & Giglio, 1993; Holler *et al.*, 2007; Thomas, 2004). The following sections will provide a brief description of why to expect these interferences as well as a few examples.

2.5.3.1. Spectral interferences

Polyatomic- and molecular spectral interference:

This type of spectral interference results from two or more atomic or molecular ions that have the same mass to charge (m/z) ratio. The formation of polyatomic or molecular ions are dependent on the plasma (Ar, H, O) nebuliser used, matrix components and elements present in the acid digestion applied (N, Cl, S, P), as well as elements present in the surrounding atmosphere (such as oxygen and/or nitrogen). Elements such as As, Cr, and Ni are extremely vulnerable to these interferences. Table 2.6 provides a more comprehensive list of the elements primarily inclined to allow polyatomic interference (Evan & Giglio, 1993; Thomas, 2004). Numerous elements are susceptible to polyatomic interference, therefore poly atomic interferences are generally subdivided into 4 main groups, including:

- Oxides: ArO^+, ClO^+, MO^+
- Hydroxides: $ArOH^+$, $ClOH^+$, MOH^+
- Hydrides: ArH^+, MH^+
- Argides: MAr^+

Table 2.6: Isotopes that commonly produce polyatomic interferences and the corresponding affected isotopes

Isotope	Affected Isotope
$^{18}H_2O^+$	^{18}O
$^{28}N^+$, $^{28}CO^+$	^{28}Si
$^{31}NOH^+$	^{31}P
$^{32}O_2^+$	^{32}S
$^{44}N_2O^+$, $^{44}CO_2$	^{44}Ca
$^{52}ArC^+$	^{52}Cr
$^{54}ArN^+$	^{54}Fe
$^{56}ArO^+$	^{56}Fe
$^{57}ArOH^+$	^{57}Fe
$^{68}ArCO^+$	^{68}Zn
$^{75}ArCl^+$	^{75}As
$^{76}Ar_2^+$	^{76}Se
$^{80}Ar_2^+$	^{80}Se
$^{103}ArCu^+$	^{103}Rh
$^{154}BaO^+$	^{154}Sm, ^{154}Gd
$^{155}BaOH^+$	^{155}Gd

Table 2.6 (continued): Isotopes that commonly produce polyatomic interferences and the corresponding affected isotopes

Isotope	Affected Isotope
$^{181}HoO^{+}$	^{181}Ta
$^{192}LuO^{+}$	^{192}Os, ^{192}Pt
$^{254}UO^{+}$	^{254}Es, ^{254}Cf
^{54}Fe	^{54}Cr; ^{54}ArN
^{56}Fe	^{56}ArO
^{57}Fe	$^{57}ArOH$
^{58}Fe	^{58}Ni
^{74}Se	^{74}Ge
^{76}Se	^{76}Ge, $^{76}Ar_2$
^{77}Se	$^{77}ArCl$
^{78}Se	^{78}Kr, $^{78}Ar_2$
^{80}Se	^{80}Kr, $^{80}Ar_2$
^{82}Se	^{82}Kr

A good and rather well-known example of polyatomic and molecular spectral interference is that of Argon (Ar). Ar is readily available as it is generally used as gas in ICP-MS systems. The most abundant isotope of Ar is $^{40}Ar^{+}$, which interferes with the signal of the most abundant Ca isotope – $^{40}Ca^{+}$. Resulting in a wrongly enlarged signal at the corresponding m/z ratio. Another example of Ar polyatomic and molecular spectral interference is when oxygen is introduced to system via aqueous sample. Ar easily binds with oxygen forming $^{40}Ar^{16}O^{+}$ with a mass at 56 amu – similar to that of Fe. Furthermore, Ar readily reacts with elements in an acidic matrix (acid digestion), such as chlorine. $^{40}Ar^{35}Cl^{+}$ (mass at 75 amu) is formed when $^{40}Ar^{+}$ binds with the most abundant isotope of chlorine, $^{35}Cl^{+}$. In turn, spectral overlaps occur between $^{40}Ar^{35}Cl^{+}$ and arsenic (mass at 75 amu) (Holler *et al.,* 2007; Thomas, 2004).

Oxides, hydroxides, hydrides & doubly charged species:

This spectral interference occurs when elements within sample bind with H^{+} (hydrides), $^{16}O^{+}$ (oxides), and $^{16}OH^{+}$ (hydroxides) present in air, plasma, or in aqueous sample self. According to Holler *et al.* (2007), oxides and hydroxides has the most serious spectral interference potential. The resulting hydrides, oxides, and hydroxides are analysed at respectively 1, 16, and 17 mass units higher than that of the element under consideration. Increasing potential of spectral overlap with isotopes of other elements with similar m/z ratios. This type of spectral interference is prominent for refractory elements, Mo, Ta, W, Re, Ti, V, Cr, Mn, Zr, Tc, Ru, and Rh, as well as rare earth elements (Thomas, 2004).

For an example of oxide interference, let us consider the 5 naturally occurring Ti isotopes. The Ti isotopes readily bind with available oxygen forming a MO^+ ion (oxides), with M being Ti. These oxides have m/z of 62, 63, 64, 65, 66, which overlaps with $^{62}Ni^+$, $^{63}Cu^+$, $^{64}Zn^+$, $^{65}Cu^+$, and $^{66}Zn^+$. This allows for a decrease in the reliability of the analytical technique (Holler *et al*., 2007).

Doubly charged species (M^{2+}), on the other hand, are generally produced by elements with low second ionisation potential (e.g. Ba, alkaline earth elements, and rare earth elements). The formation of doubly charged species allows for a decrease in the analytical techniques' sensitivity of the corresponding singly charges ion. In addition, doubly charges species are known to result in an isotopic overlap at half the m/z ratio of the parent isotope. Table 2.7 provides a list of the major elements vulnerable to produce doubly charged species as well as the isotopes that are affected by these species.

Table 2.7: Doubly charged species (M^{2+}) that commonly produce spectral interferences and the corresponding affected isotopes

Isotope	Affected Isotope
$^{88}Sr^{2+}$	^{44}Ca
$^{138}Ba^{2+}$	^{69}Ga
$^{140}Ce^{2+}$	^{70}Ge
$^{154}Sm^{2+}$	^{77}Se
$^{170}Er^{2+}$	^{85}Rb
$^{176}Yb^{2+}$	^{88}Sr

Isobaric interference:

Lastly, another spectral interference can be attributed to the interference of isotopes from different elements with the same m/z ratio. The majority of elements consist of more than one isotope that is free from isobaric interference. However, isobaric overlap primarily occurs at the most abundant and therefore the most practical isotope (Holler *et al*., 2007; Thomas, 2004). For instance, in a chloride matrix (acid digestion) $^{16}O^{35}Cl$ is available. Vanadium, which is characterised by two isotopes, i.e. ^{50}V and ^{51}V with a relative abundance of ~0.25% and ~99.75% respectively. It is clear that ^{51}V is the sensible isotope to consider. However, large isobaric interferences are measured at mass 51 amu due to $^{16}O^{35}Cl$ having a similar m/z ratio than ^{51}V. Therefore, ^{50}V is used, but not without its own limitations. ^{50}V in turn interferes with the isotopes of Ti and Cr (Evans & Giglio, 1993; Thomas, 2004). Another well-known example of isobaric interference is that of $^{58}Ni^+$ and $^{58}Fe^+$ (Holler *et al.*, 2007; Rüdel *et al.*, 2011). Table 2.8 provides a list of elements (or isotopes) generally susceptible to isobaric interferences.

Table 2.8: Isotopes that commonly produce isobaric interferences and the corresponding affected isotopes

Isotope	Isobaric Interference
^{36}S	^{36}Ar
^{40}K	^{40}Ar, ^{40}Ca
^{50}V	^{50}Ti, ^{50}Cr
^{64}Ni	^{64}Zn
^{84}Sr	^{84}Kr
^{92}Zr	^{92}Mo
^{113}In	^{113}Cd
^{115}In	^{115}Sn
^{124}Te	^{124}Sn; ^{124}Xe
^{148}Nd	^{148}Sm
^{160}Gd	^{160}Dy
^{176}Lu	^{176}Yb, ^{176}Hf
^{196}Pt	^{196}Hg
^{204}Pb	^{204}Hg

2.5.3.2. Matrix Interference

Unlike spectral interferences where the interference is due to another element with the same m/z ratio. A matrix interference (also known as a non-spectroscopic interference) is primarily due to dissolved salts in the sample. The nature and concentration of the matrix is greatly responsible for the degree of interference. This type of interferences can be characterised as either signal drift or signal suppression/enhancement (Evans & Giglio, 1993). Signal drift occurs when the dissolved salts in a sample deposit on and in turn clog the orifices of the sampling and skimmer cones. Resulting in poor ion flow into the mass spectrometer region and subsequently a considerable signal drift (Evans & Giglio, 1993). Signal suppressions/enhancements occur due to high concentration dissolved salts in the sample matrix. This type of matrix effect is not understood as well as signal drift in ICP-MS systems, with several conflicting studies about the mechanisms responsible for signal suppression/enhancement. For further reading, Olivares & Houk (1986) presents a comprehensive study about the effect of five dissolved salts on the analyte signal of cobalt (Co) and chromium (Cr) solutions, as well as the responsible mechanisms. Another study worth mentioning is Evan & Gilio (1993) in which ICP-MS interferences are comprehensively discussed, including signal enhancements and/or suppressions. In brief, they concluded that suppression of signal is affected by several factors, including: (1) the ionisation potential of elements from dissolved salt, (2) transport efficiency of solution with high concentration dissolved salts that clog orifices, (3) the prevailing sampling conditions in mass-spectrometer region and (4) the condition of plasma (Evans & Giglio, 1993; Olivares & Houk, 1986).

Space-charge induced matrix interference:

Multiple studies have recorded an increase in signal suppression with a decrease in atomic mass of an ion. This is mainly attributable to an excess of protons that repel each other within the ion beam. Resulting in poor ion transmission through the interface region and space-charge induced flow. That is, heavier elements with higher kinetic energy consists of higher transmission through ion optics. Whereas lighter elements with lower kinetic energy are more susceptible to the space-charge effect and in turn repelled from the central ion beam. Consequently, the transmission of lighter elements is poor and therefore less efficiently analysed (Thomas, 2004).

2.6. X-ray fluorescence

In 1895 Wilhelm Röntgen first discovered X-rays and by the early 1950's the first fluorescence technique became commercially available. X-ray fluorescence (also known as X-ray emission spectroscopy) is a widely applied technique in multiple industries for multi-elemental analysis of inorganic substances. The popularity of XRF can be ascribed to the significant amount of advantages it has including being a non-destructive technique, minimal sample preparation, quantitative- and qualitative analysis, short sampling period and low detection limits of ppm. XRF systems can be characterised as either energy-dispersive (ED-XRF) or wavelength-dispersive (WD-XRF), depending on how the spectra is resolved (Holler *et al.*, 2007; Tuisku, 2018). For this study, WD-XRF was applied, more specifically a PANanalytical Axios^{mAX} (sequential) WD-XRF system. A brief description of the workings of the XRF-spectrometer will be given, followed by a more comprehensive review of each individual component illustrated in Figure 2.8.

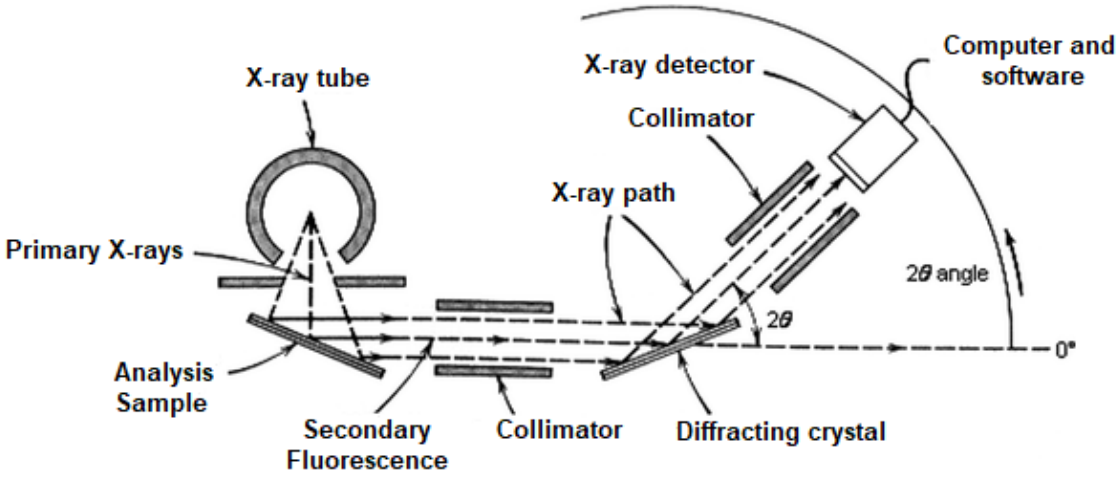

Figure 2.8: Schematic illustration of the basic components of WD-XRF system (Klein & Dutrow, 2007)

A sample is introduced to high intensity X-ray radiation generated by an X-ray tube. These X-rays are commonly called incident- or primary X-rays. The primary X-rays are absorbed by a sample according to Beer's law (see equation 2.1):

$$log\frac{I_0}{I} = K_d\Delta d \quad (2.1)$$

where I_0 is the intensity of the primary X-rays emitted by the X-ray tube, I is defined as the intensity of X-rays not absorbed by the sample, K_d is the proportionality constant, and Δd is indicates the thickness of sample.

As primary X-rays strike the sample, electron(s) of the sample is excited and removed from the most inner-electron shell(s) (K- L- M shells), resulting in a vacant orbital and consequently an unstable intermediate ion as indicated by Figure 2.9 (Holler *et al.*, 2004; Klein & Dutrow, 2007; Tuisku, 2018). It is important to note that the minimum primary X-ray energy required for the sufficient excitation of electrons is determined by the atomic number of an element. More specifically, an increase of an elements' atomic number requires an increase of primary X-ray energy. Furthermore, the primary X-ray energy should be equal or greater than the binding energy of the electrons. Binding energies are characteristic for each element. Hence, the energy of primary X-rays is also characteristic for an element (Holler *et al*., 2007; Schlotz & Uhlig, 2006; Tuisku, 2018).

In turn, an electron(s) from a higher energy-level (next outer shell) fill the vacant orbital(s). The energy released due to the electron transition from a higher- to lower energy-level is known as X-ray fluorescence or secondary X-rays which is characteristic to each element (Holler *et al*, 2007; Klein & Dutrow, 2007). This concept is perfectly illustrated by Figure 2.9. Furthermore, secondary (X-ray fluorescence) produce an emission spectrum containing groupings of K-, L-, and M spectral lines according to pattern in which outer electrons settled into lower energy orbitals. These spectral lines are ascribed to a? specific element based on wavelength (Klein & Dutrow, 2007).

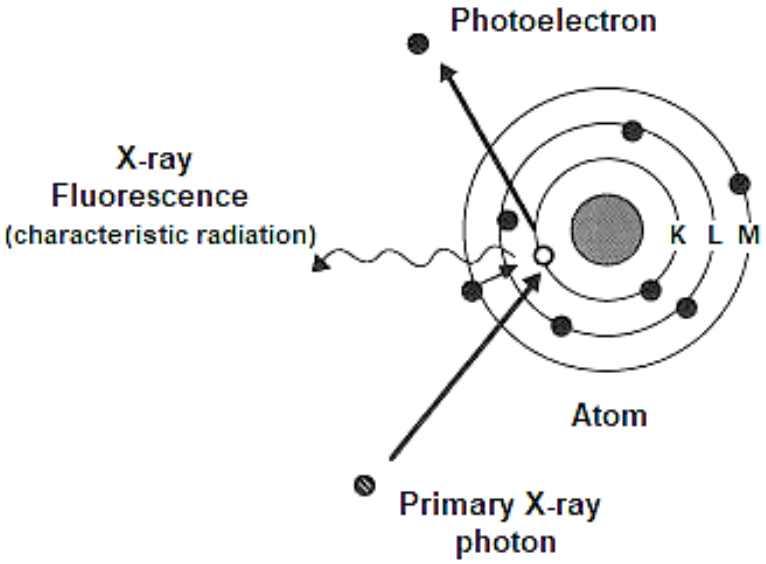

Figure 2.9: Emission of X-ray fluorescence

The detection system of a WD-XRF spectrometer includes a set of collimators, a diffraction crystal, and an X-ray detector. The secondary X-rays emitted from the sample is focused on the diffracting crystal by means of the collimators. In turn, the crystal diffracts the incoming X-rays into corresponding wavelengths (Brouwer, 2010; Schlotz & Uhlig, 2006). The detector and signal processor (an electronic counting device) records the diffracted X-rays and produce a visual display (Holler *et al*. 2007; Tuisku, 2018).

2.6.1. A comprehensive XRF review

As mentioned, this study applied the PANalytical Axios^{mAX} (sequential) WD-XRF system. A schematic illustration of the basic components in a WD-XRF system is presented in Figure 2.9. As with the ICP-MS system, a more comprehensive discussion for each will be given in the following sections

2.6.1.1. The X-ray tube

Firstly, we will consider the source of primary X-rays – namely the X-ray tube. The X-ray tube is responsible for providing a stable, high intensity X-ray beam with a wide range of energies to ensure efficient excitation of all elements under consideration (Brouwer, 2010; Holler *et al.*, 2007*;* Tuisku, 2018). Although there are multiple and different types of X-ray tubes commercially available, all function on the same fundamental principle. The most common X-ray tube, which is also operational in the a PANalytical Axios^{mAX} (sequential) WD-XRF system, is the end-window type (Brouwer, 2010; Tuisku, 2018). The basic design of an end-type X-ray tube is illustrated in Figure 2.10.

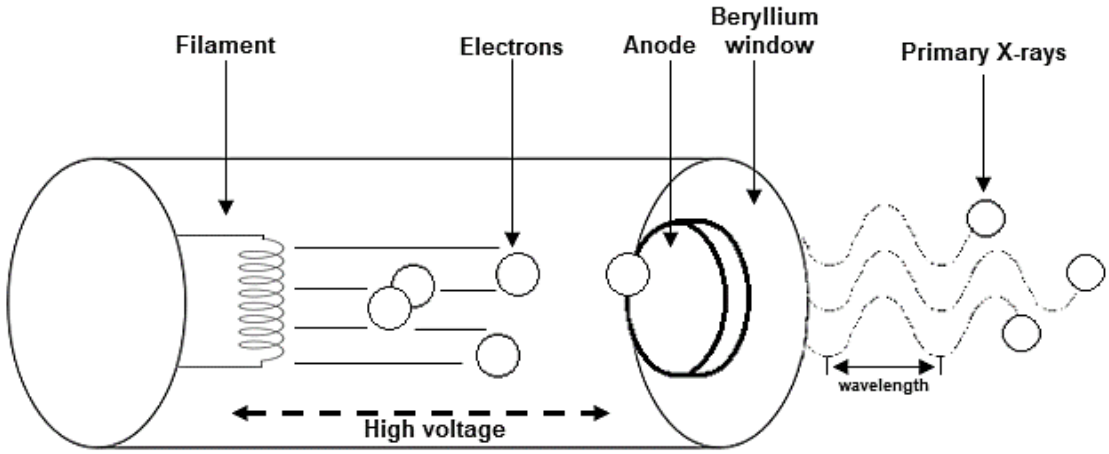

Figure 2.10: Schematic diagram of an end-type X-ray tube (Brouwer, 2010)

This design consists of an annular tungsten filament (negative potential cathode) set to zero voltage; and a large target (positive potential anode) inside a vacuum (Brouwer, 2010; Schlotz & Uhlig, 2006; Tuisku, 2018). Generally, the anode is made from copper with a metal target on its surface or embedded in it. The target metal can be made from numerous metals such as tungsten, chromium, silver, iron, rhodium and cobalt.

For this case, the metal target is comprised of rhodium (Holler *et al*., 2007). Rhodium is the most popular metal used for the target as it allows effective excitation for the majority of elements with atomic number between 4 (Be) and 92 (U) (Tuisku, 2018). A high voltage direct current is applied on the filament, causing a negative potential and subsequently allows for the emission of electrons. An increase of potential difference between the filament (negative) and target (positive) allows electrons to accelerate towards the anode. However, the electrons decelerate once it strikes the anode, losing 1-2% of their (its) energy. Resulting in the emission of the primary X-rays. The primary X-rays exit the tube through a beryllium (Be) window situated at the front of the X-ray tube housing as indicated in Figure 2.11 and move towards the sample (Brouwer, 2010; Schlotz & Uhlig, 2006; Tuisku, 2018).

2.6.1.2. Scattering of primary radiation

The X-ray tube generates primary X-rays characterised by the entire range of energy required for multi-elemental analysis. This energy spectrum is referred to as the Bremsspectrum. As mentioned previously, when the primary X-rays interact with sample matter secondary X-rays (X-ray fluorescence) are generated. However, it is important to note that partial scattering of primary X-ray energy (Bremsspectrum) may also occur (see Figure 2.11).

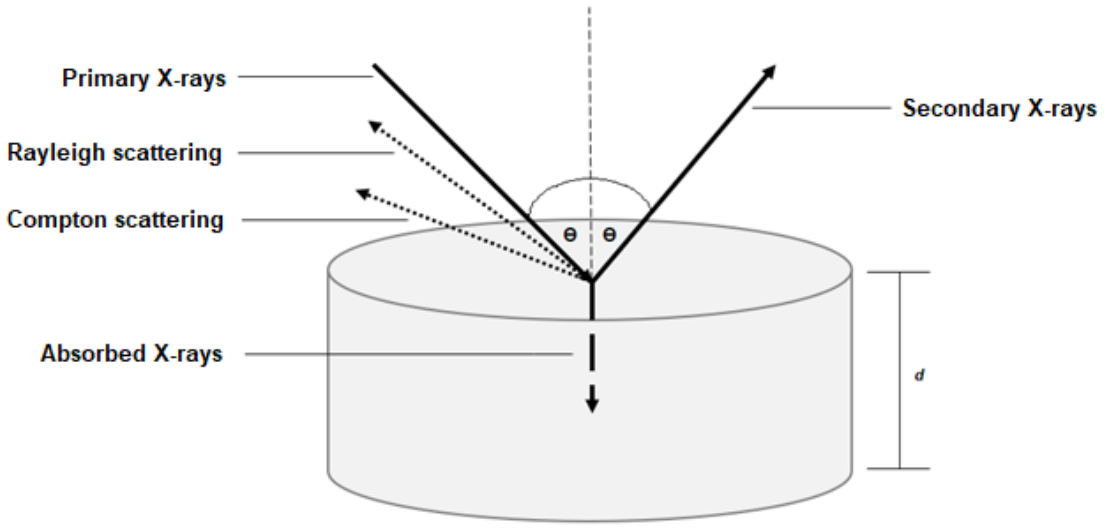

Figure 2.11: Interaction of X-ray radiation with sample matter (Brouwer, 2010)

Scattering of primary X-ray generate spectral lines that are characteristic to the anode material and not only to the sample material. Detection of such scattered primary X-rays is recognised as background radiation. Background radiation can be attributed to two types of scattering, namely Rayleigh- and Compton scattering (Brouwerr, 2010; Schlotz & Uhlig, 2006; Tuisku, 2018).

Rayleigh scattering (elastic scattering) occurs when the primary X-rays interact with strongly bound electrons of the sample. The energy of the X-rays are insufficient to remove an electron from its orbital, but enough to allow an electron to vibrate at same frequency as the primary X-rays. Furthermore, the vibrating electron discharges an energy similar to that of the primary X-ray, giving the impression that the primary X-rays are scattered by atoms (Brouwer, 2010). Therefore, Rayleigh scattering is recognised as the direct scattering of primary X-ray from sample to the detector without loss of any energy (Schlotz & Uhlig, 2006; Tuisku, 2018).

In contrast, Compton scattering (inelastic scattering) occurs when primary X-rays lose energy due to interaction with the electrons of the sample matter (Schlotz & Uhlig, 2006; Tuisku, 2018). The scattering potential vary for different samples and primarily depends on the thickness (*d*) of the sample as well as the sample matrix. Compton scattering more readily occurs with samples containing light elements. Rayleigh scattering, on the other hand, occurs to a lesser degree for light elements that consists of more loosely bound electrons and to a higher degree for heavy elements (Brouwer, 2010).

2.6.1.3. The collimator

As previously mentioned, secondary X-rays are emitted when primary X-rays strike the sample. These secondary X-rays are scattered in every direction. The collimator is responsible

to deliver these secondary X-rays in a consistent and orderly fashion to the diffraction crystal and X-ray detector as indicated in Figure 2.9. The collimator together with the diffraction crystal is accountable(responsible?) for the optic sensitivity and resolution of the WD-XRF system (Tuisku, 2018). The collimators are comprised of parallel slits in sets of metal plates. Scattered secondary X-rays are directed through these slits in orderly fashion towards the diffraction crystal and X-ray detector. Logically, one can conclude that if spacing between slits are small, the less secondary X-rays are allowed through. Consequently, spacing between metal plates influence the sensitivity and resolution of the WD-XRF system (Tuisku, 2018).

2.6.1.4. The diffraction crystal

The diffraction crystal (also known as the analysing crystal) diffracts the polychromatic secondary X-ray beams emitted by the sample into the appropriate separate wavelengths according to Bragg's Law. Figure 2.12 illustrates the diffraction of X-rays by the crystal in WD-XRF systems according to Bragg's Law. Crystals consist of ordered three-dimensional structures with characteristic scattering units (i.e. atoms or molecules) evenly distributed along crystallographic axes. When electromagnetic radiation, such as X-ray radiation, collides with such an orderly structure, the radiation interacts with the electrons in the atomic structure of the sample. The electrons are triggered to "vibrate" at a frequency similar to that of the primary radiation (Holler *et al*., 2007; Klein & Dutrow, 2007; Schlotz & Uhlig, 2006).

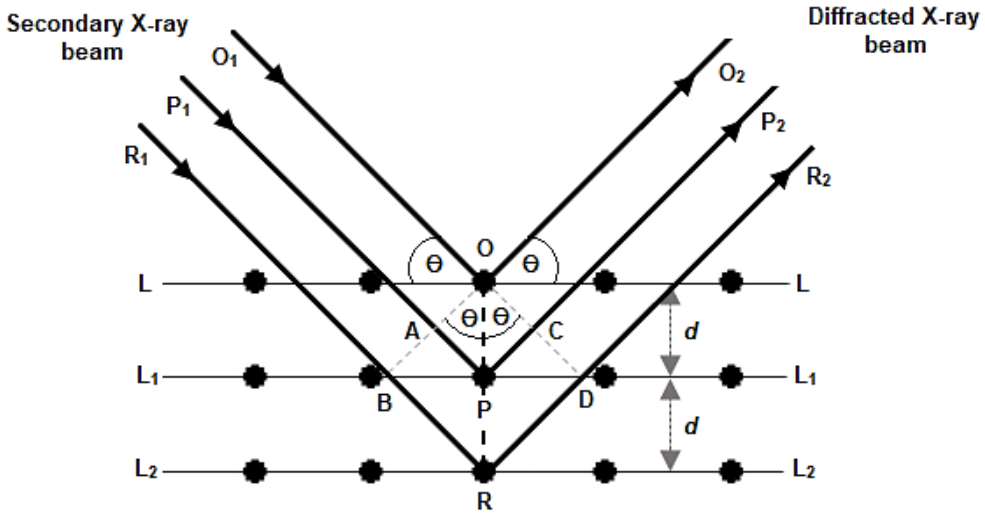

Figure 2.12: Diffraction of X-rays by a crystal according to Bragg's Law (Holler et al., 2007)

When the secondary X-rays strike the diffraction crystal at a certain angle (Θ), a fraction of the X-rays are scattered by the outer layer of atoms in the crystal lattice (L). Whereas the remaining fraction is absorbed by the vibrating electrons and allowed to penetrate deeper into the crystal surface to the first lattice plane (L_1). Almost an infinite number of lattice planes (n)

undergo the afore-mentioned penetration, absorption and scattering of primary radiation and are evenly spaced throughout the crystal structure (*d)*. Considering that each lattice plane contributes only a small fraction towards the total diffraction effect, it is vital that scattered radiation is in-phase to deliver a sufficient and quantifiable intensity. However, the path length of (P_1-P-P_2)-radiation is longer than the path length of (O_1-O-O_2)-radiation as indicated by Figure 2.13. If the scattered radiation, O-O_2 and P-P_2, is to be in-phase – the path difference must be equal to a whole multiple of the wavelength (*nλ*). Furthermore, as indicated by Figure 2.13, OA and OC are perpendicular to P_1-P and P-P_2. Thus, it is concluded that P_1-P = O_1-O = R_1-R and P-P_2 = O-O_2 = R-R_2. If scattered radiation is in-phase, PA + PC must be a multiple number of wavelengths. That is PA + PC = 2d sinϴ = nλ as ∆OPA, *d* sinϴ = PA and ∆OPC = *d* sinϴ = PC. This equation is known as Braggs equation (see equation 2.2):

$$n\lambda = 2d \sin\theta \tag{2.2}$$

where *n* is the reflection order, *λ* is defined as the radiation wavelength in nanometres (nm), *d* is the distance between crystal lattice planes (nm), and *ϴ* is ascribed to the diffractions angle (Klein & Dutrow, 2007; Schlotz & Uhlig, 2006; Tuisku, 2018). Multiple crystals are commercially available for diffraction in WD-XRF systems. However, selecting the appropriate crystal for multi-elemental analysis of both light- and heavy elements may be a difficult task. The ideal crystal for heavy element analysis is generally characterised by lattice planes close to each other (small *d*), whereas the ideal crystal for light elements are characterised by a larger distance between the crystal lattice Tuisku, 2018).

2.6.1.5. The X-ray detector

The purpose of the detector is to convert the energy of secondary X-rays into quantifiable voltage pulses. The pulse heights correspond with the energies of observed secondary X-rays. Furthermore, the resulting pulses are amplified and counted by an electronic counting device (signal processor) and displayed as an X-ray spectrum. Semi-quantitative/quantitative analysis are obtained by careful measurement of spectral peak heights for each element. The concentration of an element can be determined by equation 2.3:

$$P_x = P_s W_x \tag{2.3}$$

Where: (1) P_x is the line intensity of measured in counts per second (cps) of element under consideration, (2) P_s is defined as the the line intensity measures (cps) for an element/standard of known concentration, and (3) W_x is the weight fraction of the element under consideration.

X-ray detectors are set at an angle, which allows for the measurement of wavelengths diffracted in different directions by the diffraction crystal. In some systems, as with the one used for this case study, the detector is placed on a rotating goniometer. This allows the detector to move through a certain angular range, measuring several different wavelengths one after another. Systems that employ moving detectors are called sequential XRF-systems (Brouwer, 2010).

Three vital properties that asserts the WD-XRF system as such a robust and competitive analytical technique, depends on the detector, namely (Brouwer, 2010):

(1) sensitivity, which defines the efficiency with which X-rays are counted. Sensitivity is considered high if the ratio between the number of pulses against the number of incoming X-rays is high,

(2) resolution, which indicates the competence of the detector and signal processor to discriminate between different energy levels, and

(3) dispersion, which defines the capability of the detector to separate different energy X-rays. WD-XRF spectrometers mainly use gas-filled and scintillation detectors (Brouwer, 2010; Schlotz & Uhlig, 2006; Tuisku, 2018).

A scintillation detector:

Figure 2.13 is an illustration of the basic component within a scintillation detector. The four main components of the scintillation detector can be identified as a (1) Be window, (2) scintillator crystal, and a (3) photo multiplier tube consisting a (4) photo cathode (Brouwer, 2010).

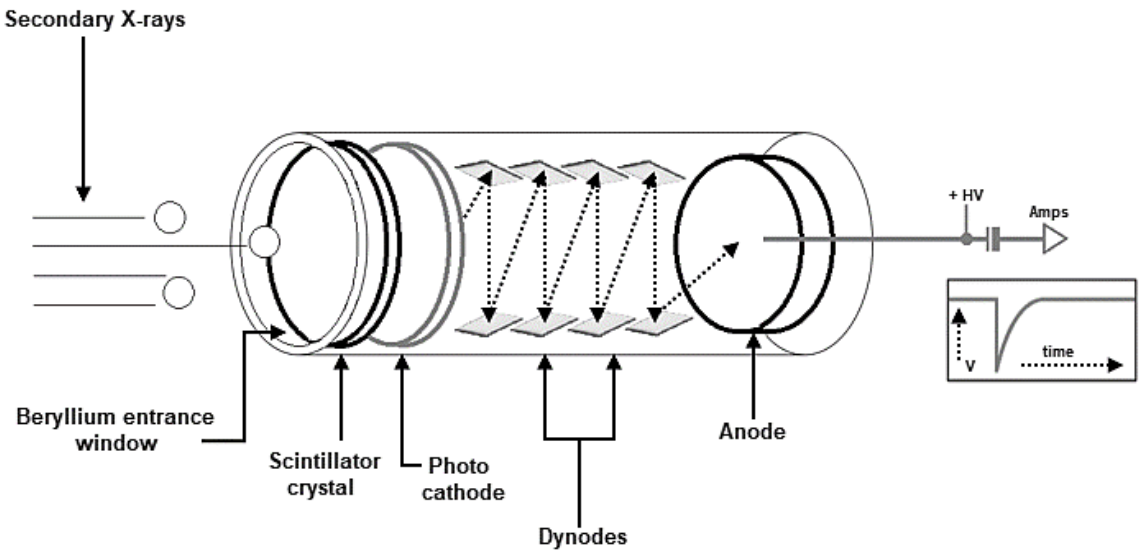

Figure 2.13: Basic illustration of a Scintillation detector (Brouwer, 2010)

The secondary X-rays are directed towards the detector from the diffraction crystal by means of collimators. In turn, the X-rays pass through the Be window of the detector and strike the scintillator crystal. The scintillator crystal is a sodium iodide crystal with thallium atoms evenly dispersed throughout the crystal lattice (NaI(Tl)). The high density of the scintillator crystal allows for the absorption of all secondary X-ray energies. This generates a light flash with the same energy as the absorbed secondary X-rays and the emission of light photons. These photons continue through a photomultiplier tube until striking the cathode and subsequently releasing a cloud of electrons. The electrons are accelerated through towards an anode by means of several dynodes as indicated in Figure 2.14. A negative voltage pulse is recorded as electrons strike the anode with the energy being directly proportional to the number of electrons. In turn the MCA counts the pulses generated by the detector (Brouwer, 2010; Schlotz & Uhlig, 2006).

A Gas-Filled (Flow) Detector:

As gas-filled detector can be described as a metal cylindrical cathode consisting of two main components, including (1) an anode (generally constructed from tungsten) with an applied voltage and (2) a thin Be entrance window (as indicated in Figure 2.14). Additionally, the cylinder is filled with an inert counting gas such as Ne, Ar, Kr, Xe or He. Loss of inert counting gas frequently occurs if the Be window is too thin. To compensate for this loss, detectors are often connected to a bottle of the inert gas so as to continuously replace gas that penetrates through the window. These detectors are referred to as flow detectors (Brouwer, 2010; Schlotz & Uhlig, 2006).

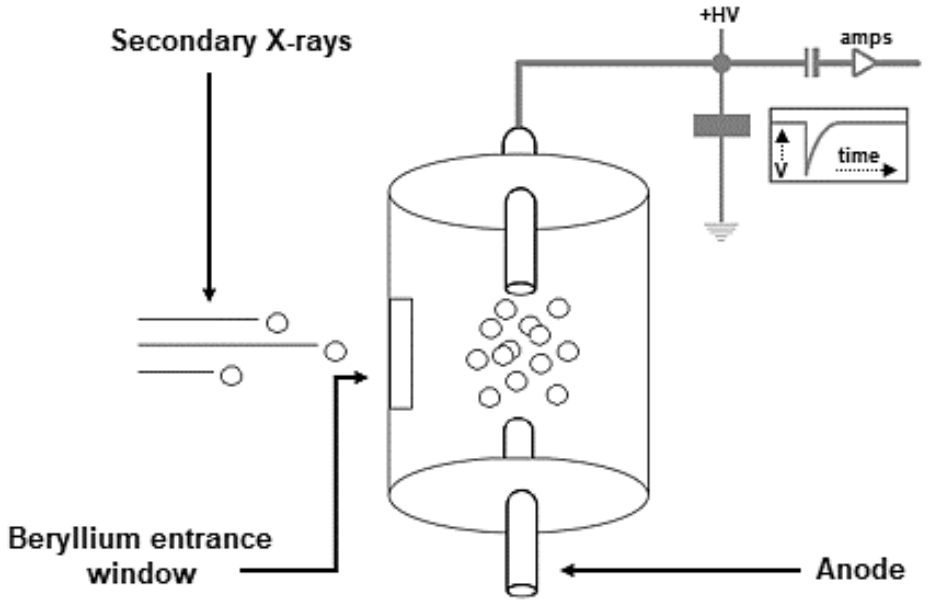

Figure 2.14: Basic illustration of a Gas-filled detector (Brouwer, 2010)

Secondary X-rays pass through the Be window into the gas-filled detector. In turn, the X-ray ionise the atoms and molecules of inert gas, resulting in the formation of protons and primary electrons. The protons move towards the cathode. Whereas, the emitted primary electrons accelerate towards the anode with voltage between 1300 V and 2000 V. The number of electron pairs that formed is equal to the energy of the secondary X-rays. Furthermore, gas amplification allows for the formation of secondary electrons. That is, the primary electrons experience an increase in voltage *en route* to the anode, providing them with sufficient energy to ionise additional gas atoms and molecules (Brouwer, 2010; Schlotz & Uhlig, 2006). According to Schlotz & Uhlig (2006), a single primary electron has the potential to generate 10 000 secondary electron pairs by means of gas amplification. This allows XRF-systems to accurately measure light elements such as Boron and/or Molybedenum. As with the scintillation detector, once the primary and secondary electrons reach the anode – a drop in voltage pulse is recorded. Allowing the signal processor to count the pulses generated by the detector (Brouwer, 2010).

2.6.2. WD-XRF spectrometer interferences

As previously mentioned, the net energy of the secondary X-rays that arrive at the detector is responsible for the signal recorded and therefore also responsible for the spectral line indicating the concentration of an element. However, it is important to note that the energy of secondary X-rays is influenced by the composition and mass absorption coefficient of the

matrix. Matrix interference can be divided into two categories, namely absorption effect and enhancement effect.

The absorption effect is mainly attributable to the presence of an element within the matrix that absorbs either the primary X-ray or the emitted secondary X-rays more strongly than the elements under consideration. Consequently, the concentration calculated by equation 2.3 can either be too high or too low due to absorption effect of matrix. That is, if an element in the matrix more readily absorbs the primary- or secondary X-rays, the weight fraction of the element under consideration will be underestimated as P_s is determined with a standard in which absorption was smaller. Whereas, if the element absorbed lees primary- or secondary X-rays, W_x will be overestimated as P_s determined for a standard is larger. Usually, absorption more readily occur for heavy elements (Brouwer, 2010; Holler *et al.*, 2007).

As indicated by its name, enhancement effects produce results of higher concentrations than what is expected for an element. This is attributable to the secondary excitation of an analytical line when the characteristic emission spectrum is excited by the primary X-ray beam or the secondary X-rays emitted by other elements. The degree of the enhancement effect depends on the element and its concentration (Brouwer, 2010; Holler *et al.*, 2007).

CHAPTER 3: DATA ACQUISITION & ANALYSIS METHODOLOGY

In this chapter the research design and methodologies applied to achieve the objectives set out in Chapter 1 are presented. Detailed descriptions of the sampling sites, sample collection methods, sample analytical procedures, as well as the statistical approaches applied are discussed.

3.1. Research design

In Figure 3.1 a flow diagram is presented, which outlines the general research design followed in order to achieve the objectives of this study. Particulate matter (PM) samples were collected on filters through two independent sampling campaigns conducted at two different sampling sites. 24-hour indoor particulate samples were collected during the one campaign, while weekly ambient aerosol samples were collected during the other sampling campaign. Detailed descriptions of these two sampling sites and sampling methodologies are presented in a subsequent section. All samples collected during these two sampling campaigns were initially subjected to wavelength-dispersive X-ray fluorescence (WD-XRF), after which inductively coupled plasma mass-spectrometry (ICP-MS) analysis of these samples were conducted. WD-XRF is a non-destructive analytical technique, while samples are destroyed during ICP-MS analysis. The trace metal concentrations which were determined with the two analytical methods were processed and subjected to statistical analysis in order to compare the concentrations of different trace metals determined with the WD-XRF and ICP-MS respectively.

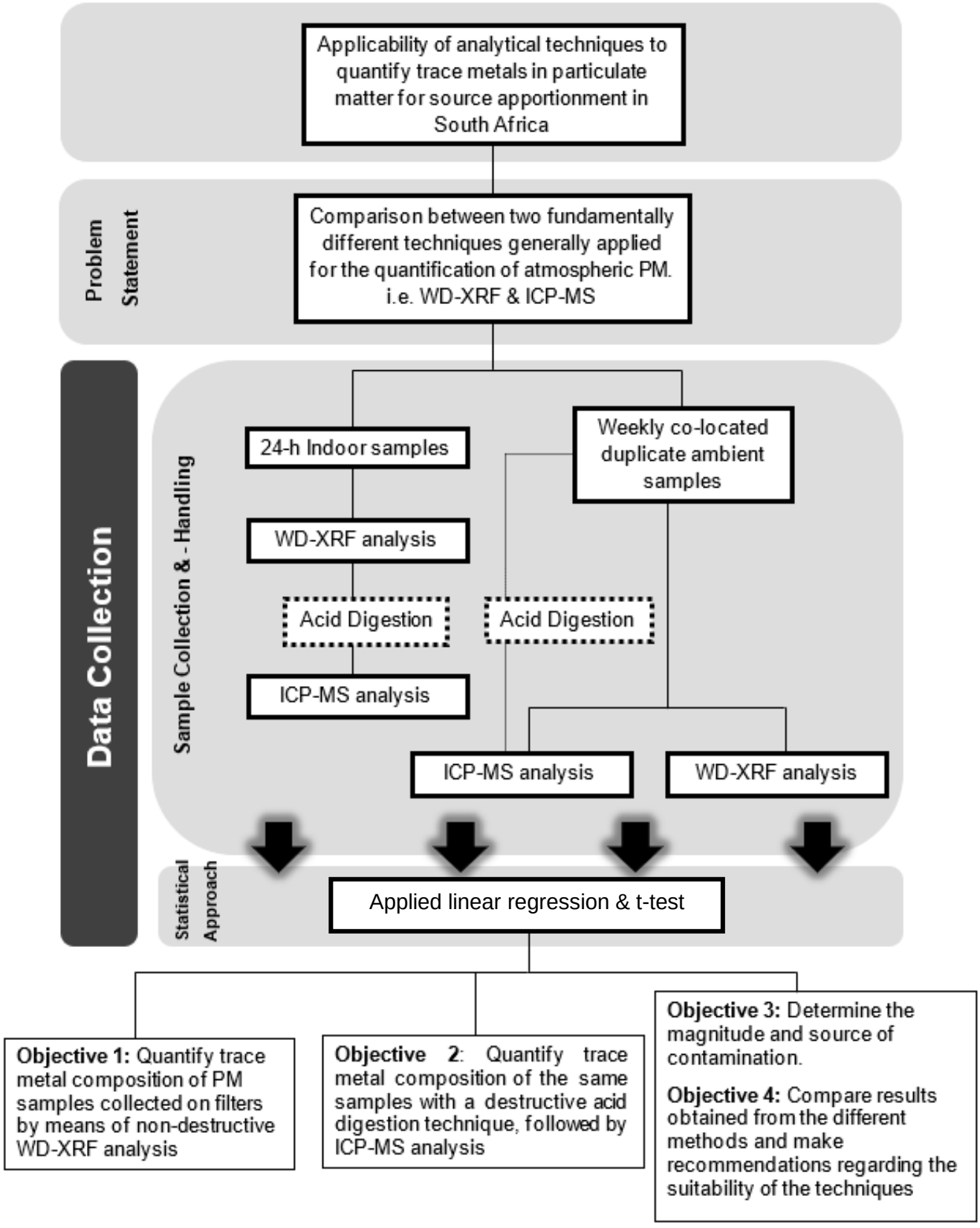

Figure 3.1: Conceptual flow-diagram outlining the research design of this case study

3.2. Sampling sites

3.2.1. Ambient samples: Welgegund monitoring station

3.2.1.1. Regional meteorology

Samples were collected at one of the most extensively equipped atmospheric measurement stations in South Africa – i.e. the Welgegund station (Beukes *et al.*, 2013; Venter *et al.*, 2017). The station is situated on a commercial farm (26°34′10″S, 26°56′21″E) in the North West province as indicated in Figure 3.2 (Booyens *et al.*, 2015; Booyens, 2018; Jaars *et al.*, 2014; Jaars *et al.*, 2016; Venter *et al.*, 2017).

Figure 3.2: Location of the Welgegund monitoring station with reference to South Africa and neighbouring countries

Welgegund is located within the South African Highveld region. The Highveld is characterised by two distinct seasons, i.e. the wet season and the dry season. The wet season generally prevails during summer (October to April) whereas the dry season coincide with winter (May to September). Another distinctive characteristic of the Highveld is the continental-high pressure cell (anti-cyclone) present over the interior of southern Africa during the dry season (winter). In turn the high-pressure cell promotes the development of definite inversion layers within the atmosphere. Consequently, vertical mixing of the atmosphere is restricted and/or weakened. Resulting in the increase of atmospheric PM concertation during winter as PM are

"trapped" between earth surface and inversion layers and/or different inversion layers in the atmosphere. During summer, however, the continental high-pressure cell moves in a southern direction allowing for easterly flow over South Africa. As the high-pressure cell weakens over the interior of southern Africa, the resulting inversion layers also weaken and are observable at greater height in the atmosphere. The low-pressure cell prevailing during summer allows for unstable meteorological conditions and free vertical mixing of atmosphere. In turn, allowing decrease in atmospheric PM concentration due to greater dispersal of PM (Booyens *et al*., 2015; Booyens, 2018; Jaars *et al.*, 2016; Laakso *et al.*, 2012).

3.2.1.2. Vegetation & geology

The Welgegund station is situated within a grassland biome. More specifically – the Vaal-Vet Sandy Grasslands, which covers the majority of the North West and Free State provinces. As mentioned, the station is located on a commercial farm, with activities including grazing of livestock (cattle) as well as cultivation of primarily maize and to a lesser degree sunflower (Jaars *et al.*, 2016; Vakkari *et al.*, 2014). The primary grass species in proximity of station include *Hypparrhenia hirta*, C*ynodon dactylon*, *Eragrostis chloromelas*, *Sporobolus pyramidalis*. Whereas non-grassy species include *Acacia sieberiana*, *Rhus rehmanniana*, *Walafrida densiflora*, *Spermacoce natalensis*, *Kohautia cynanchica* and *Phyllanthus glaucophyllus* (Booyens, 2018; Jaars *et al.*, 2016). The Welgegund station is situated in the Transvaal Supergroup. Jaars *et al*. (2016) describes the soil surrounding the station as heterogeneous – varying from rocky to sandy to clayey due to underlying geology. The underlying geology include andesite, chert, dolomite, mudstone, quartzite, sandstone and shale.

3.2.1.3. Major pollution sources

As mentioned, Welgegund is a great representation of the regional background air quality for the interior region of South Africa, as it has no major anthropogenic pollution sources in its nearby surroundings (Booyens *et al.*, 2015; Jaars *et al.*, 2014, Jaars *et al.*, 2016; Venter *et al.*, 2017). Having said that, Welgegund is frequently affected by air plumes that have moved over areas associated with the worst air pollution in the country, such as the Waterberg-bonjala Priority Area, Highveld Priority Area as well as the Vaal Triangle Air Shed Priority Area (Booyens *et al.*, 2015; Jaars *et al.*, 2014, Jaars *et al.*, 2016; Venter *et al.*, 2017). Figure 3.3 indicates the three priority areas mentioned above with reference to the Welgegund Monitoring Station. Figure 3.4 present some of the major pollution sources (power station, pyrometallurgical- and petrochemical operations) situated within areas that affect the Welgegund measurements.

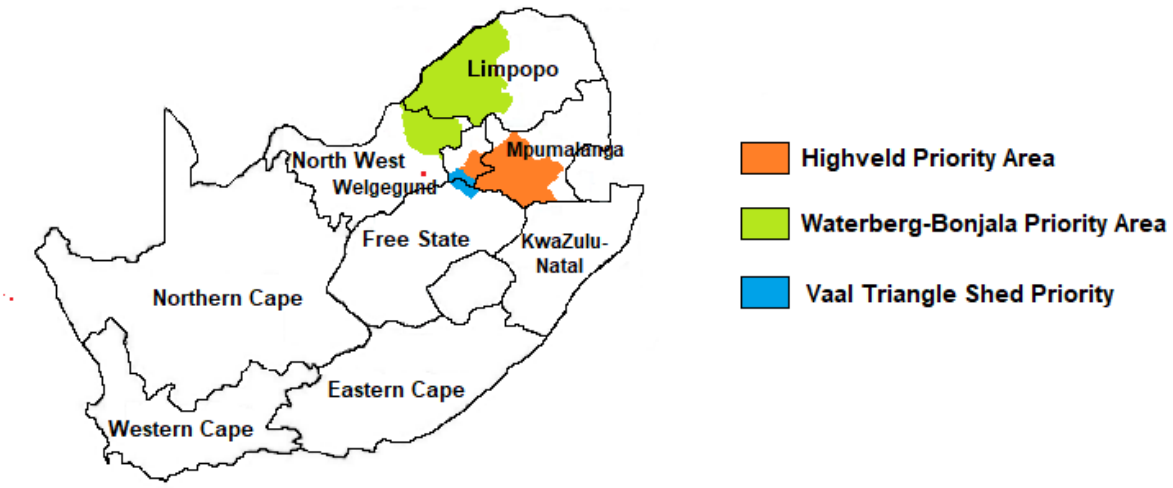

Figure 3.3: Location of ambient PM sampling site (Welgegund) indicated by the red dot in reference to several major air quality priority areas

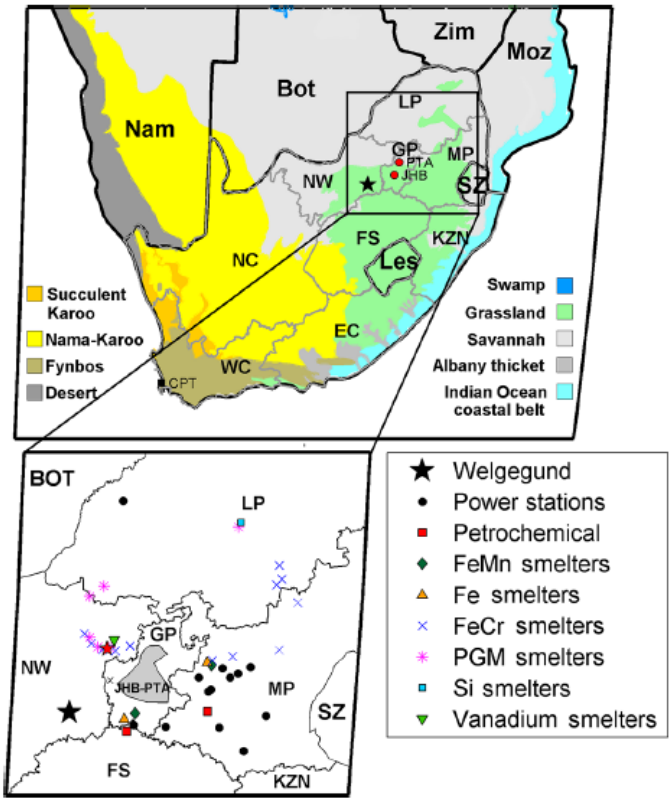

Figure 3.4: Major anthropogenic source pollution surrounding the Welgegund monitoring station (Venter et al., 2017)

The Vaal Triangle Airshed Priority Area situated in a south and south-easterly direction from Welgegund. Not only is most of South Africa's petrochemical industries located within the Vaal Triangle. But also other major anthropogenic pollution sources such as coal power plants (without denitrification and desulfurisation technologies) and pyrometallurgical smelters (responsible for emission of significant amounts of Cr, Ni, Zn, Fe, Mn) (Booyens *et al.*, 2015;

Jaars *et al.*, 2014; Venter *et al.*, 2017). North and north-east from Welgegund lies the western limb of the Bushveld Igneous Complex (BIC) situated within the Waterberg-Bojanala Priority Area. The BIC covers over 66 000 km^2 across Gauteng, Limpopo, Mpumalanga, and the North West. The BIC contains large deposits of V, Ni, Cu, Cr, and Sn. As well as, approximately 80% of the world's platinum group metals (PGMs). Thus, it is without surprise that the BIC is known as a highly industrialised region with multiple mining facilities and pyrometallurgical operations. These pyrometallurgical operation are responsible for significant emissions of Cr, Fe, Ni, and V. Whereas, the tailing storage facilities (TSFs) are responsible for substantial amount of wind-blown dust and emissions of large transport vehicles (Booyens *et al.*, 2015; Jaars *et al.*, 2014; van Zyl *et al.*, 2014; Venter *et al.*, 2017).

Another major pollution source from the north and north-easterly direction is the Johannesburg-Pretoria metropolitan with approximately 10 million residents. The Johannesburg-Pretoria conurbation is well known for its high volumes of traffic, which consequently leads to high amounts of fuel emissions (Pb, Fe, Cu, Zn, Ni, Cd). As well as the formation of particles due to road and tyre abrasion. Another major source of pollution from the megacity is wind-blown dust from gold TSFs (Booyens *et al.*, 2015; Jaars *et al.*, 2014; Venter *et al.*, 2017). From an eastern direction, Welgegund is affected by air plumes that have moved over the Highveld Priority area situated in Mpumalanga. The air quality of the Mpumalanga Highveld region is considered amongst the poorest in the country. This region is characterised by hundreds of coal mines, multiple pyrometallurgical operations, a large petrochemical plant, as well as 11 of Eskom's coal-fired power stations (without denitrification and desulfurisation technologies), brick and stone work, fertilise producers, as well as chemical and explosive producers, and other smaller industrial operations (Booyens *et al.*, 2015; Department of Co-operative Governance and Traditional Affairs, 2018; Jaars *et al.*, 2014; Venter *et al.*, 2017).

3.2.2. Indoor samples: Agincourt

3.2.2.1. Regional meteorology

Indoor samples were collected from a rural informal settlement, namely Agincourt (24°43′30″S, 31°13′55″E). Agincourt is situated in north-eastern Mpumalanga in the Lowveld region of South Africa as indicated by Figure 3.5. The Lowveld encompass approximate 56 853 km^2 in area – extending from the coast of Mozambique to the foot slopes of the Drakensberg mountain range. Similar to the Highveld, the Lowveld is characterised by a distinct wet- and dry season. Which is primarily during late spring to summer and winter respectively. However, the Lowveld region is considered to have a sub-tropical climate and consists of much higher temperatures during the summer and winter than the Highveld region. This can mainly be

attributed to the weaker influence of the high-pressure cell active over the interior region of South Africa during winter. As well as the influence of the warm Agulhas ocean current running past on the eastern coast of Southern Africa. The Lowveld summers consist of a highest maximum temperature average of 41°C - 43°C. Whereas the highest winter averages recorded are 34°C - 38°C (Department of Co-operative Governance and Traditional Affairs, 2018; Language, 2019).

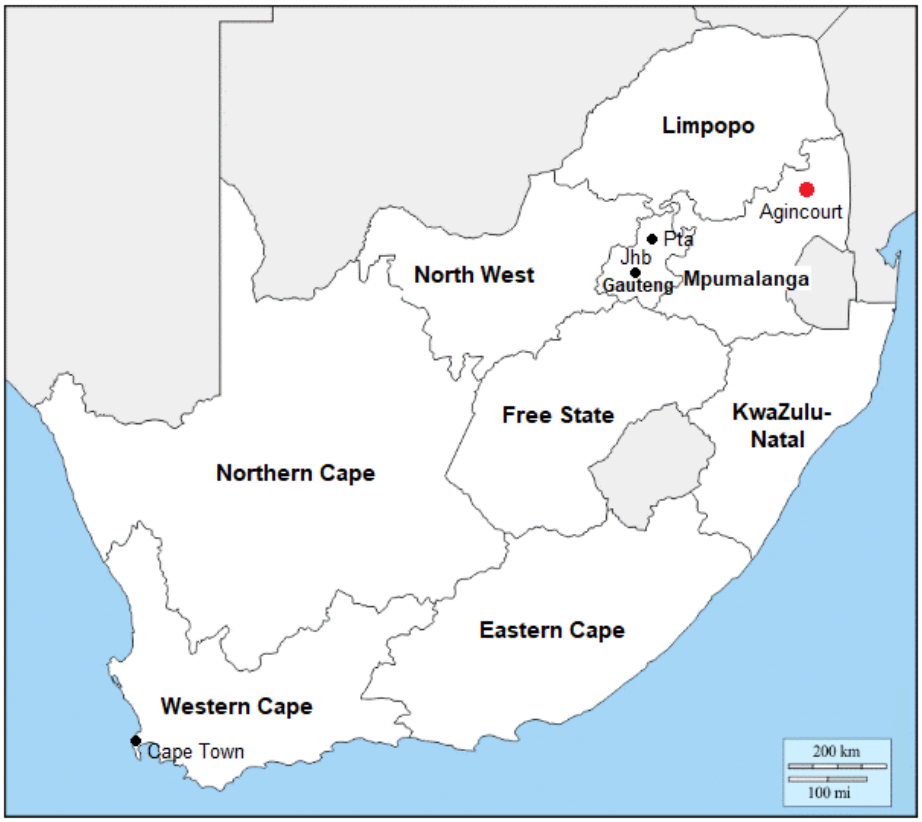

Figure 3.5: Location of the Agincourt monitoring station with reference to South Africa and neighbouring countries

3.2.2.2. Vegetation & geology

Agincourt is situated in what is considered a savannah-dominated biome with minor grassland in the surrounding area, which is characterised by a mixture of African trees, grass and shrubs (Department of Co-operative Governance and Traditional Affairs). According to Language (2019) approximately 48,2% of the land coverage in a 50km^2 radius of Agincourt settlement can be ascribed to woodland/open bush and 10.1% to plantations. The Mpumalanga province has numerous geological formations and mineral deposits. Consequently, Mpumalanga consists of extensive mining and metallurgical activities. Some of the largest and most well-known deposits include PGMs deposited in the eastern limb of the BIC, gold (Witwatersrand Supergroup) and furthermore Sb, Fe, Hg, Cu-Zn, asbestos, talc and other gemstones in the Barberton Supergroup. Various rock types are found throughout the province, including

dolerite, granite, gabbro, gneiss, norite, tuff, and shale. Agincourt, however, is located within the Cunning Moor lithostratigraphic unit, which is characterised by coarse grained deep intrusives with high silica content, i.e. Tonalite (Department of Co-operative Governance and Traditional Affairs). These rocks have weathered throughout the years to produce some of the most naturally fertile soils in the country – including sandy loam in the western region of the Lowveld and clays in the eastern region.

3.2.2.3. Major pollution sources

Four villages within the Agincourt region were identified as suitable sampling sites. These villages included Cunningmoore A, Croquet Lawn A, Merry Pebble Stream, and Rolle. Over a 5-year period one-hundred-and-three houses were selected for sample collection of which 50 contributed to the summer sampling campaign of 2016. No major anthropogenic air pollution sources are in the nearby proximity of Agincourt, with the closest being a gold mine at Graskop approximately 57 km away. . Houses were selected at random and were categorised as either:

- Formal – houses built by residents and/or traditional houses,
- Formal RDP – reconstruction and development programme-built houses, or
- Informal – Houses commonly referred to as *shacks.*

Although all houses in Agincourt have access to electricity, the selected houses were sub-categorised according to the solid fuel practices cooking and heating. Categories were assigned as follow:

- Indoor solid fuel burning (ISFB)
- Outdoor solid fuel burning (OSFB)
- Non-solid fuel burning (NSFB)

Table 3.1 provides a summary of the above-mentioned categories and the corresponding number of houses for each during the 2016 summer sampling campaign. 12% of the households sampled at Agincourt during the summer of 2016 burned solid fuel (wood, coal, animal dung, or crop waste) indoors, 80% burned solid fuel outdoors, and 8% did not burn solid-fuel (e.g. gas, paraffin, electricity). Wood emissions are associated with emission of Ca, Cu, K, Mn, P, Zn, while paraffin emissions could include Cd, Fe and Zn.

Table 3.1: Summary of the type of fuel use for households during the 2016 summer campaign and the corresponding number households for each

Summer 2016 (*n = 50*)	
Fuel Use	**Household number**
ISFB	6
OSFB	40
NSFB	4

Furthermore, according to Language (2019) approximately 40% of the households sampled on the Agincourt region over the 5-year period used electricity for cooking, and roughly 60% of the households used wood. It was found that approximately 20% of the households used electricity,60-70% wood which allows for emission of Ca, Cu, K, Mn, P, Zn and 10-20% used paraffin which is associate with the emission of Cd, Fe, Zn.

3.3. Sample collection & sample handling

Section 3.3. will mainly focus on the procedures followed for the collection of ambient PM, as indoor samples were collected by the CRG prior to this research study. A brief description will be given for indoor samples where deemed necessary, but for a comprehensive review about the sample collection and -handling (experimental procedures), refer to the thesis of Language, B. Table 3.2 indicates the sampling scheme for this case study

Table 3.2: Sampling scheme

Sample Type	Sampling Time	Collecting Environment	Particle Size	Sample numbers
Non-duplicates	24-h	Indoor	PM4	40
Co-located Duplicates	1-week	Outdoor	PM1	16
			PM2.5	16
			PM10	15
Reagent blanks				1 for each 15 samples
Lab Blanks	24-h	Indoor		5
	1-week	Outdoor		9

3.3.1. Pre- & post sample handling: gravimetric mass analysis of filters

For this case study 37 mm MCE filters were used for the collection of ambient and indoor PM samples. The filters were weighed in a controlled environment in the laboratory (T = 20°C ±2°C and RH = 37.2%) before and after sampling with a six-decimal Mettler-Toledo (XP26 DeltaRange) micro balance. Filters were pre-conditioned for approximately 2 days and visually inspected for any flaws 24 hours before weighing. Since the Mettler-Toledo balance consists

of an internal electrostatic unit, no additional procedures were required for static and air buoyancy corrections. Filters were placed into labelled petri dish slides prior to sampling.

3.3.2. Sample collection: ambient PM

Weekly ambient PM samples were collected for a period of two months (December 2018 – February 2019). Samples were collected by means of fix-point sampling, which entails two inlets placed within a few meters from each other. PM ambient samples were collected with Dekati PM_{10} three-stage cascade impactors at a flow rate of 30L/min for (Pump A & Pump B) as indicated in Figure 3.6 The impactor allowed for the collection different PM size fractions, which included PM_{10} (coarse), $PM_{2.5}$ (fine), and PM_1 (ultra-fine). Filters were solely handled, inserted and removed from impactors with forceps. Collected samples placed in petri dish slides were stored in an additional container in the laboratory up until chemical analysis.

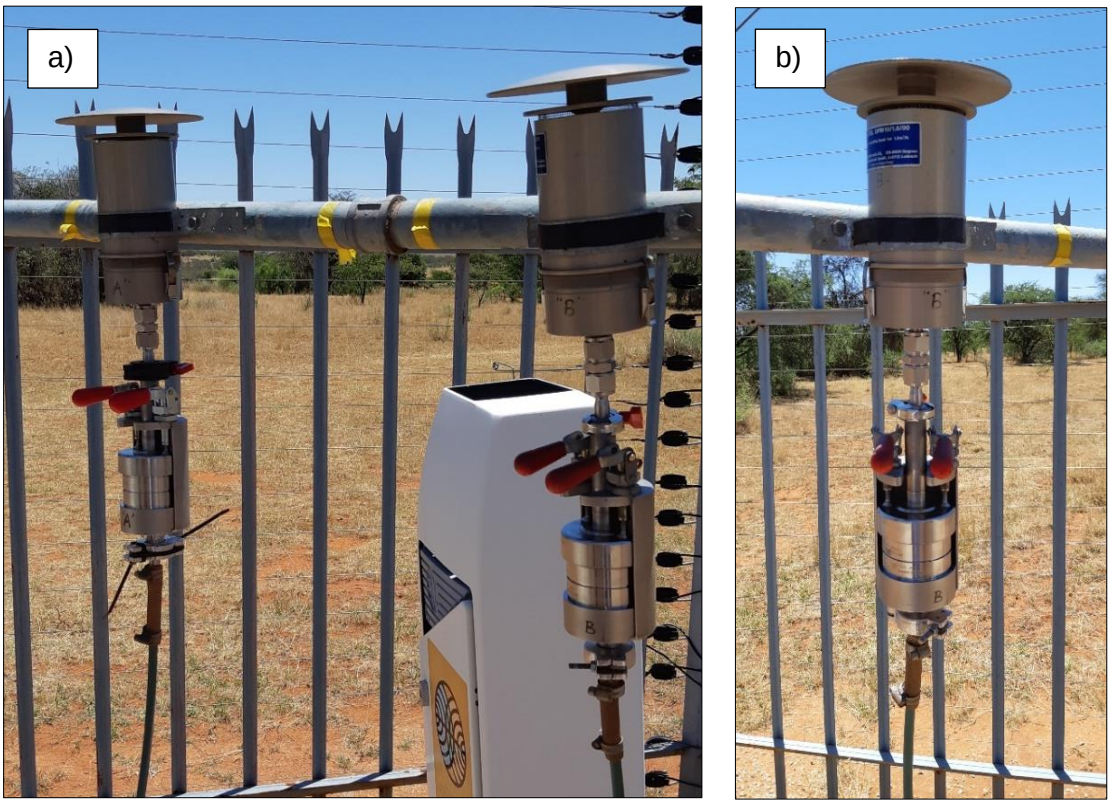

Figure 3.6: Cascade impactor set-up at the Welgegund monitoring station for the collection of ambient PM

3.3.3. Sample collection: indoor PM

Daily (24-h) intermittent indoor samples were collected by means of PM_4 cyclone inlets. The collection of indoor samples for this case study was by means of a GX Cyclone calibrated at 2.2 $L.min^{-1}$±5%. Furthermore, the sampling inlets were assembled at a fixed height of approximately 1.6 m, which is representative of the average breathing height (Language, B. 2019). As previously mentioned, the indoor samples were collected for a previous study.

Therefore, it is highly recommended that the reader refers to the PhD thesis of B. Language – *Characterisation of respirable indoor particulate matter in South African low-income settlements,* for a more comprehensive understanding about entire sample collection and methodology applied at each site.

3.4. Laboratory procedures

3.4.1. Acid digestion

HNO_3-HCl (4:1) acid mixture on a hot-plate (conventional heating) connected to a reflux system that is presented in Figure 3.7 was applied for the extraction of PM samples from filters for ICP-MS analysis (Mouli *et al*., 2006; Salcedo *et al*., 2014), which also resembles the US-EPA recommended acid digestion technique for the decomposition for PM collected on filter material. The PM loaded filter was placed in a 100 ml Erlenmeyer flask after which 20 mL concentrated nitric acid (HNO_3) and 40 mL MilliQ water (18.2 MΩ) was added. The mixture was boiled for 5-10 minutes, after which 5 mL hydrochloric acid (HCl) was added. The mixture was then refluxed for 3 hours whilst continuously being stirred after which the HNO_3-HCl mixture were allowed to cool down and diluted to a 100 mL volumetric flask. Filter material and Erlenmeyer flask was washed twice with MilliQ-water so as to ensure complete transference of sample. Since acid digestion is considered one of the largest sources of contamination when quantifying atmospheric PM, great attention was given to the cleanliness of laboratory glassware and equipment used. Glassware was immediately rinsed and washed with MilliQ-water after acid mixture was decanted. Afterwards, glassware was left to soak in diluted HNO_3 for 24-h and rinsed again with MilliQ-water before use.

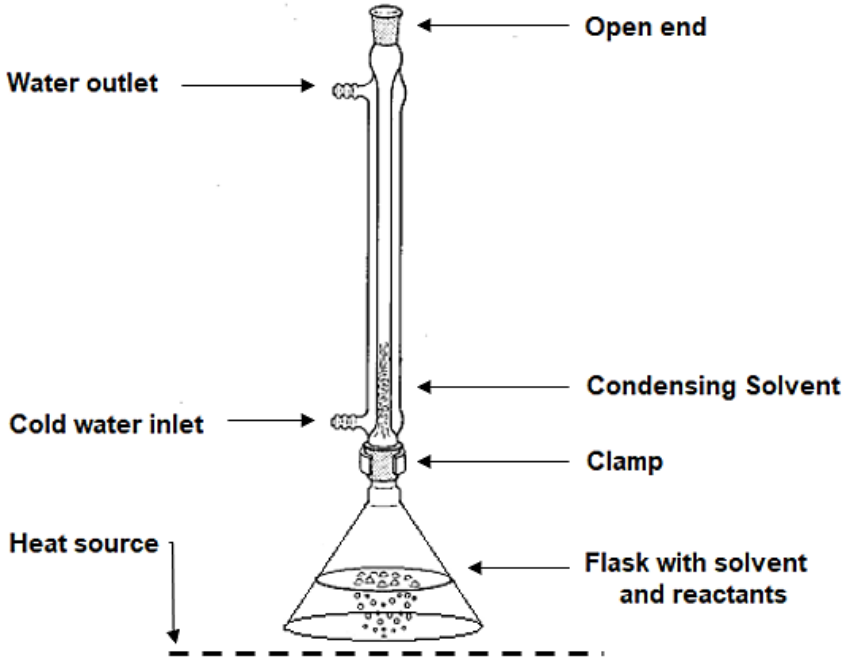

Figure 3.7: Schematic illustration of acid digestion set-up applied for this case study (Zubrick, 2019).

3.4.2. WD-XRF analysis

WD-XRF analysis for this study was conducted by a PANalytical Axios ^{mAX} (sequential) WD-XRF spectrometer was used. The spectrometer consisted a rhodium (Rh) X-ray tube and a 4 kW generator. Furthermore, the spectrometer was equipped with a 20 mm collimator and helium (He) counting-gas in the gas-filled detector. MICROMATTER^{TM} calibration standards were applied for the calibration of the WD-XRF system. Each element in the standards were characterised by two calibration points, i.e. light standard (3-8 µg.cm^{-2}) and heavier standard (40-60 µg.cm^{-2}). The following elements were analysed: Na, Mg, Al, Si, P, S, Cl, K, Ca, Ti, V, Cr, Mn, Fe, Co, Ni, Cu, Zn, Ga, Ge, As, Se, Br, Rb, Sr, Y, Zr, Nb, Mo, Pd, Ag, Cd, In, Sn, Sb, I, Cs, Ba, Ce, W, Pt, Hg, Tl, Pb and Bi. Although only 31 of the elements mentioned above were considered for this case study, i.e. Na, Mg, Al, P, K, Ca, Ti, V, Cr, Mn, Fe, Co, Ni, Cu, Zn, As, Se, Rb, Sr, Mo, Pd, Ag, Cd, Sb, Ba, Pt, Au, Hg, Tl, Pb and Bi.

Elements with concentration below detection limits were considered to have a concentration equivalent to half of the detection limit. This is a precautionary statement frequently made in numerous environmental studies (Venter, 2015).

3.4.3. ICP-MS analysis

Trace metal analysis were conducted by using an Agilent 7500 CE ICP-MS system. The system is calibrated by using a certified mixed multi-elemental stock standard solution containing all the elements of interest. For this study, the following elements were analysed:

Na, Mg, Al, P, K, Ca, Ti, V, Cr, Mn, Fe, Co, Ni, Cu, Zn, As, Se, Rb, Sr, Mo, Pd, Ag, Cd, Sb, Ba, Pt, Au, Hg, Tl, Pb and Bi. The instrumental conditions are displayed in Table 3.3.

Table 3.3: Parameters of the ICP-MS system applied in case study

Parameter	Value
Forward Power	1550 W
Plasma Gas Flow	15 L/min
Nebuliser Gas Flow	1,2 L/min
Sampling Depth	8 mm
Spray Chamber Temp	2°C

As with the WD-XRF results obtained, elements with concentration below detection limits were considered to have a concentration equivalent to half of the detection limit. This is a precautionary statement frequently made in numerous environmental studies (Venter, 2015).

3.5. Statistical Approach

3.5.1. Assessment Criteria

Firstly, a "pass-fail" assessment criterion similar to the one in Niu *et al.* (2010) was applied to the ICP-MS and WD-XRF datasets for both ambient and indoor samples. An element either received a "pass" if 70% of dataset exceeded the detection limit (LOD) of the analytical technique – either XRF or ICP-MS. An element received a "partially pass" if between 20% and 70% of dataset exceeded the LOD and/or a "fail" if ≤ 20% exceeded the LOD. LOD was calculated as three times the standard deviation of gravimetric blanks for both WD-XRF and ICP-MS (see equation 3.1). Elements that received a "fail" criterion was not considered reportable.

$$LOD = 3 \cdot \sigma_{Blanks} \quad (3.1)$$

Table 3.4 indicates the elements that "passed" and/or "partially passed" the assessment criterion with an "X".

Table 3.4: Trace metals that "passed" and/or partially passed" the assessment criteria

Elements	Indoor		Ambient	
	WD-XRF	ICP-MS	WD-XRF	ICP-MS
Na	X	X	X	X
Mg	X	X	X	X
Al	X	X	X	X
P	X	X	X	X
K	X		X	X

Table 3.4 (continued): Trace metals that "passed" and/or partially passed" the assessment criteria

Elements	Indoor		Ambient	
	WD-XRF	ICP-MS	WD-XRF	ICP-MS
Ca	X	X	X	X
Ti	X	X	X	X
V		X		X
Cr	X	X		X
Mn	X	X	X	X
Fe	X	X	X	X
Co	X	X		X
Ni	X	X	X	X
Cu	X	X	X	
Zn	X	X	X	X
As		X	X	X
Se		X		X
Rb	X	X		X
Sr	X	X	X	X
Mo	X	X		X
Pd	X	X	X	X
Ag				X
Cd		X		
Sb	X	X		X
Ba		X		X
Pt		X	X	X
Au				X
Hg		X		X
Tl				
Pb			X	X
Bi		X		X

Only elements that received an "X" for both WD-XRF and ICP-MS was used for further data processing. As indicated by Table 3.4, for the indoor samples only 18 of the 31 elements received a "pass" and/or "partially pass" criteria for both ICP-MS and WD-XRF including Na, Mg, Al, P, Ca, Ti, Cr, Mn, Fe, Co, Ni, Cu, Zn, Rb, Sr, Mo, Pd, and Sb. For the ambient samples only a mere 16 of the 31 elements received exceeded the criteria, including Na, Mg, Al, P, K, Ca, Ti, Mn, Fe, Ni, Zn, As, Sr, Pd, Pt and Pb.

3.5.2. Linear regression

Linear regression analysis was applied to the datasets in order to determine the comparison between the WD-XRF and ICP-MS. For this study, the correlation coefficient (*r*) was calculated. The correlation coefficient indicates the strength of the linear relationship between

the values obtained by the analytical techniques. As indicated in Table 3.5, the correlation coefficient can be described by four properties.

Table 3.5: Description of the r-value

r - value	Correlation	Indication
$0 < r < 1$	Positive correlation	A larger *r*-value indicates a stronger positive fit.
$-1 < r < 0$	Negative correlation	A smaller *r*-value indicate a negative linear fit.
$r = 0$	No correlation	The closer the *r*-value is to 0 - the weaker linear fit.
$r = \pm 1$	Strong correlation	Indication of a perfect linear fit. That is, all data points lie on the 1:1 line.

The rule of thumb that is usually followed states that any *r*-value between ±0.8 and ±1 indicates a strong linear relationship. Whilst a *r*-value below ±0.5 indicates a poor/weak linear relationship (Greyling, S., 2016).

3.5.3. T-test

Numerous studies have indicated that linear regression isn't always the best method to determine the comparison between two techniques. It is suggested that multiple statistical approaches are applied in order to get a more comprehensive view of the comparison between two datasets. Therefore, a tow-tailed t-test was also applied as statistical analysis in this case study.

A two-tailed t-test refers to the statistical analysis and comparison between two averages of different datasets. The first step for a t-test is to establish a null-hypothesis. Generally, the null hypothesis (H_0) states that there is no difference between the two datasets. In other words, there is no difference in the measured concentrations between WD-XRF and ICP-MS. Secondly, an alternative hypothesis (H_1) is formulated, which is generally the exact opposite of the null-hypothesis. That is, there is a significant difference between the two averages of each dataset.

The two-tailed t-test produces a p-value (α) smaller or greater than 0.05 when a confidence level of 95% is chosen. Table 3.6 indicates what the p-value statistically describes

Table 3.6: Description of the α-value

p-value (α)	Indication
$\alpha < 0.05$	significant difference between the two averages. Therefore, the H_0 hypothesis is rejected.
$\alpha > 0.05$	No significant difference. The H_0 is accepted as true.

CHAPTER 4: RESULTS & DISCUSSION

As indicated in preceding chapters, the main aim and research question of the study was to compare ICP-MS and WD-XRF generally utilised to determine atmospheric trace metal concentrations. In this chapter these two analytical methods are evaluated in terms of (1) precision and the influence of contaminants, and (2) trace metal concentrations determined with these two methods for particulate samples collected on filters at two monitoring sites, i.e. an ambient and indoor site. Trace metal concentrations determined in different particulate size fractions in ambient samples are also presented. Concentration determined for specific trace metal species with ICP-MS and WD-XRF are statistically correlated, while differences in concentrations determined for each of these trace metal species with the two methods are assessed in detail.

4.1. Evaluation of analysis

4.1.1. Precision of analytical techniques

The precision of each analytical technique utilised to quantify trace metal concentrations in this study was assessed by analysing 4 samples, i.e. gravimetric blank filters, with each analytical method. Eight ambient gravimetric blank filters were selected of which four was analysed with ICP-MS and the other four with WD-XRF. In Figure 4.1 the correlation between concentrations determined for 31 ambient trace metal species of the gravimetric blank samples with ICP-MS (a and c) and WD-XRF (b and d) are presented. The results are presented on a linear scale in the top panes (with 0 values) and on a log scale in the bottom panes (without 0 values) similarly (Herner *et al.*, 2006). The same calibration curve sets were used for each analytical method. It is evident from Figure 4.1 that precision of both analytical methods can be considered very good in the entire concentration range for trace metal levels above the limit of detection (LOD) of the analytical techniques, with ICP-MS indicating marginally better reproducibility. Furthermore, it also seems that the reproducibility slightly decreases for the WD-XRF at lower trace metal concentrations close to the LOD of the analytical technique. The trends at very low concentrations can be better viewed on the log scale presented in Figure 4.1. This decrease in precision associated with XRF at lower concentrations of trace metal species was also observed by Herner *et al.* (2006) who also compared trace metal concentrations determined with ICP-MS and XRF. However, in this study the extent of the decreased reproducibility at lower trace metal concentrations associated with XRF was not as pronounced as observed by Herner *et al.* (2006). For WD-XRF, only Cu and Zn had relative standard deviation (RSD) smaller than 10%, while the remaining elements had RSD > 10%. The RSD percentage for the majority trace metals determined with ICP-MS were smaller than 10% with the exception of Al (12.85%), K

(11.26%), Ca (16.73%), Mn (10.12%), Fe (24.70%), Zn (12.93%), Sr (10.57%) and Pd (14.63%).

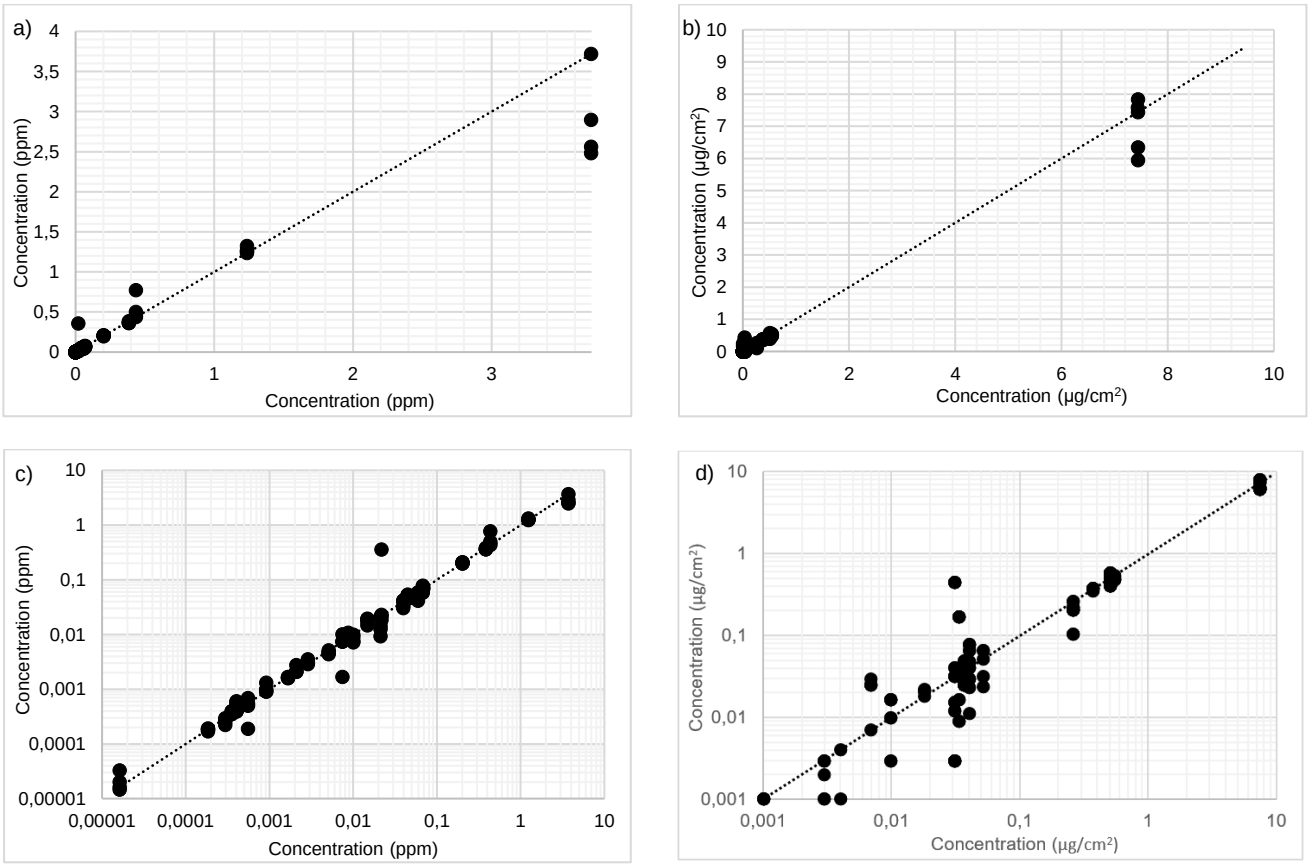

Figure 4.1: Correlation between ambient trace metal concentrations determined in duplicate samples with (a), (c) ICP-MS and (b), (d) WD-XRF. (a) and (b) present results on a linear scale, while the concentrations are presented on a log scale in (c) and (d)

4.1.2. Source & magnitude of contamination

For this study, the gravimetric blank contamination, laboratory procedural blank contamination and particle contamination of ambient- and indoor samples sent for ICP-MS analysis were determined according to calculations used in Rasmussen *et al.* (2007). The laboratory procedural blanks consist only of reagents. That is, the lab procedural blanks represent combination of contamination sources including contamination introduced by reagent, laboratory glassware and containers used during aid digestion. The gravimetric blank contamination is defined as any contamination that occurs during the pre- and post-sample weighing of filters. The gravimetric blank contamination was calculated by subtracting the laboratory procedural blank concentration from the concentration of the gravimetric blanks. Particle contamination, defined as contamination due to the unintended introduction of trace metals by means of sampling equipment, was calculated by multiplying the median of gravimetric blanks with the median of the particle metal concentration collected (Rasmussen *et al*., 2007).

Figure 4.2 and 4.3 indicates the magnitude of contamination associated with laboratory procedures and weighing of filters determined during the ambient- and indoor sampling campaigns, respectively. In each of these figures (b) presents trace metal concentrations on a smaller y-axis scale in order to observe differences for trace metal species present at lower concentrations.

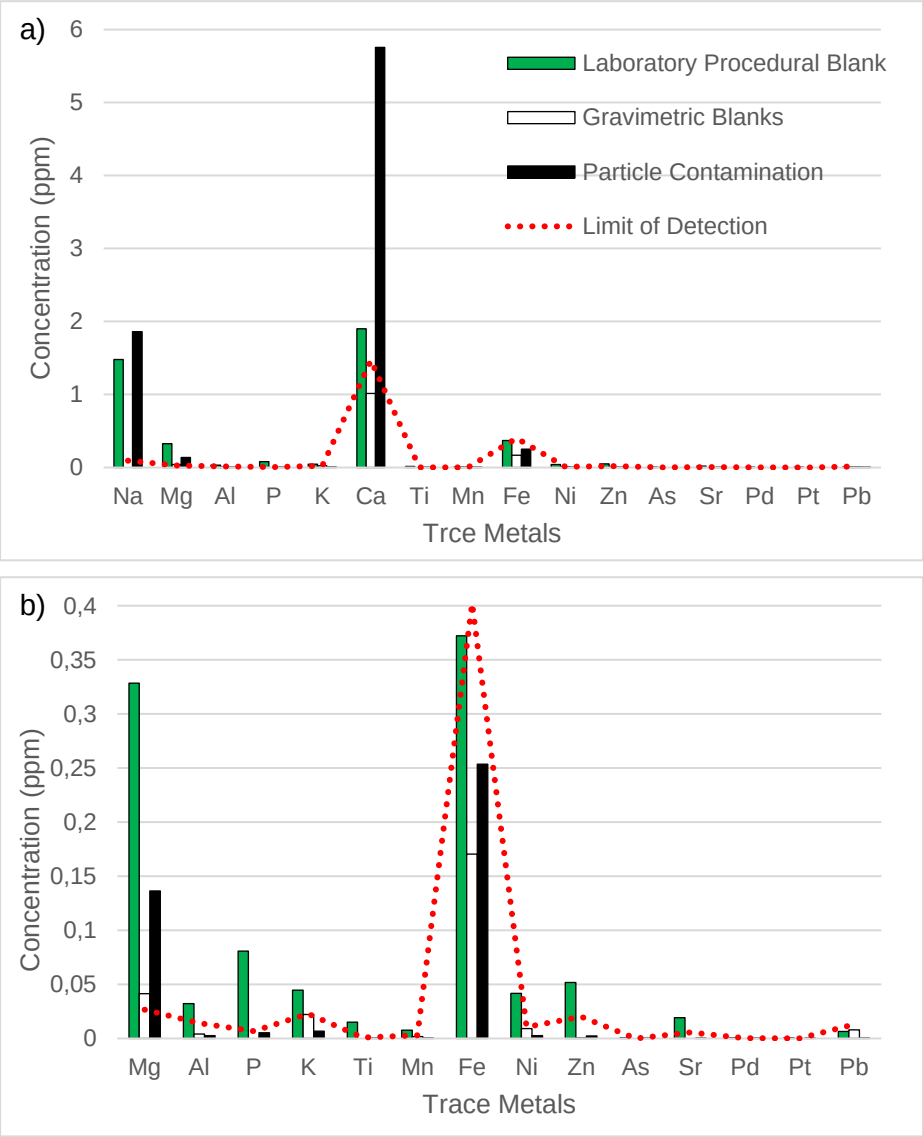

Figure 4.2: Contamination during ICP-MS analysis of ambient samples

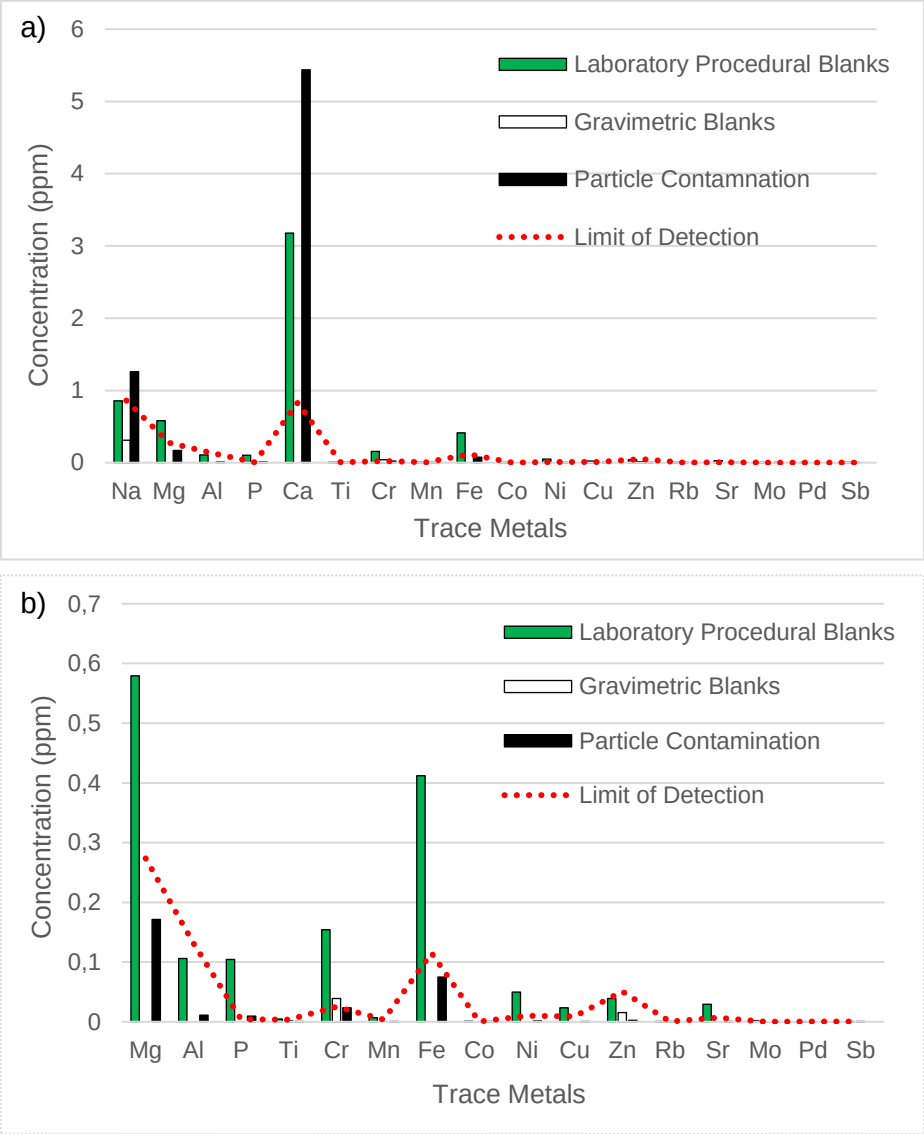

Figure 4.3: Contamination during ICP-MS analysis of indoor samples

It is clear from Figure 4.2 and 4.3 that significantly higher contamination is associated with Na and Ca, while relatively higher contributions to contamination are evident for Fe and Mg. Particle contamination is the main source of Na and Ca contamination, while laboratory procedural contamination also contributes to Na and Ca concentrations in samples. Procedural contamination makes the largest contribution to Fe and Mg contamination, while the influence of particle contamination on Fe and Mg levels are also evident. Laboratory procedural contamination made the largest contribution to contamination in samples for most trace metal species presented in Figure 4.2 and 4.3. Concentrations of Al, P, K, Ti, Mn, Ni, Zn, Sr, Cr and Cu associated with laboratory procedural contamination were above the DL of ICP-MS, with the contamination of these trace metal species associated with other sources being below the DL. According to Jalkanen & Häsänen (as stated in Rasmussen *et al.*, 2007) Pb and Ni contamination in laboratory procedures result from reagents. Whereas

contamination of Al, As, Cr, Zn in laboratory procedure blanks are primarily due to leaching of trace metals from glassware being used.

4.2. Trace metal concentration

In Table 4.1 the concentration ranges and medians of the trace metal species determined with the two analytical methods utilised in this study are presented for ambient particulate samples collected at Welgegund and indoor aerosol samples collected at Agincourt. Although 31 trace metal species could be detected with both analytical techniques as indicated in Chapter 3, only 16 and 18 trace metal species in ambient and indoor samples, respectively, passed the assessment criteria described in Chapter 3 (percentage of time above the DL of ICP-MS and WD-XRF) in all the samples collected, which are listed in Table 4.1.

Table 4.1: Summary of trace metal concentrations determined in indoor- and ambient samples

Element		Method	Concentration Range (µg/m³)
Na	Indoor	WD-XRF	< DL - 7,681388
		ICP-MS	< DL - 11,37035
	Ambient	XRF	< DL - 0,211450
		ICP-MS	0,01687 - 0,209160
Mg	Indoor	WD-XRF	< DL - 1,053476
		ICP-MS	< DL - 10,04637
	Ambient	XRF	< DL - 0,072070
		ICP-MS	0,00042 - 0,071640
Al	Indoor	WD-XRF	< DL - 3,475509
		ICP-MS	< DL - 12,77449
	Ambient	XRF	< DL - 0,350754
		ICP-MS	0,00323 - 0,026820
P	Indoor	WD-XRF	0,000863 - 0,055181
		ICP-MS	0,119025 - 0,875966
	Ambient	XRF	< DL - 0,002219
		ICP-MS	0,0001 - 0,006040
K	Ambient	XRF	< DL - 0,028060
		ICP-MS	0,0012 - 0,043240
Ca	Indoor	WD-XRF	0,129652 - 2,818623
		ICP-MS	3,012491 - 89,87588
	Ambient	XRF	< DL - 0,054690
		ICP-MS	0,17255 - 0,786100
Ti	Indoor	WD-XRF	< DL - 0,187849
		ICP-MS	< DL - 0,260165
	Ambient	XRF	< DL - 0,022600
		ICP-MS	2,26E-05 - 0,000770

Table 4.1 (continued): Summary of trace metal concentrations determined in indoor- and ambient samples

Element		Method	Concentration Range (µg/m³)		
Cr	Indoor	WD-XRF	< DL	-	0,026035
		ICP-MS	N/A	-	N/A
Mn	Indoor	WD-XRF	< DL	-	0,050191
		ICP-MS	< DL	-	0,505124
	Ambient	XRF	< DL	-	0,018197
		ICP-MS	0,000161	-	0,001604
Fe	Indoor	WD-XRF	0,003739	-	0,8304
		ICP-MS	0,044893	-	149,5359
	Ambient	XRF	< DL	-	0,336240
		ICP-MS	0,00601	-	0,061250
Co	Indoor	WD-XRF	< DL	-	0,012049
		ICP-MS	0,001029	-	0,191754
Ni	Indoor	WD-XRF	0,001345	-	0,005891
		ICP-MS	0,001114	-	1,624229
	Ambient	XRF	< DL	-	0,001600
		ICP-MS	0,00036	-	0,036880
Cu	Indoor	WD-XRF	0,003055	-	0,017322
		ICP-MS	0,004778	-	0,867277
Zn	Indoor	WD-XRF	0,000292	-	0,126648
		ICP-MS	< DL	-	2,406386
	Ambient	XRF	0,00023	-	0,024210
		ICP-MS	0,0012	-	0,043290
As	Ambient	XRF	< DL	-	0,000210
		ICP-MS	2,06E-06	-	0,000036
Rb	Indoor	WD-XRF	< DL	-	0,089335
		ICP-MS	< DL	-	0,220148
Sr	Indoor	WD-XRF	< DL	-	0,057915
		ICP-MS	0,005176	-	0,366066
	Ambient	XRF	< DL	-	0,009422
		ICP-MS	3,58E-05	-	0,006699
Mo	Indoor	WD-XRF	< DL	-	0,147411
		ICP-MS	0,011123	-	0,406679
Pd	Indoor	WD-XRF	0,020316	-	0,407954
		ICP-MS	< DL	-	0,024514
	Ambient	XRF	0,00011	-	0,130180
		ICP-MS	1,26E-05	-	0,000107
Sb	Indoor	WD-XRF	< DL	-	0,624306
		ICP-MS	< DL	-	0,068165

Table 4.1 (continued): Summary of trace metal concentrations determined in indoor- and ambient samples

Element		Method	Concentration Range (µg/m³)
Pt	Ambient	XRF	< DL - 0,000820
		ICP-MS	1,09E-06 - 0,000021
Pb	Ambient	XRF	< DL - 0,002380
		ICP-MS	< DL - 0,007100

Na, Mg, Al, P, Ca, Ti, Mn, Fe, Ni, Zn, Sr and Pd passed the assessment criteria in ambient samples collected at Welgegund and indoor particulates collected at Agincourt. K, As, Sr, Pt and Pb passed the assessment criteria only in ambient samples, while only Cr, Co, Cu, Rb, Sr Mo and Sb in indoor samples passed the assessment criteria. The concentration ranges of trace metal species indicate that trace metal concentrations in indoor samples were generally higher than levels thereof in ambient samples, which could also contribute to slightly more trace metal species determined in indoor samples. These observed differences in trace metal concentrations and –compositions in aerosol samples collected at the two sites can be expected due to ambient aerosols being more dispersed compared to particulates associated with indoor emissions. In addition, different sources will contribute to variances in aerosol composition of samples collected indoor compared to ambient samples, while the two sites are also located in two diverse regions of South Africa with different sources influencing aerosol composition as indicated in Chapter 2. However, the aim of this study was not to compare trace metal concentrations determined at these two sites, but to collect sufficient aerosol samples in order to compare the two analytical techniques generally used for trace metal analysis as indicated in Chapter 1. The collection of indoor and ambient aerosols in different regions of South Africa did, however, allow the collection of aerosol samples representing different concentration ranges of trace metal species. From Table 5.1 it is evident that the highest concentrations were associated with Na, Mg, Ca and Al.

In Figure 4.4 and 4.5 the percentages of samples in which the concentrations of specific trace metals were above the DLs of the two analytical methods are presented for ambient and indoor samples, respectively. It is evident that the percentages of trace metal concentrations above the DLs of the analytical instrumentation ranged from 20 to 100% and 30 to 100% for WD-XRF and ICP-MS, respectively. For indoor samples, the concentrations of Mg, P, Ca, Ti, Fe, Mn, Ni, Cu and Pd were >80% of the time above the DL of ICP-MS and WD-XRF, while Al, P, K, Ca, Ti, Mn, Fe, Zn and Pd concentration in >80% ambient samples were above the DL of both analytical methods. The percentages of samples in which concentrations of specific trace metals were above the DLs of WD-XRF and ICP-MS also differed for the two analytical

techniques. It seems from Figure 4.4 and 4.5 that higher percentages of concentrations of specific trace metals were above the DL of ICP-MS compared to WD-XRF, especially, for ambient samples. Most trace metals in ambient samples were 100% of the time above the DL of ICP-MS, while the percentages of times that trace metal concentrations were above the DL of WD-XRF differed in ambient samples. However, it is evident that detection efficiencies of WD-XRF exceeded ICP-MS for certain trace metals in indoor samples. For instance, Na. Al and Zn in indoor samples were > 95% of the time above the DL of WD-XRF, while these species were > 65% of the time above the DL of ICP-MS. It seems that lower trace metal concentrations correspond to higher percentages above the DLs of ICP-MS, whereas WD-XRF are less sensitive at lower trace metal concentrations. Furthermore, lower concentrations of trace metal species associated with mineral dust is expected with ICP-MS, which is observed for Na, Mg and Al in indoor samples. However, this is not the case for the percentage of time that these species are detected in ambient samples with ICP-MS. These observed differences in the detection of trace metal species with ICP-MS and WD-XRF will be further explored for each of the trace metal species determined.

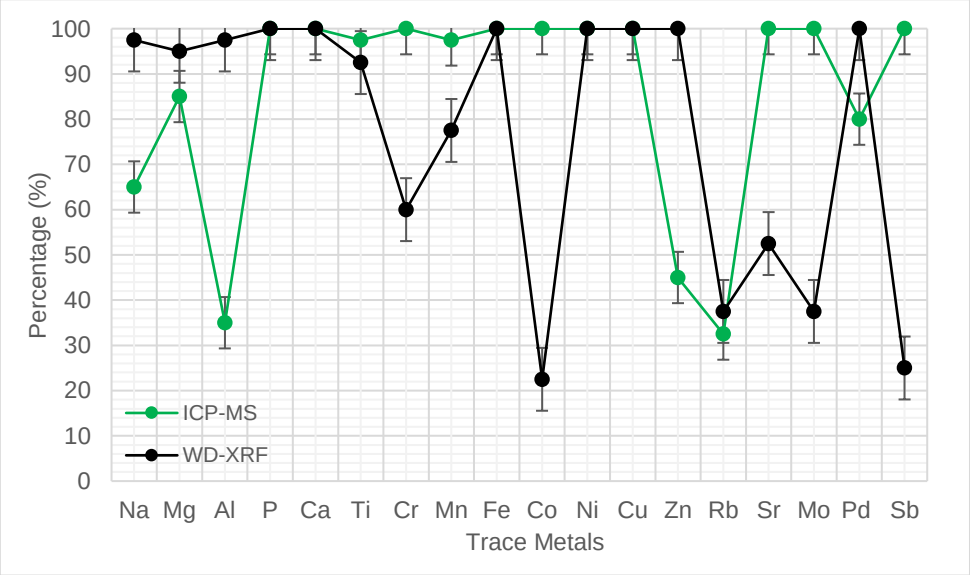

Figure 4.4: Comparison of the percentage indoor samples that passed the assessment criteria for both the ICP-MS and WD-XRF.

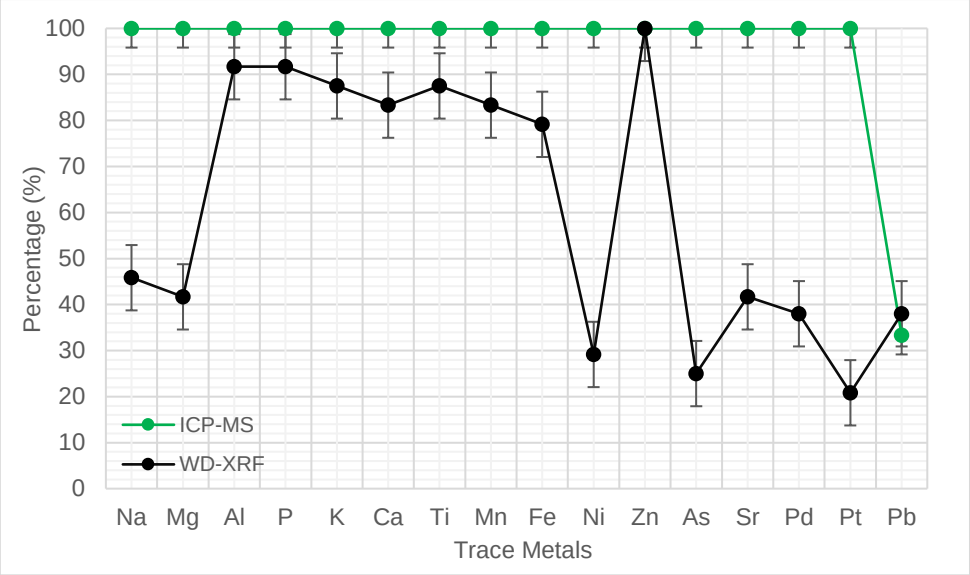

Figure 4.5: Comparison of the percentage ambient samples that passed the assessment criteria for ICP-MS and WD-XRF

4.3. PSD in ambient samples

Since ambient particulate matter was determined at Welgegund with a size segregated impactor (Dekati PM_{10} impactors, see section 3.3.2.) the size distribution of aerosols could be determined, which also allowed determining the particle size distribution of each trace metal measured in this study. In Figure 4.6 the particles size distribution of aerosols collected with the two impactors are presented. It is evident that most particulates measured at Welgegund are associated with the ultra-fine (PM_1) size fraction (42 and 44%), while only 25 and 27 % of aerosols collected were in the coarse size fraction. This aerosol size distribution was also indicated in other studies where samples were collected at this site, which can mainly be attributed to the sources impacting air measured at Welgegund. As indicated in Chapter 3, Welgegund is a background sites influenced by the major anthropogenic source region in the north-eastern interior of South Africa. Smaller particulates are generally associated with industrial and other anthropogenic activities (Venter *et al.*, 2017), In addition, Welgegund is also impacted by a relatively clean background site that could contribute to larger aerosols usually related to wind-blown dust, i.e. crustal species (Venter, 2015) . Lower aerosol concentrations in the coarser size fraction could also be attributed to sampling conducted during the wet season, which contribute to wash-out of coarser particulates form the atmosphere (Booyens *et al*., 2015; Booyens, 2018).

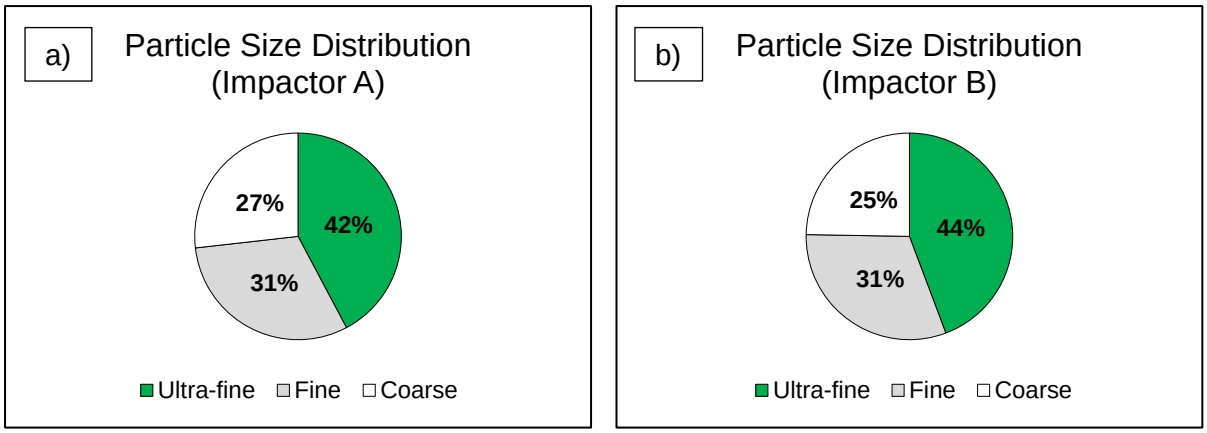

Figure 4.6: Particle size distribution of mass concentration in total suspended particulate matter for a) impactor A & b) impactor B

Each trace metal species (detected above the detection limit) in the ambient samples was fractionalised separately between the three size fractions, which are presented in Figure 4.7. It is evident that trace metal species in ambient samples occurred in all three size fractions. However, the largest fraction of trace metal species was present in the ultra-fine size fraction except for Al and K that had the highest occurrence (>35%) in the coarse size fraction. Except for Al and K, more than 30% of the specific trace metals were present in the PM_1 size fraction. In addition, >60% of all trace metals were in the fine ($PM_{2.5}$) and ultrafine size fractions. This signifies the strong influence of industrial activities in the source regions (e.g. the Western Bushveld Ingenious Complex,) impacting air masses measured at Welgegund on atmospheric trace metal concentrations determined at this site (Venter *et al.*, 2017). Trace metal species such as Cr, Mn, V, Zn and Ni are typically associated with metallurgical activities (Venter *et al.*, 2017). Higher occurrences of Al and K in the coarse size fraction are indicative of wind-blown dust being major sources of these species at Welgegund.The higher occurrence of other trace metal species usually associated with wind-blown dust, e.g. Fe, Na, Mg and Ti in the fine size fractions, indicate the influence of anthropogenic sources on levels of these species in air masses measured at Welgegund.

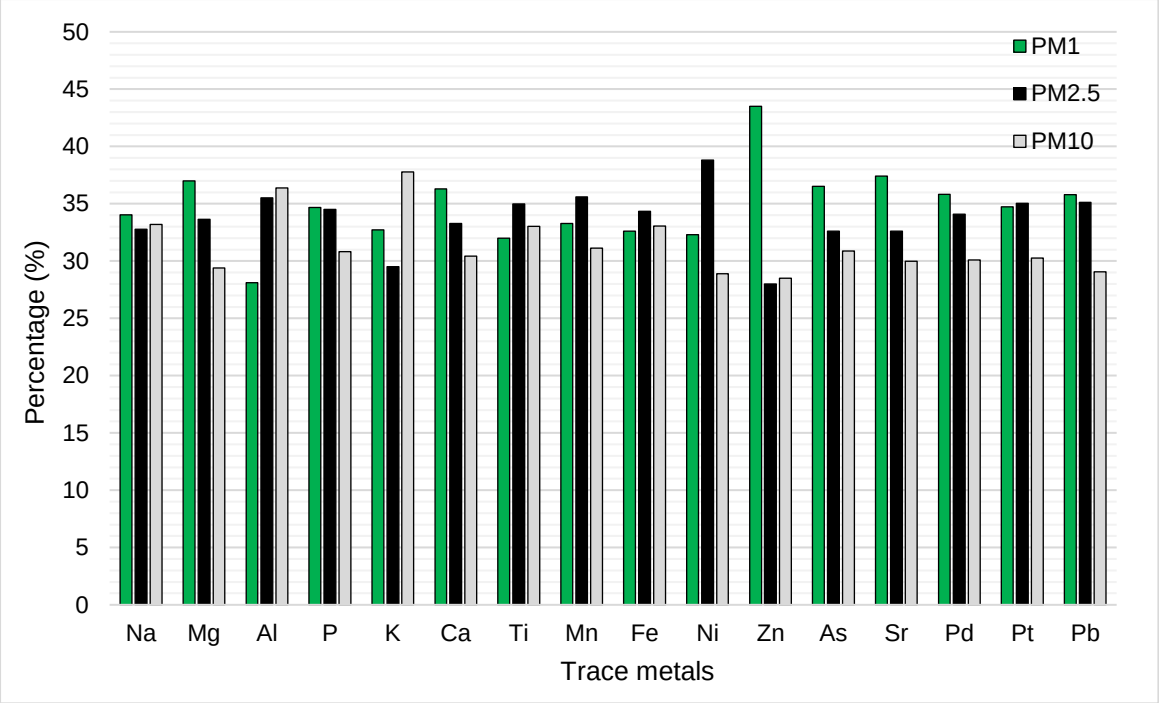

Figure 4.7: Particle size distribution of each trace metal in ambient samples

4.4. Comparison of trace metal concentration determined with IC-MS & WD-XRF

4.4.1. Statistical correlation

In Table 4.2 correlation coefficients (r) for the comparisons between trace metal concentrations determined for ambient and indoor samples with ICP-MS and WD-XRF are presented. As mentioned in Section 3.5.2 in Chapter 3, complete correlations correspond to an $|r|$ value of 1, while correlations ≥0.7 are generally considered to be strong/significant (Greyling, S., 2016). $|r|$ values ranging between 0.3 and 0.7 are considered to be moderate correlations, with $|r|$ values <0.3 being regarded as weak correlations. It is evident from Table 4.2 that the correlations between the concentrations determined for almost all the trace metal species with the two analytical techniques can be considered weak. A few trace metal concentrations determined with ICP-MS and WD-XRF showed moderate correlations, i.e. Mg in ambient and indoor samples, Mn and Pd in indoor samples, and Pt in ambient samples. Therefore, according to the *r* values, very poor correlations are observed between trace metal concentrations determined with the two analytical techniques in general.

Table 4.2: Correlation between trace metal concentrations determined with ICP-MS and WD-XRF

Trace Metals	Ambient (*r*)	Indoor (*r*)
Na	0,0472	0,0292
Mg	0,3378	0,4429
Al	0,158	0,0098
P	0,1434	0,0667
K	0,0804	-
Ca	0,2306	0,1596
Ti	0,0091	0,1343
Cr	-	-
Mn	0,1478	0,4583
Fe	0,0610	0,1526
Co	-	0,1000
Ni	0,0427	0,1579
Cu	-	0,0162
Zn	0,1980	0,0782
As	0,0267	-
Rb	-	0,1654
Sr	0,1626	0,1201
Mo	-	0,0997
Pd	0,1360	0,3197
Sb	-	0,0861
Pt	0,3821	-
Pb	0,0743	-

In addition to Pearson correlations, a two-tailed t-test was also performed in order to further statistically explore comparisons of trace metal concentrations determined with ICP-MS and WD-XRF, which are presented in Table 4.4. An α-values < 0.05 indicates a significant difference between the two analytical techniques. Table 4.3 indicates that there was no significant difference (α > 0.05) between the ICP-MS and WD-XRF analysis of ambient sample for Na Al, P, K, Mn, Ni, Zn, Sr, Pd and Pb. Whilst, Mg, Ca, Ti, Fe, As and Pt is characterised by a α < 0.05, indicating a significant difference between the techniques. For the indoor samples significant difference (α < 0.05) was found for majority of elements except Al, Fe, Rb, Mo and Pd. Therefore, according to correlation statistics, very weak correlations are observed between trace metal concentrations determined with ICP-MS and WD-XRF. These weak correlations can be attributed to a number of factors, which will be explored in the subsequent section through direct comparison of the concentrations determined for specific trace metal species with ICP-MS and WD-XRF.

Table 4.3: Two-tailed t-test for comparison between trace metal concentrations determined with ICP-MS and WD-XRF

Trace Metal	Ambient (α-value)	Indoor (α-value)
Na	0,3955	5E-11
Mg	0,0426	0,0065
Al	0,6450	0,0860
P	0,1794	2E-05
K	0,7905	
Ca	0,0458	7E-12
Ti	0,0292	5E-07
Cr	-	2E-24
Mn	0,1555	8E-05
Fe	0,0374	0,1449
Co	-	0,0348
Ni	0,2345	4E-08
Cu	-	3E-05
Zn	0,2824	0.,0102
As	0,0011	-
Rb	-	0,2688
Sr	0,9894	0,0315
Mo	-	0,1616
Pd	0,1277	0,7882
Sb	-	3E-07
Pt	0,0010	-
Pb	0,7754	-

4.4.2. Specific trace metal comparison

In this section, the concentrations determined for each trace metal species with ICP-MS and WD-XRF are compared by means of bar graphs. A brief discussion will be given about possible reason for the trend seen in the bar graphs. It should be noted, trace metals that had a measured concentration smaller than the gravimetric blank concentration were recorded as 0 µg/m^3.

Na

Comparison of the Na concentrations determined with ICP-MS and WD-XRF in Figure 4.8, indicate that Na in ambient samples were detected more frequently with ICP-MS, while in indoor samples, Na concentrations were above the DL of WD-XRF in most samples with Na only determined in one indoor sample with ICP-MS. According to the particle size distribution conducted for ambient samples, Na were predominantly in the fine size fraction that can contribute to Na not being detected with WD-XRF. Fine particles easily penetrate deeper into

the substrate medium with impaction, which can result in an increase of X-ray scattering and background noise, especially for light metals such as Na In samples where Na was above the DLs of both analytical techniques, differences are observed for Na concentrations determined with the two analytical methods. In certain samples higher Na concentrations was determined with ICP-MS, while in other samples higher Na levels corresponded to WD-XRF. No clear trend is evident from the comparison of the detection of Na with ICP-MS and WD-XRF.

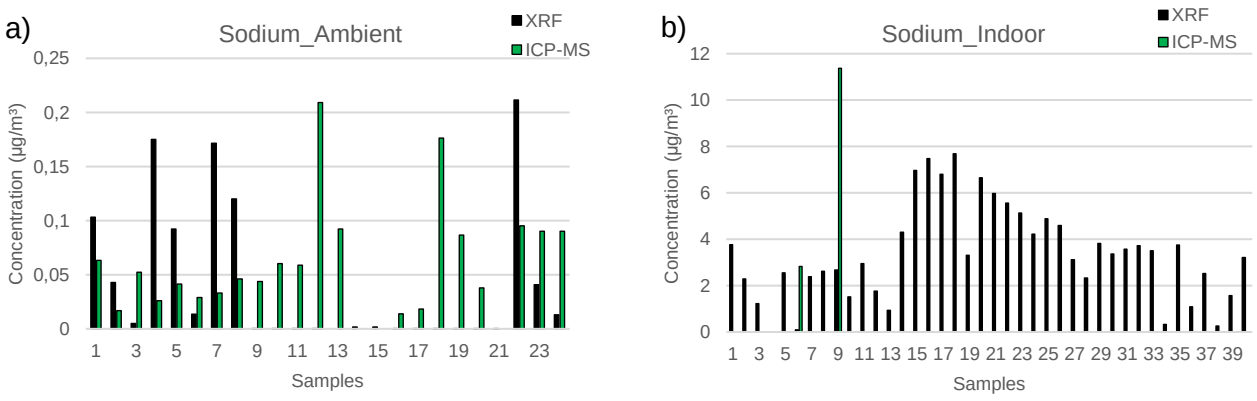

Figure 4.8: Comparison between the WD-XRF & ICP-MS for a) ambient and b) indoor sodium (Na)

K

K concentrations were only measured in ambient samples with both analytical techniques, which are presented in Figure 4.9. Although no distinct trend can be observed from the comparison of K levels determined with the two analytical methods, it seems that higher K concentrations were generally determined with ICP-MS. However, in a few instances higher K levels were determined with WD-XRF in samples where K was determined with both analytical methods. A larger percentage (~60%) of K also occurred in the fine size fraction, which could contribute to underestimation with WD-XRF as shown for Na. The t-test (α = 0.7905) indicated no significant differences between the K concentration measured with two analytical techniques.

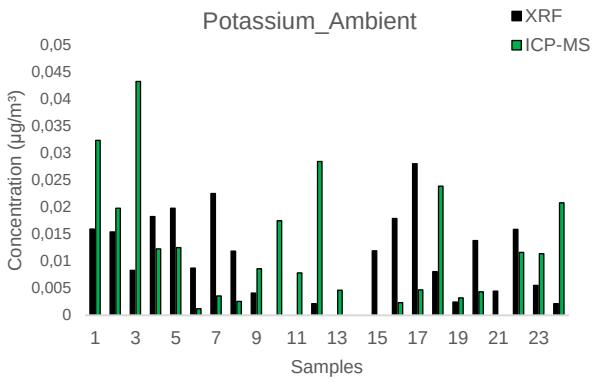

Figure 4.9: Comparison between the WD-XRF & ICP-MS for a) ambient and b) indoor potassium (K)

Mg

It is evident from Figure 4.10 in which Mg concentrations determined with the two analytical techniques are compared, that Mg was more frequently above the detection limits of WD-XRF, with Mg concentrations determined in almost all the samples with WD-XRF. However, in indoor samples, Mg concentrations determined with ICP-MS were significantly higher in a number of samples compared to Mg levels determined with WD-XRF. Underestimation of Mg concentrations with WD-XRF can also possibly be attributed to Mg occurring mainly in the fine fraction. Particle size distribution of ambient samples indicated that >70% of Mg was in the fine fraction. Deficiencies associated with ICP-MS analysis of Mg can be attributed Mg occurring in crustal species, which is generally underestimated by ICP-MS when nitric digestion is conducted (Venter et al).

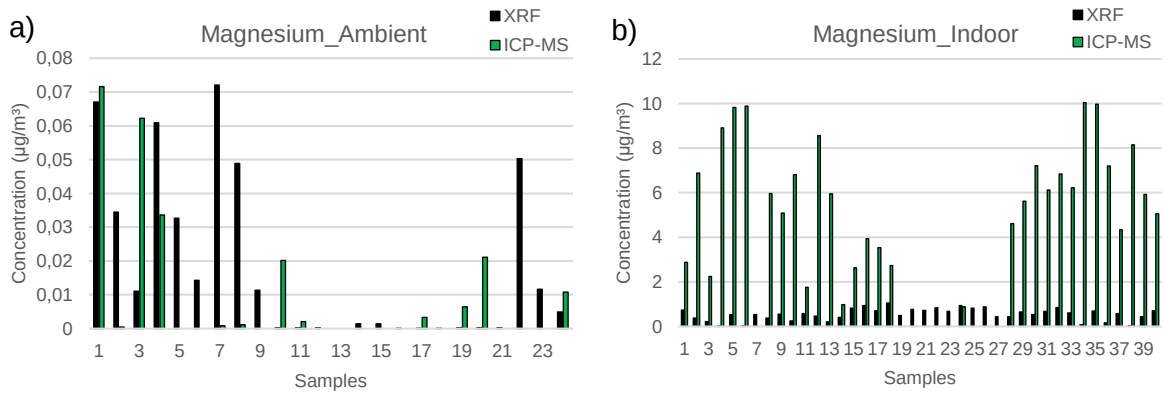

Figure 4.10: Comparison between the WD-XRF & ICP-MS for a) ambient and b) indoor magnesium (Mg)

Al

In Figure 4.11 Al concentrations determined with ICP-MS and WD-XRF are presented. A clear trend can be observed for Al concentrations determined with the two analytical methods, i.e.

Al levels determined with WD-XRF were consistently higher in all samples with the exception of few samples. This is expected, since nitric acid digestion utilised to extract and dissolve trace metals for ICP-MS analysis could allow for underestimation of Al associated with silicate minerals in dust (Venter et al). Si and Al are considered to be the most abundant crustal elements (Klein & Dutrow, 2007), while it is estimated that approximately only 30 % Al in silicate minerals is extracted by nitric acid leaching. The particle size distribution of Al is also indicative of Al being mainly associated with crustal species with 42% of Al occurring in the coarse size fraction. Silicate minerals can be dissolved through hydrofluoric acid digestion for ICP-MS analysis. However, it is a very difficult procedure resulting in the formation of gaseous SiF_3, which was therefore not conducted in this study.

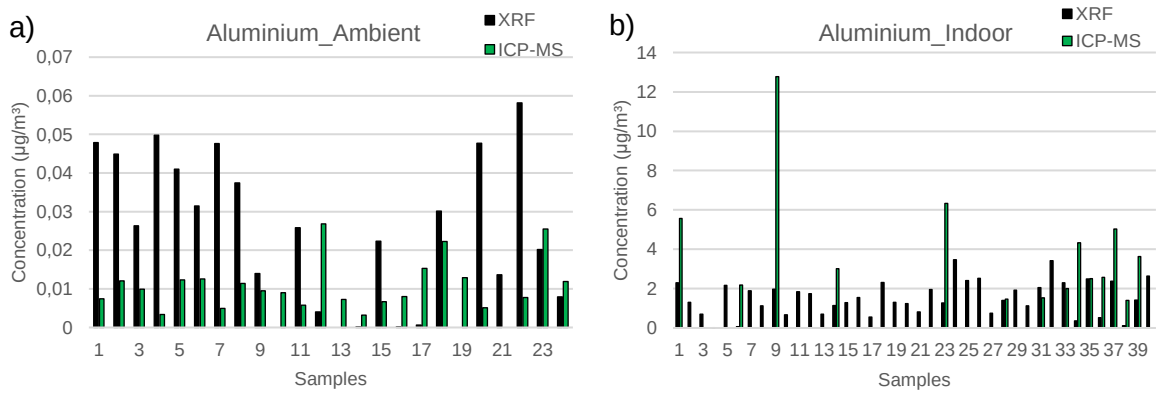

Figure 4.11: Comparison between the WD-XRF & ICP-MS for a) ambient and b) indoor aluminium (Al)

Fe

Comparison of Fe concentrations determined with ICP-MS and WD-XRF presented in Figure 4.12 indicates that Fe concentrations were above the DL of WD-XRF in almost all the ambient and indoor samples, while Fe was less frequently determined with ICP-MS. Similarly as indicated for Al above, particulate Fe can also be associated with silicate minerals in dust, which could result in not all particulate Fe being measured with ICP-MS when nitric acid dilution is utilised. These species will be determined with WD-XRF. Polyatomic interference of ions such as $^{54}ArN^+$, $^{56}ArO^+$, $^{57}ArOH$ with ^{54}Fe, ^{56}Fe and ^{57}Fe could also contribute to lower Fe concentrations measured with ICP-MS. However, in a number of samples where Fe concentrations were measured with ICP-MS and WD-XRF, Fe levels determined with ICP-MS were higher than Fe concentrations determined with WD-XRF. As indicated by the particle size distribution of ambient samples, a large fraction of Fe occurred in the fine size fraction (~65%), which is indicative of Fe not only being associated with crustal elements and other source also contributing to atmospheric Fe. Therefore, this could partially explain instances

when Fe concentrations determined with ICP-MS were higher than levels thereof determined with WD-XRF.

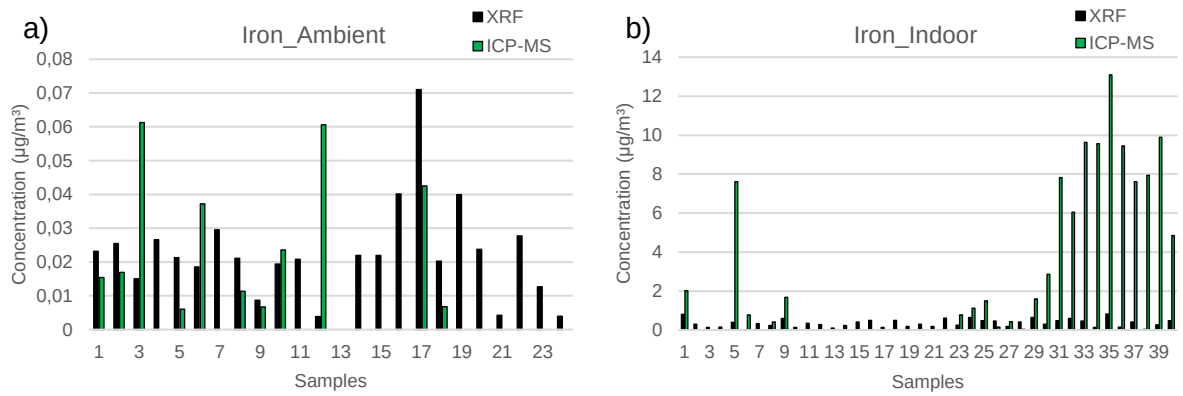

Figure 4.12: Comparison between the WD-XRF & ICP-MS for a) ambient and b) indoor iron (Fe)

Ca

Figure 4.13 indicates the Ca concentrations determined with the two analytical methods. Although Ca concentrations in ambient samples were above the DL of WD-XRF in more samples, the four instances when Ca was determined in ambient samples with ICP-MS, significantly higher Ca concentrations were determined. Ca levels determined for indoor samples were more frequently detected with ICP-MS compared to WD-XRF, with significant differences observed in Ca concentrations determined in samples detected with both analytical methods. It is expected that WD-XRF will be more efficient for the measurement of Ca associated with silicate minerals as indicated above for Al, Fe and Mg. However, higher Ca concentrations determined with ICP-MS compared to levels thereof determined with WD-XRF could be attributed to other sources of Ca. The particle size distribution also indicated > 65% of Ca occurring in the fine fraction, which is indicative of other source that dust. Measurement of Ca with ICP-MS could also provide challenges associated with interferences relating to the argon gas used during ICP-MS analysis.

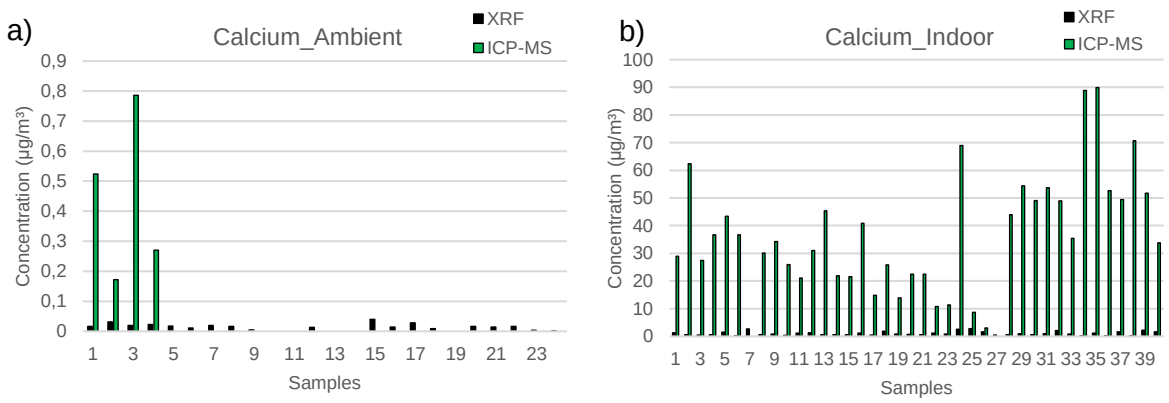

Figure 4.13: Comparison between the WD-XRF & ICP-MS for a) ambient and b) indoor calcium (Ca)

Ti

A clear trend is observed when comparing Ti concentrations determined with the two analytical methods presented in Figure 4.14. Ti concentrations were determined more frequently in ambient and indoor samples with WD-XRF, while, with the exception of a few samples, higher Ti concentrations were also determined in most samples with WD-XRF. The t-test also indicate significant difference in concentrations measured with the analytical techniques. This result was surprising, since it was expected that ICP-MS will perform better in the quantification of Ti. However, this could also be attributed to Ti associated with silicate minerals in dust (Klein & Dutrow, 2007). A possible explanation for the poor ICP-MS results obtained for the Ti measurements can be attributed to (1) the multiple oxidation states of Ti that readily form insoluble oxides and hydrides, as well as other metal complexes and (2) Ti is one of the most hydrolysed transition metals during ICP-MS, which can increase hydrolytic instability and formation of insoluble oxychlorides such as $TiOCl_2$.

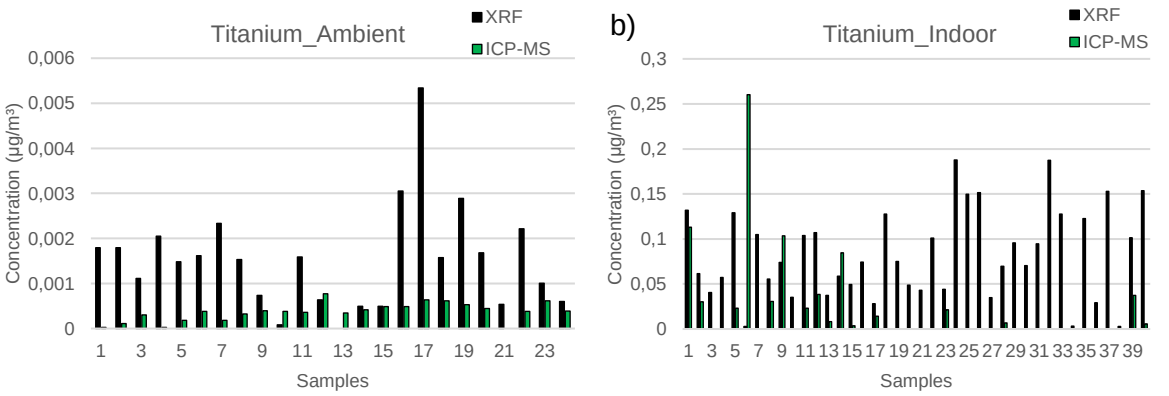

Figure 4.14: Comparison between the WD-XRF & ICP-MS for a) ambient and b) indoor titanium (Ti)

Cr

Cr concentrations were only determined in indoor samples and comparison between levels thereof determined with the two analytical techniques are presented in Figure 4.15. Cr levels were only determined with WD-XRF, while it was only measured in a few samples. In addition, very low concentrations were determined for Cr. Analysis of Cr with ICP-MS is susceptible to interferences e.g. polyatomic interference with ions such as $^{52}ArC^{+}$ or ^{54}Fe, which would affect measurement of Cr, especially, at very low concentrations.

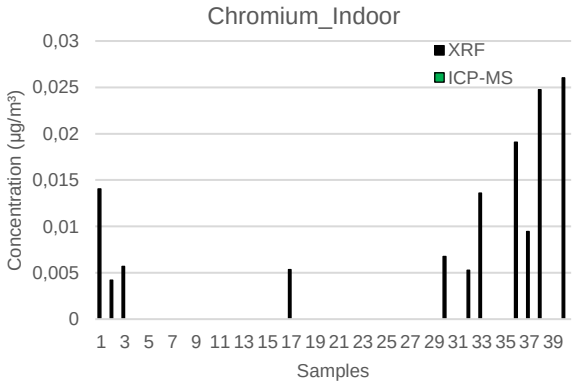

Figure 4.15: Comparison between the WD-XRF & ICP-MS for a) ambient and b) indoor chromium (Cr)

Mn

It evident from the comparisons of Mn concentrations determined with ICP-MS and WD-XRF in ambient and indoor samples presented in Figure 4.16, that Mn levels were determined in approximately the same number of ambient and indoor samples by both analytical methods. However, differences are observed for the Mn concentrations determined with the two analytical techniques. Mn concentrations determined with ICP-MS were higher in certain samples, while higher Mn levels corresponded to WD-XRF in other samples. No clear trend is evident from the comparison of the detection of Mn with ICP-MS and WD-XRF. The t-test value also indicated no significant difference between Mn concentrations determined with ICP-MS and WD-XRF. In general, relatively good comparison are observed for Mn determined with both analytical methods, especially for lower concentrations thereof associated with ambient samples.

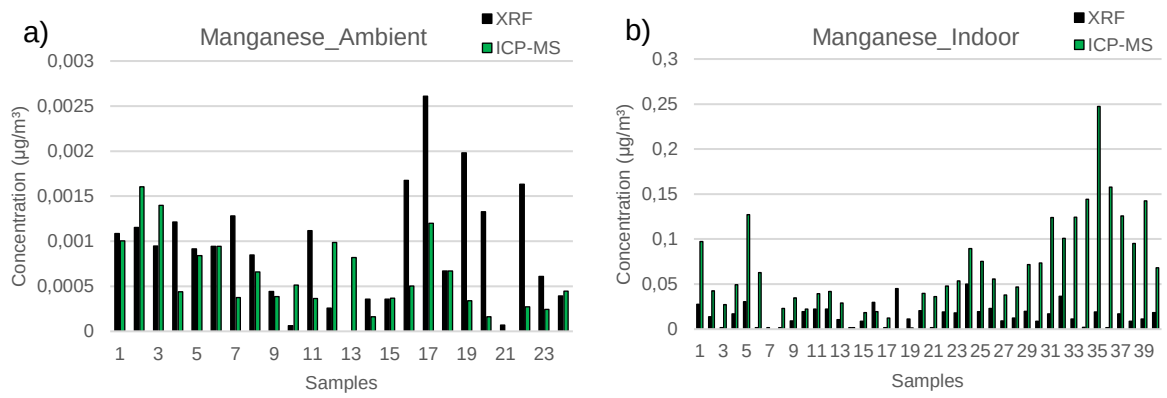

Figure 4.16: Comparison between the WD-XRF & ICP-MS for a) ambient and b) indoor manganese (Mn)

Co

Figure 4.17 indicates the Co concentrations determined with ICP-MS and WD-XRF indoor samples. Co was not detected in ambient samples. No significant trend in the compassion of analysis of Co with the two analytical methods is evident. In some samples higher Co levels were determined with ICP-MS, while WD-XRF analysis yielded higher Co concentrations in other samples, similar to that observed for Na and Mn. The highest Co concentrations, however, were determined with ICP-MS. In general, Co concentrations were very low, especially, considering that these levels are associated with indoor samples that had higher concentrations of trace metals. These low concentrations could contribute to artefacts associated with both analytical methods. It is expected that ICP-MS should more accurately analyse Co concentrations, since it has a lower DL for Co compared to WD-XRF.

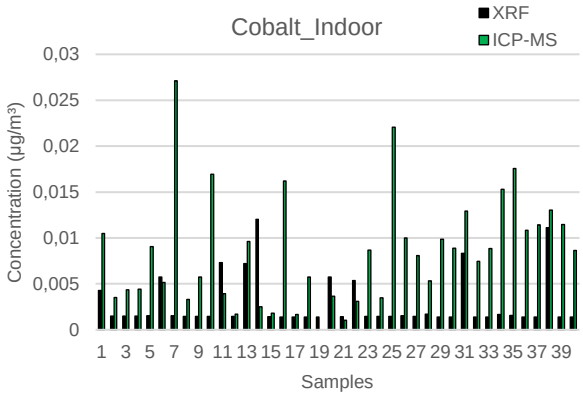

Figure 4.17: Comparison between the WD-XRF & ICP-MS for a) ambient and b) indoor cobalt (Co)

Ni

It is evident form Figure 4.18 that Ni concentrations in ambient samples were almost exclusively determined with ICP-MS with very low levels determined with WD-XRF. Although Ni were detected by both analytical methods in indoor samples, Ni levels were determined in

more samples with WD-XRF. In addition, relatively large differences are observed for samples in which Ni levels were determined with both analytical methods. These observed differences between Ni concentrations determined with the two analytical techniques could be attributed to relatively low concentrations of these species. Furthermore, as indicated by the PSD in ambient samples, Ni predominantly occurred in the fine fraction, which could also contribute to biases in concentrations determined with WD-XRF. As indicated for other species predominantly in the fine fraction, Ni-particles could therefore penetrate deeper into the collection substrate, which could contribute to increased scattering of X-ray radiation and background noise.

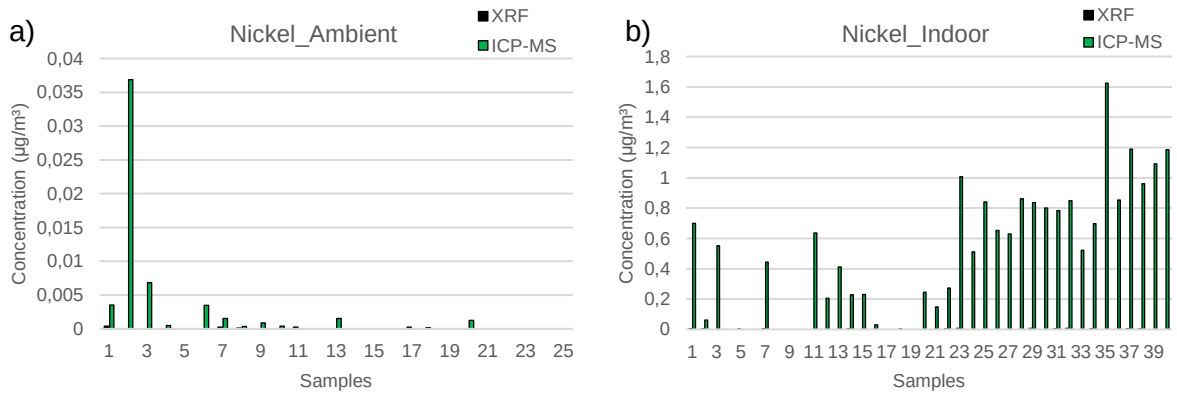

Figure 4.18: Comparison between the WD-XRF & ICP-MS for a) ambient and b) indoor nickel (Ni)

Cu

Cu only passed the basement criteria in samples collected indoor and in Figure 4.19 Cu concentrations determined with ICP-MS and WD-XRF in these samples are presented. It is evident that relatively low concentrations were determined for Cu that were predominately detected with ICP-MS. Significant differences are observed for the Cu concentrations determined in samples where Cu was detected with the two methods. Significantly higher Cu levels were determined with ICP-MS, while low Cu concentrations were determined with WD-XRF. The t-tests also indicated significant differences between C concentrations determined with both analytical methods. It seems that ICP-MS is more sensitive for lower concentrations of Cu compared to WD-XRD with ICP-MS having a lower DL for Cu. However, Cu concentrations could also be underestimated with ICP-MS due to complex formation in aqueous solutions.

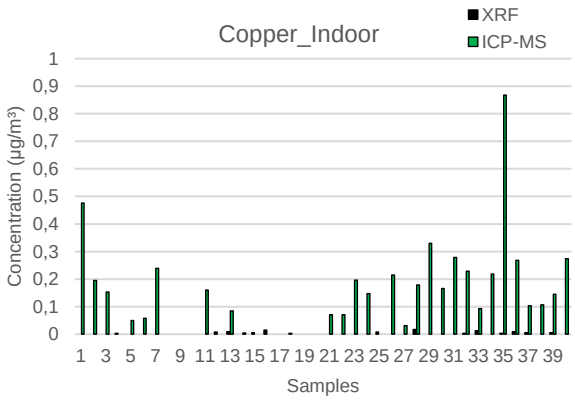

Figure 4.19: Comparison between the WD-XRF & ICP-MS for a) ambient and b) indoor copper (Cu)

Zn

Figure 4.20 indicates the Zn concentrations determined with the two analytical methods in ambient and indoor samples. Although it is evident that Zn was detected more frequently with WD-XRF than with ICP-MS in both sets of samples, higher Zn concentrations were generally determined with ICP-MS. Therefore, significant differences are observed in samples where Zn was detected with both analytical techniques. Zn was also determined in most of the indoor samples, while it was measured in <50% of ambient samples. Differences associated with Zn measured with the two techniques could be related to similar reasons that contributed to inconsistencies in concentrations determined for other base metals (e.g. Ni and Cu), which can be related to relatively low Zn concentrations and Zn mainly occurring in the fine fraction, as well as complex formation in aqueous solutions.

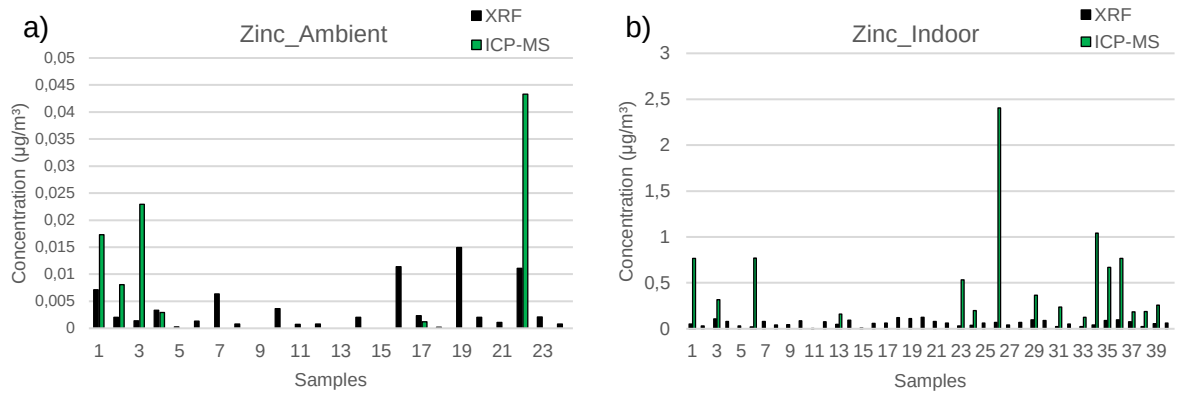

Figure 4.20: Comparison between the WD-XRF & ICP-MS for a) ambient and b) indoor zinc (Zn)

Sb

Sb was only determined in indoor samples. It is evident form the comparison of Sb concentrations presented in Figure 4.21 that Sb was predominantly detected with WD-XRF, with significantly lower concentration thereof detected in only a few samples with ICP-MS. It

is also of interest to note that Sb was detected with WD-XRF in all the indoor samples. The poor quantification of Sb with ICP-MS can be attributed to hydrolyses of Sb during the nitric acid digestion, which results in the formation of SbOCl and/or $Sb_4O_5Cl_2$ precipitates.

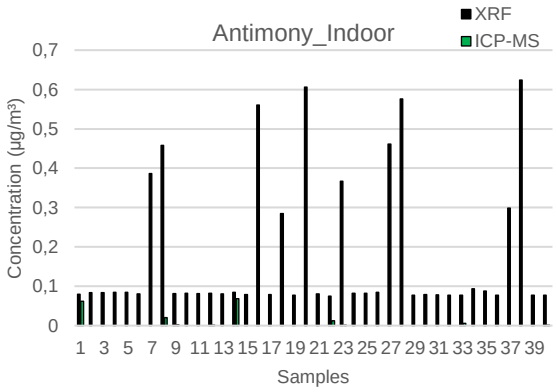

Figure 4.21: Comparison between the WD-XRF & ICP-MS for indoor antimony (Sb)

Sr

Comparison of Sb concentration determined with ICP-MS and WD-XRF in ambient and indoor samples presented in Figure 4.22 indicate that, although Sb was determined with both analytical methods in most samples, significantly higher concentrations were determined with ICP-MS. However, considerably higher Sb concentrations were determined with WD-XRF in two ambient samples. The t-test indicated no significant difference in Sr determined in ambient samples. However, a significant difference was determined for indoor samples.

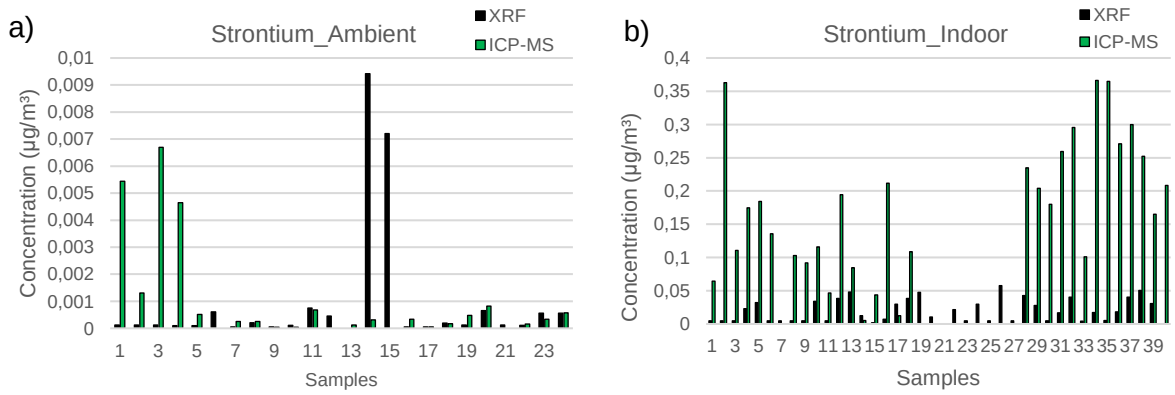

Figure 4.22: Comparison between the WD-XRF & ICP-MS for ambient strontium (Sr)

Pd

It is evident form the comparison of Pd concentrations determined in ambient and indoor samples with both analytical techniques presented in Figure 4.23, that Pd was predominantly determined with WD-XRF in both sets of samples. Pd was only detected in a few instances

with ICP-MS in indoors samples, with significant lower measured concentrations. It is important to mention that Pd concentrations determined with WD-XRF could be influenced by spectral overlap with Rh, which could contribute to an overestimate of Pd concentrations determined with WD-XRF. Scattering of the Rh X-ray tube (applied in this case study) during WD-XRF analyses could enhance the signal of Pd. Therefore, great care should be taken when analysing Pd with Rh X-ray tube. Limitations associated with ICP-MS for measurement of Pd relates to interferences with other species, while Pd could also form insoluble complexes in acidic solutions.

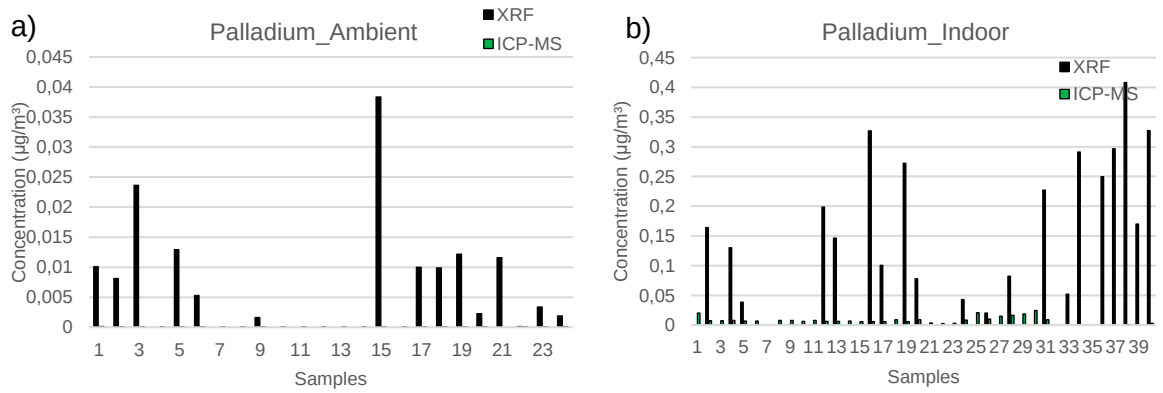

Figure 4.23: Comparison between the WD-XRF & ICP-MS for a) ambient and b) indoor palladium (Pd)

P

In Figure 4.24 P concentrations determined with ICP-MS and WD-XRF in ambient and indoor samples are presented. Although P was detected with both analytical methods in most the samples, significantly higher P concentrations were determined with IC-MS. However, P levels were determined in a few ambient samples only with WD-XRF. With the exception of these few samples, a clear trend is evident for measurement of P concentrations with ICP-MS preforming generally better than WD-XRF. The t-test also indicate significant differences in P concentrations determined with the two analytical techniques in door samples. P concentrations measured with ICP-MS could be overestimated by interferences. Lower P levels determined with WD-XRF could be attributed to P, which is a light element, mainly occurring in the fine fraction, as well as the relatively low P concentrations.

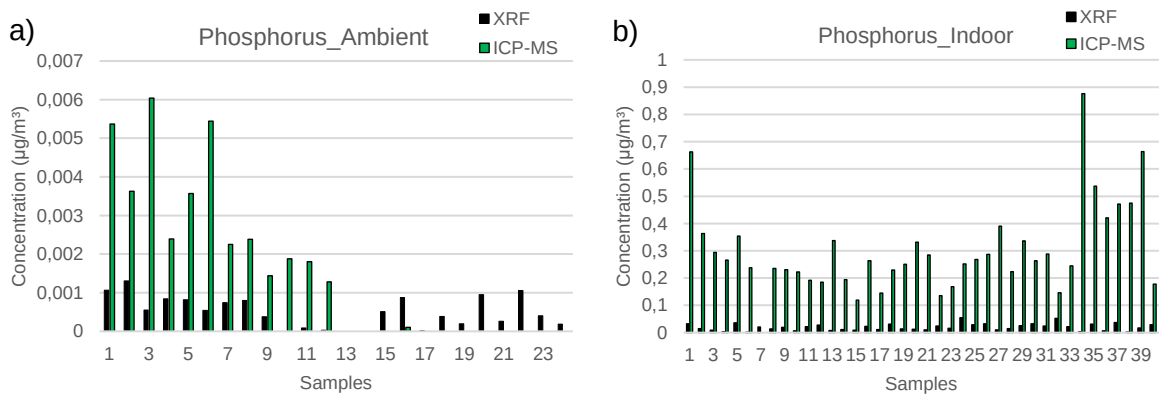

Figure 4.24: Comparison between the WD-XRF & ICP-MS for a) ambient and b) indoor phosphorus (P)

As, Pt and Pb

Very low concentrations were determined for As, Pt and Pb as indicated in Figure 4.25, 4.26 and 4.27, respectively, while these species only occurred in ambient samples. As was predominantly determined with ICP-MS, while Pb was determined with both analytical methods in different samples. Pt was also mainly measured with ICP-MS, while a relatively higher Pt concentration was determined in the only sample in which Pt was detected with WD-XRF. These very low concentrations of As, Pt and Pb does not allow for further interpretation of results. Low concentrations of these species will contribute to very low concentrations passing the assessment criteria applied.

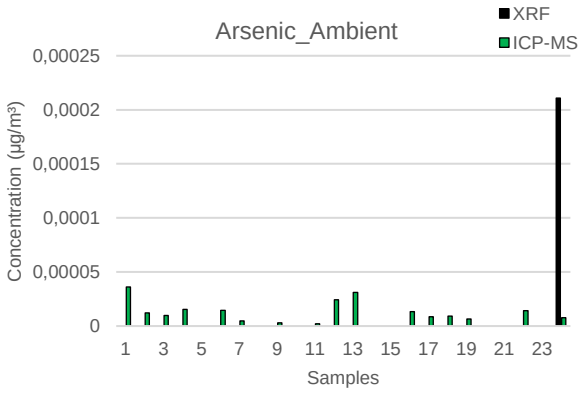

Figure 4.25: Comparison between the WD-XRF & ICP-MS for ambient arsenic (As)

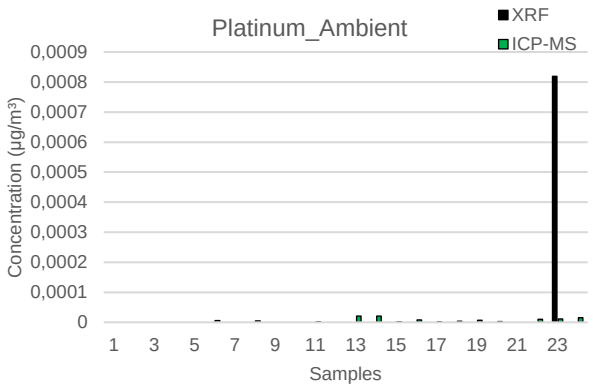

Figure 4.26: Comparison between the WD-XRF & ICP-MS for ambient indoor platinum (Pt)

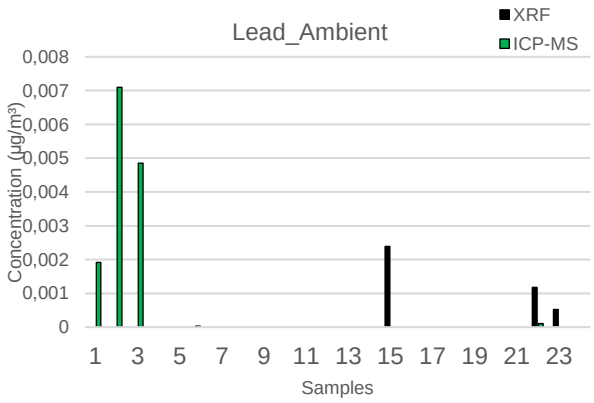

Figure 4.27: Comparison between the WD-XRF & ICP-MS for ambient and lead (Pb)

5.5 Conclusions

From the results presented in this chapter, it is evident that weak correlations were determined between the concentrations of trace metals determined with ICP-MS and WD-XRF as indicated by Pearson correlations and t-tests. Comparison of concentrations determined for each trace species with the two analytical methods did not reveal distinct validations with regard to the suitability of ICP-MS and WD-XRF for determination of concentrations of specific trace metal. However, it seemed that WD-XRF did perform better for the analysis of trace metals associated with silicate mineral in dust (e.g. Al and Fe), while lighter trace metals are most-likely underestimated with this analytical technique. It was also indicated that the particle size distribution could contribute to lower trace metal concentrations determined with WD-XRF, i.e. trace metals predominantly occurring in the fine size fraction. In addition, the influences associated with interferences attributed to the nitric acid digestion of trace metal species for ICP-MS analysis, could contribute to under- and overestimations of trace metal concentrations determined with ICP-MS. Furthermore, it could also be established that laboratory procedural contamination was the major factor contributing to contamination of

samples prepared for ICP-MS analysis while the influence of gravimetrical contamination was also evident for both analytical techniques.

CHAPTER 5: PROJECT EVALUATION

This chapter presents a critical evaluation of the most important aspects and findings of this case study regarding the suitability of analytical techniques generally used for the quantification of atmospheric particulate matter. Successes and shortcomings will be highlighted, while possible key areas for future studies will also be identified.

5.1. Project evaluation

The reliable quantification of atmospheric particulate matter is greatly influenced by the physical properties and chemical composition. Two of the most widely used analytical techniques utilised in the characterisation and quantification of trace metals in atmospheric particulate matter (PM), i.e. the inductively coupled mass spectrometer (ICP-MS) and the wavelength-dispersive X-ray fluorescence spectrometer (WD-XRF were compared in this study. This aim was to assess the applicability of these techniques for source apportionment studies in South Africa, as well as to assess the strengths and limitations of these two methods. Below the project is assessed in terms of the shortcomings and successes in view of each specific objective listed in Chapter 1.

Objective 1: Quantify the trace metal composition of the PM samples collected on filters by means of non-destructive WD-XRF analysis.

Ambient and indoor PM samples were collected at two sites located in different regions in the interior of South Africa. Duplicate weekly samples were successfully collected in duplicate at the regional atmospheric background site, Welgegund, while 24-hour indoor samples were collected in Agincourt. In this case study, 40 of the PM samples collected during the indoor sampling campaign was applied for WD-XRF and ICP-MS analysis. While 24 ambient aerosol samples were collected. Thirty-one (31) trace metals (Na, Mg, Al, P, K, Ca, Ti, V, Cr, Mn, Fe, Co, Ni, Cu, Zn, As, Se, Rb, Sr, Mo, Pd, Ag, Cd, Sb, Ba, Pt, Au, Hg, Tl, Pb, Bi) were analysed by means of the WD-XRF and ICP-MS. PM samples extracted from filters were subjected to ICP-MS and 19 indoor- and 17 ambient trace metal species could be detected. Application of an assessment criteria resulted in the successful quantification of 18 indoor- and 16 ambient trace metal species, which were considered for comparison with ICP-MS. These species included ambient Na, Mg, Al, P, K, Ca, Ti, Mn, Fe, Ni, Zn, As, Sr, Pd, Pt, Pb and indoor Na, Mg, Al, P, Ca, Ti, Cr, Mn, Fe, Co, Ni, Cu, Zn, Rb, Sr, Mo, Pd, Sb. Trace metal species that were consistently below the detection limit (DL) of the analytical technique included ambient V, Cr, Co, Se, Rb, Mo, Ag, Cd, Sb, Ba, Au, Hg, Tl, Bi as well as indoor V, As, Se, Ag, Cd, Ba, Pt, Au, Hg, Tl Pb, Bi.. The precision of the WD-XRF method could also be successfully indicated, which indicated good comparison between trace metal concentrations determined.

However, there are limitations associated with the method utilised in this study to establish precision.

Objective 2: Quantify trace metal composition of PM samples with a destructive acid digestion technique for ICP-MS analysis.

The same indoor filters subjected to non-destructive WD-XRF could be subjected to acid digestion in preparation for analysis with ICP-MS. Whereas the duplicate weekly ambient PM samples were collected allowing each analytical technique its own set of 24 PM samples Collected PM samples were successfully extracted from filters with a nitric- and hydrochloric acid digestion method commonly used for ICP-MS. However, a limitation associated with extraction of aerosol samples was that hydrofluoric acid extraction could not be successfully performed due limitations associated with the laboratory setup and safety concerns due to this method resulting in the formation of hazardous gaseous SiF_3. PM samples extracted from filters were subjected to ICP-MS and 26 indoor- and 28 ambient trace metal species could be detected. Application of the assessment criteria resulted in the successful quantification of 18 indoor- and 16 ambient trace metal species, which were considered for comparison with WD-XRF. These species included ambient Na, Mg, Al, P, K, Ca, Ti, Mn, Fe, Ni, Zn, As, Sr, Pd, Pt, Pb and indoor Na, Mg, Al, P, Ca, Ti, Cr, Mn, Fe, Co, Ni, Cu, Zn, Rb, Sr, Mo, Pd, Sb. Trace metal species that were consistently below the detection limit (DL) of the analytical method included indoor K, Ag, Au, Tl, Pb, Bi and ambient Cu, Cd, Tl. Assessment of the precision of ICP-MS also revealed good correlations, while the influence of contamination from different sources related to ICP-MS analysis could also be indicated. The influence of contamination associated with WD-XRF could, however, not be quantified.

The trace metal concentrations determined with both analytical methods generally indicated higher levels of these species indoor samples compared to ambient samples, which was expected due to ambient aerosols being more dispersed compared to particulates associated with indoor emissions and different sources impacting the two sites. Furthermore, the highest indoor trace metal concentrations were determined for Na, Mg, Al, and Ca.

Since size segregated ambient samples were collected at Welgegund, the particle size distribution of each trace metal species could also be determined. As previously stated in Chapter 3, Welgegund is frequently affected by anthropogenic air plumes from the Vaal Triangle Airshed Priority Area, Waterberg-Bojanala Priority Area, Johannesburg-Pretoria metropolitan, and the Highveld Priority Area. Consequently, it is without surprise that the PSD of the collected ambient samples indicated that the majority (except Al and K) of trace metal

species occurred in the fine- ($PM_{2.5}$) and ultra-fine (PM_1) size fraction, which is generally affiliated with anthropogenic emissions.

Objective 3: Compare results obtained from the different methods to identify possible biases of techniques with regard to composition and source apportionment of PM.

Initial comparison of the trace metal detected with the two analytical methods, indicated that the percentages of samples in which concentrations of specific trace metals were above the DLs of WD-XRF and ICP-MS differed for the two analytical techniques, which reflected inconsistencies between the two analytical methods. Statistical correlation between trace metal concentrations with ICP-MS and WD-XRD also indicated very weak relationship in general for the concentrations determined for most trace metal species. In order to further assess these differences in the detection of trace metal species with ICP-MS and WD-XRF, as well as the weak statistical correlations, concentrations determined for each trace metal species in each sample collected during the ambient and indoor campaigns with the two analytic methods were directly compared.

These direct comparisons of concentrations determined for specific trace metals in each sample did not reveal distinct trends in the concentrations determined for most species with WD-XRF. However, it did seem that higher concentrations of trace metal species associated with crustal sources were determined with WD-XRF, which was expected due to the nitric acid digestion underestimating silicate minerals in dust. This could be successfully indicated for, especially, Al in this study. Lower trace metal concentrations determined with ICP-MS was also attributed to interferences during the analysis of extracted samples. Lower trace metal concentrations determined with WD-XRF compared to ICP-MS was generally attributed to most trace metal species occurring in the fine size fraction. Fine particles easily penetrate deeper into the substrate medium with impaction, which can result in an increase of X-ray scattering and background noise, especially for light metals.

Although trace metal species were successfully detected with the two analytical techniques and could be assessed, comparison of the concentrations determined for each trace species with the two analytical methods did not reveal distinct confirmations with regard to the suitability of ICP-MS and WD-XRF for determination of concentrations of specific trace metals. Therefore, future studies in order to improve the comparison of these two analytical methods are suggested as indicated below.

5.2. Future perspectives

Numerous studies have been conducted in order to compare different analytical methods and procedures utilised for the characterisation and quantification of atmospheric trace metal

species. These other studies also indicated the complexities associated with establishing the most suitable method for the analysis of trace metal species in specific environments as revealed in this study. In view of the weak correlation between trace metal concentrations determined with ICP-MS and WD-XRF, as well as other limitations associated with this study, the following recommendations for future studies are presented.

- Other extraction methods for the preparation of aerosol samples for ICP-MS analysis must be explored. This, especially, includes the use of hydrofluoric acid as an extractant, which would elucidate uncertainties associated with silicate mineral determined with ICP-MS in this study.
- Efforts must be undertaken to minimise problems associated with interferences relating to both analytical techniques. As indicated in Chapter 2, there are several possible interferences associated with these analytical techniques, especially, for ICP-MS.
- An improved study on the influence of contamination could also be conducted, especially, for WD-XRF. Many inconsistencies relating to trace metal concentrations determined with both analytical methods can be attributed to the influences of contamination during various steps associated with sampling and analysis of PM.
- Trace metal concentrations determined with the two analytical methods could also be included as input data in source apportionment models in order to determine the characteristics of sources according to trace metal concentrations determined with the two analytical techniques.

REFERENCES

Alfarra, M.R. 2004. Insights into atmospheric organic aerosols using an aerosol mass spectrometer. Manchester: University of Manchester. (Thesis – PhD).

Allen, A.G., Nemitz, E., Shi, J.P., Harrison, R.M. & Greenwood, J.C. 2001. Size distribution of trace metals in atmospheric aerosols in the United Knigdom. *Atmospheric Environment*, 35(27):4581-4591.

Bazilio, A. & Weinrich, J. 2012. The easy guide to: inuctively coupled plasma mass spectrometry (ICP-MS). http://www.ecs.umass.edu/eve/facilities/equipment/ICPMS/ICPMS%20quick%20guide.pdf Date of access: 3 Aug. 2018.

Bettinelli, M, Baroni, U. & Pastorelli, N. 1989. Microwave oven sample dissolution for the analysis of environmental and biological materials. *Analytica Chimica Acta*, 225:159-174.

Beukes, J.P., Vakkari, V., van Zyl, P.G., Venter, A.D., Josipovic, M., Jaars, K., Tiitta, P., Kulmala, M., Worsnop, D., Pienaar, J.J., Virkkula, A & Laakso, L. 2013. Source region plume characterisation of the interior of South Africa as observed at Welgegund. *Clean Air journal*, 23(1):7-10.

Bo, M., Salizzoni, P., Clerico, M. & Buccolieri, R. 2017. Assessment of indoor-outdoor particulate matter air pollution: a review. *Atmosphere*, 8. https://www.mdpi.com/2073-4433/8/8/136 Date of access: 4 November 2018

Booyens W. 2018. Measurment of organic compounds in atmospheric aerosols collected at Welgegund, South Africa. Potchefstroom: NWU. (Thesis – PhD).

Booyens, W., van Zyl, P.G., Beukes, J.P., Ruiz-Jimenez, J., Kopperi M., Riekkola, M-L., Josipovic, M., Venter, A.D., Jaars, K., Laakso, L., Vakkari, V., Kulmal, M. & Pienaar, J.J. 2015. Size-resolved characterisation of organic compounds in atmospheric aerosols collected at Welgegund, South Africa. *Journal of Atmospheric Chemistry*, 72(1):43-64.

Boss, C.B. & Fredeen, K.J. 2004. Concepts, instrumentation and techniques in inductively coupled plasma optical emission spectrometry. 3rd ed. Shelton, CT: Perkin Elmer.

Brimblecombe, P. 1996. Air: composition and chemistry. 2nd ed. Cambridge University Press.

Brouwer, P. 2010. Theory of XRF. https://www.iotcco.com/uploads/VirtualTeaching/Articles/PANanalytical/PANanalytical%20XRF%20theory.pdf Date of access: 5 Jan. 2019

Brown, R.J.C. & Milton, M.J.T. 2005. Analytical techniques for trace element analysis: an overview. *Trends in Analytical Chemistry*, 24(3):266-274.

Brunekreef, B. & Holgate, S.T. 2002. Air pollution and health. *The Lancet*, 360:1233-1242.

Butterfield, D. & Quincy, P. 2007. Measurement science issues relating to PM_{10} and $PM_{2.5}$ airborne particles. http://eprintspublications.npl.co.uk/4023/1/AS15.pdf Date of access: 18 May 2019

Chow, J.C. 1995. Measurement methods to determine compliance with ambient air quality standards for suspended particles. *Journal of the Air & Waste Management Association*, 45(5):320-382.

Davidson, C.I., Phalen, R.F. & Solomon, P.A. 2005. Airborne particulate matter and human health: a review. *Aerosol Science & Technology*, 39(8):737-749.

Deguillaume, L., Leriche, M., Desboeufs, K., Mailhot, G., George, C. & Chaumerliac, N. 2005. Transition metals in atmospheric liquid phases: sources, reactivity, and sensitive parameters. *Chemical Reviews*, 105(9):3388-3431.

Evans, E.H. & Giglio, J.J. 1993. Interferences in inductively coupled plasma mass spectrometry. A review. *Journal of Analytical Atomic Spectrometry*, 8(1):1-18.

Feldmann, J., Salaün, P. & Lombi, E. 2009. Critical review perspective: elemental speciation analysis methods in environmental chemistry – moving towards methodological integration. *Environmental Chemistry*, 6:275-289.

Fuzzi, S., Baltensperger, U., Carslaw, K., Decesari, S., Denier Van Der Gon, H., Facchini, M.C., Fowler, D., Koren, I., Langford, B., Lohmann, U., Nemitz, E., Pandis, S., Riipinen, I., Rudich, Y., Schaap, M., Slowik, J.G., Spracklen, D.V., Vignati, E., Wild, M., Williams, M. & Gilardoni, S. 2015. Particulate matter, air quality and climate: lessons learned and future needs. *Atmospheric Chemistry and Physics*, 15(14):8217-8299.

Gilstrap, R.A. 2009. A colloidal nanoparticle form of indium tin oxide: system development and characterization. Georgia: Georgia Institute of Technology. (Dissertation – PhD).

Graney, J.R., Landis, M.S. & Norris, G.A. 2003. Concentrations and solubility of metals from indoor and personal exposure $PM_{2.5}$ samples. *Atmospheric Environment*, 38(2):237-247.

Greyling, S. 2016. Development of a hydrocyclone separation efficiency model using artificial neural networks. Potchefstroom: NWU. (Dissertation – MSc).

Harrison,R.M. & Yin, J. 2000. Particulate matter in the atmosphere: which particle properties are important for its effects on health? *The Science of the Total Environment,* 249:85-101

Herner, J.D., Green, P.G. & Kleeman, M.J. 2006. Measuring the trace elemental composition of size-resolved airborne particles. *Environmental Science & Technology*, 40(6):1925-1933.

Holler, E.J., Skoog, D.A. & Crouch, S.R. 2007. Principles of instrumental analysis. 6th ed. Belmont, CA: Brooks/Cole Cengage Learning.

Irshad, M., Malik, A.H., Shaukat, S., Mushtaq, S. & Ashraf, M. 2013. Characterization of heavy metals in livestock manures. *Polish Journal of Environmental Studies*, 22(4):1257-1262.

ISO, DINEN. 1972. Theory of sample preparation using acid digestion, pressure digestion and microwave digestion (microwave decomposition).

Jaars, K., Beukes, J.P., van Zyl, P.G., Venter, A.D., Josipovic, M., Pienaar, J.J., Vakkari, V., Aaltonen, H., Laakso, H., Kulmala, M., Tiitta, P., Guenther, A., Hellén, H., Laakso, L. & Hakola, H. 2014. Ambient aromatic hydrocarbon measurements at Welgegund, South Africa. *Atmospheric Chemistry and Physics*, 14(13):7075-7089.

Jaars, K., van Zyl, P.G., Beukes, J.P., Hellén, H., Vakkari, V., Josipovic, M., Venter, A.D., Räsän, M., Knoetze, L., Cilliers, D.P., Siebert, S.J., Kulmala, M., Rinne, J., Guenther, A., Laakso, L. & Hakola, H. 2016. Measurements of biogenic volatile organic compounds at a grazed savannah grassland agricultural landscape in South Africa. *Atmospheric Chemistry and Physics*, 16:15665-15688.

Karanasiou, A.A., Thomaidis, N.S., Eleftheriadis, K. & Siskos, P.A. 2004. Comparative study of pretreatment methods for the determination of metals in atmospheric aerosol by electrothermal atomic absorption spectrometry. *Talanta*, 65(5):1196-1202.

Kgabi, N.A. 2006. Monitoring the levels of toxic metals of atmospheric particulate matter in the Rustenburg district. Potchefstroom: NWU. (Thesis – PhD).

Kgabi, N.A. 2010. An assessment of common atmospheric particulate matter sampling and toxic metal analysis methods. *African Journal of Environmental Science and Technology*, 4(11):718-728.

Khoder, M.I., Hassan, S.K. & El-Abssawy, A.A. 2010. An evaluation of loading rate of dust, Pb, Cd, and Ni and metals mass concentration in the settled surface dust in domestic houses and factors affecting them. *Indoor and Built Environment*, 19(3):391-399.

Klein, C. & Dutrow, B. 2007. Manual of mneral science. 23rd ed. USA: John Wiley & Sons

Kulshrestha, A., Massey, D.D., Masih, J. & Taneja, A. 2014. Source characterisation of trace elements in indoor environments at urban, rural and roadside sites in a semi-arid region of India. *Aerosol and Air Quality Research*, 14:1738-1751

Laakso , L., Vakkari, V., Virkkula, A., Laakso, H., Backman, J., Kulmala, M., Beukes, J.P., van Zyl, P.G., Tiitta, P., Josipovic, M., Pienaar, J.J., Chiloane, K., Gilardoni, S., Vignati, E., Wiedensohler, A., Touch, T., Birmili, W., Piketh, S., Collett, K., Fourie, G.D., Komppula, M., Lihavainen, H., de leeuw, G. & Kerminen, V.M. 2012. South African EUCAARI measurements: seasonal variation of trace gases and aerosol optical properties. *Atmospheric Chemistry and Physics*, 12(4):1847-1864.

Lachas, H., Richaud, R., Jarvis, K.E., Herod, A.A., Dugwell, D.R. & Kandiyoti, R. 1998. Determination f 17 trace elements in coal and ash reference materials by ICP-MS applied to milligram sample size. *Analyst*, 124:177-184.

Language, B., Piketh, S.J. & Burger, R.P. 2016. Correcting respirable photometric particulate measurements using a gravimetric sampling method. *The Clean Air Journal*, 26(1):10-13.

Language, B. 2019. Characterisation of respirable indoor particulate matter in South African low-income settlements. Potchefstroom: NWU. (Thesis – PhD).

Liu, K., Shang, Q., Wan, C., Song, P., Ma, C. & Cao, L. 2017. Characteristics and sources of heavy metals in $PM_{2.5}$ during a typical haze episode in rural and urban areas in Taiyuan, China. *Atmosphere*, 9(2). https://www.mdpi.com/2073-4433/9/1/2 Date of access: 4 November 2018.

Marconi, M., Sferlazzo, D.M., Becagli, S., Bommarito, C., Calzolai, G., Chiari, M., di Sara, A., Ghedini, C., Gómez-Amo, J.L., Lucarelli, F., Meloni, D., Monteleone, F., Nava, S., Pace, G., Piacentino, S., Rugi, F., Severi, M., Traversi, R. & Udisti, R. 2014. Saharan dust aerosol over the central Mediterranean Sea: PM_{10} chemical composition and concentration versus optical columnar measurements. *Atmospheric Chemistry and Physics*, 14:2039-2054

Matusiewicz, H. 2016. Sample decomposition techniques in inorganic trace elemental analysis. (*In* Baranowska, I., *ed*. Handbook of trace analysis: fundamentals and applications. Switzerland:Springer. p. 75-122).

McMurry, P.H. 2000. A review of atmospheric aerosol measurements. *Atmospheric Environments*, 34:1959-1999.

Monks, P.S., Granier, C., Fuzzi, S., A. Stohl, A., Williams, M.L., Akimoto, H., Amann, M. Baklanov, A., Baltensperger, U., Bey, I. , Blake, N. , Blake, R.S., Carslaw, K., Cooper, O.R., Dentener, F., Fowler, D., Fragkou, E., Frost, G.J., Generoso, S., Ginoux, P., Grewe, V., Guenther, A., Hansson, H.C., Henne, S., Hjorth, J., Hofzumahaus, A., Huntrieser, H., Isaksen, I.S.A., Jenkin, M.E., Kaiser, J., Kanakidou, M., Klimont, Z., Kulmala, M., Laj, P., Lawrence, M.G., Lee, J.D., Liousse, C., Maione, M., McFiggans, G., Metzger, A., Mieville, A., Moussiopoulos, N., Orlando, J.J., O'Dowd, C.D., Palmer, P.I., Parrish, D.D., Petzold, A., Platt., U., Poschl, U., Prévôt, A.S.H., Reeves, C.E., Reimann, S., Rudich, Y., Sellegri, K., Steinbrecher,R., Simpson, D., ten Brink, H., Theloke, J., van der Werf, G.R., Vautard, R., Vestreng, V., Vlachokostas, C. & von Glasow, R. 2009. Atmospheric composition change – global and regional air quality. *Atmospheric Environment*, 43(33):5268-5350.

Mouli, P.C., Mohan, S.V., Balaram, V., Kumar, M.P. & Reddy, S.J. 2005. A study on trace elemental composition of atmospheric aerosols at a semi-arid urban site using ICP-MS technique. *Atmospheric Environment*, 40:136-146.

Mudway, I.S., Duggan, S.T., Venkataraman, C., Habib, G., Kelly, F.J. & Grigg, J. 2005. Comnustion of dried animal dung as biofuel results in the generation of highly redox active fine particulates. *Particle and Fibre Toxicology*, 2(6). https://particleandfibretoxicology.biomedcentral.com/articles/10.1186/1743-8977-2-6 Date of access: 4 November 2018.

Nazir, R., Shaheen, N. & Shah, M.H. 2011. Indoor/outdoor relationship of trace metals in the atmospheric particulate matter of an industrial area. *Atmospheric Research*, 101(3):765-772.

Niu, J., Rasmussen, P.E., Wheeler, A., Williams, R. & Chénier, M. 2009. Evaluation of airborne particulate matter and metals data in personal, indoor and outoor environments using ED-XRF and ICP-MS and co-located duplicate samples. *Atmospheric Environment*, 44(2):235-245.

Okuda, T., Fujimori, E., Hatoya, K., Takada, H., Kumata,H., Nakajima, F., Hatakeyama, S., Uchida, M., Tanaka, S., He, K., Ma, Y. & Haraguchi, H. 2013. Rapid and simple determination of multi-elements in aerosol samples collected on quartz fiber filters by using EDXRF coupled with fundamental parameter quantification technique. *Aerosol and Air Quality Research*, 13:1864-1876.

Olivares, J.A. & Houk, R.S. 1986. Suppression of analyte signal by various concomitant salts in inductively coupled plasma mass spectrometry. *Analytical Chemistry*, 58(1):20-25.

Onabowale, M.K. & Owoade, O.K. 2015. Assessment of residential indoor-outdoor airborne particulate matter in Ibadan, Southwestern Nigeria. *Donnish Journal of Physcal Sciences*, 1(1):1-7.

Pacyna, J.M. & Pacyna, E.G. 2001. An assessment of global and regional emissions of trace metals to the atmosphere from anthropogenic sources worldwide. *Environmental Reviews*, 9(4):269-298.

Pope, C.A. & Dockery, D. 2006. Health effects of fine particulate air pollution: lines that connect. *Journal of Air & Waste Management Association*, 56(6):709-742.

Pöschl, U. 2005. Atmospheric aerosols: composition, transformation, climate and health Effects. *Angewandte Chemie International Edition*, 44(46):7520-7540.

Prospero, J.M., Charlson, R.J., Mohnen, V., Jaenicke, R., Delany, A.C., Moyers, J., Zoller, W. & Rahn, K. 1983. The atmospheric aerosol system: an overview. *Reviews of Geophysics and Space Physics*, 21(7):1607-1629.

Ramanathan, V., Crutzen, P.J., Kiehl, J.T. & Rosenfeld, D. 2001. Aerosols, climate, and the hydrological cycle. *Science*, 294(5549):2119-2124.

Rasmussen, P.E., Wheeler, A.J., Hassan, N.M., Filiatreault, A. & Lanouette, M. 2007. Monitoring personal, indoor, and outdoor exposures to metals in airborne particulate matter: risk of contamination during sampling, handling and analysis. *Atmospheric Environment*, 41(28):5897-5907.

Raynor, P.C., Leith, D., Lee, K.W. & Mukund, R. 2011. Sampling and analysis using filters. (*In* Kulkarni, P., Baron, P.A. & Willeke, K., ed. 2011. Aerosol measurements: principles, techniques, and applications. 3rd ed. Hoboken, NJ: John Wiley & Sons. p. 107-127.)

Rüdel, H., Kösters, J.& Schörmann, J. 2011. Guidelines for chemical analysis – determination of the elemental content of environmental samples using ICP-MS. https://www.ime.fraunhofer.de/content/dam/ime/en/documents/AE/SOP_ICP-MS_en.pdf Date of access: 27 October 2018.

Salcedo, D., Bernal, J.P., Pérez-Arvizu, O. & Lounejeva, E. 2014. Assessment of sample preparation methods for the analysis of trace elements in airborne particulate matter. *Journal of Analytica Atomic Spectrometry*, 29(4):753-761.

Schlotz, R. & Uhlig, S. 2006. Introduction to X-ray fluorescence. http://www.fem.unicamp.br/~liqcqits/facilities/xrf/%5BBruker_2006%5D%20Introduction%20to%20X-ray%20Fluorescence%20(XRF).pdf Date of access: 30 October 2019.

Smith, K.R. 2002. Indoor air pollution in developing countries: recommendations for research. *Indoor Air*, 12:198-207.

Swami, K., Judd, C.D., Orsini, J., Yang, K.X. & Husain, L. 2001. Microwave assisted digestion of atmospheric aerosol samples followed by inductively coupled plasma mass spectrometry determination of trace elements. *Fresenius' Journal of Analytical Chemistry*, 369(1):63-70.

Swartz, J. 2016. Long-term measurements of concentration and dry deposition of atmospheric inorganic gaseous species at Cape Point, South Africa. Potchefstroom: NWU. (Dissertation – MSc).

Sundström, A.M., Nikandrova, A., Atlaskina, K., Nieminen, T., Vakkari, V., Laakso, L., Beukes, J.P., Arola, A., van Zyl, P.G., Josipovic, M., Venter, A.D., Jaars, K., Piernaar, J.J., Piketh, S., Wiedensohler, A., Chiloane, E.K., de Leeuw, G. & Kulmala, M. 2015. Characterization of satellite-based proxies for estimating nucleation mode particles over South Africa. *Atmospheric Chemistry and Physics*, 15:4983-4996.

Thomas, R. 2004. Practical guide to ICP-MS. Gaithersburg, MD: Marcel Dekker.

Tuisku, A. 2018. Wavelength dispersive X-ray fluorescence method development for asphaltene samples. Helsinki: Metropolia University of Applied Sciences. (Thesis – Bachelor of Laboratory Services).

United States Environmental Protection Agency (EPA). 1999. Compendium methods for the determination of inorganic compounds in ambient air. Washington, DC.

Vakkari, V., Kerminen, V.M., Beukes, J.P., Tiitta, P., van Zyl, P.G., Josipovic, M., Venter, A.D., Jaars, K., Worsnop, D.R., Kulmala, M. & Laakso, L. 2014. Rapid changes in biomass burning aerosols by atmospheric oxidation. *Geophysical Research Letters*, 41(7):2644-2651.

Vanhoof, C., Chen, H., Berghman, P., Corthouts, V., De Brucker, N. & Tirez, K. 2003. A risk assessment study of heavy metals in ambient air by WD-XRF spectrometry using aerosol generated filter standards. *X-ray Spectrometry*, 32:129-138.

van Zyl, P.G., Beukes, J.P., du Toit, G., Mabaso, D., Hendriks, J., Vakkari, V., Tiitta, P., Pienaar, J.J., Kulmala, M. & Laakso, L. 2014. Assessment of atmospheric trace metals in the western Bushveld Igneous Complex, South Africa. *South African Journal of Science*, 110:1-10.

Venter, A.D., Jaars, K., Booyens, W., Beukes, J.P., van Zyl, P.G., Josipovic, M., Hendriks, V., Vakkari, V., Hellén, H., Hakola, H., Aaltonen, H., Ruiz-Jimenez, J., Riekkola, M-L. &

Laakso, L. 2015. Plume characterization of a typical South Afrian braai. *South African Journal of Chemistry*, 68:181-194.

Venter, A.D. 2015. Assessment of atmospheric trace metals and water soluble ionic species at two regional background sites. Potchefstroom: NWU. (Thesis – PhD).

Venter, A.D., van Zyl, P.G., Beukes, J.P., Josipovic, M., Hendriks, J., Vakkari, V. & Laakso, L. 2017. Atmospheric trace metals measured at a regional background site (Welgegund) in South Africa. *Atmospheric Chemistry and Physics*, 17(6):4251-4263.

Vousta, D. & Samara, C. 2002. Labile and bioaccessible fractions of heavy metals in the airborne particulate matter from urban and industrial areas. *Atmospheric Environment*, 36(22):3583-3590.

Watson, J.G., Chow, J.C., Chen, L. & Wang, X. 2010. Measurement system evaluation for fugitive dust emissions detection and quantification. https://www.dri.edu/images/stories/editors/eafeditor/Watsonetal2010SCAQMDFugDustReport.pdf Date of access: 7 June 2019.

Woo, K.S., Chen, D.R., Pui, D.Y.H. & McMurry, P.H. 2001. Measurement of atlanta aerosol size distributions: observation of ultra-fine particle events. *Aerosol Science & Technology*, 34(1):75-87.

Yli-Juuti, T., Niemenin, T., Hirsikko, A., Aalto, P.P., Asmi, E., Hõrrak, U., Patokoski, J., Dal Maso, M., Petäjä, T., Rinne, J., Kulmal, M. & Riipinen, I. 2011. Growth rates of nucleation mode particles in Hyytiälä during 2003-2009: variation with particle size, season, data analysis method and ambient conditions. *Atmospheric Chemistry and Physics*, 11(24):12865-12886.

Zubrick, J.W. 2019. What-when-How: in depth tutorials and information. http://what-when-how.com/organic-chemistry-laboratory-survival-manual/reflux-laboratory-manual/ Date of access: 9 January 2019.